In search of a physiological role for amine oxidase,copper containing-3 (AOC3) in adipocytes

By

Sam Hsien-I Shen

A thesis submitted in partial satisfaction of the

requirements for the degree of

Doctor of Philosophy

in

Chemistry

in the

Graduate Division

of the

University of California, Berkeley

Committee in charge:

Professor Judith P. Klinman, Chair
Professor Christopher J. Chang
Professor Gary Firestone

Spring 2010

Dedication

I would like to dedicate this Doctoral dissertation to both my father and mother,

Dr. Thomas C. Shen and Mrs. Mayling C. Shen.

Without their undying support and advice, this work would not have been possible.

Acknowledgements

I would like to acknowledge the guidance and instruction of Professor Judith Klinman. Her keen insights, comments, and suggestions will undoubtedly be a part of all my future scientific endeavors.

I would also like to acknowledge Professor Sirpa Jalkanen at the University of Turku, Finland for providing me an opportunity to work in her lab and giving me important insights into my project. Ann Fisher provided invaluable counsel on all things tissue culture.

.

Table of Contents

Chapter 5: Monocyte chemoattractant protein-1 (MCP-1) production by adipocytes

Chapter 6: Involvement of adipocyte-derived chemokine(s) in macrophage chemotaxis

Table of Figures

Figures

Figures

List of Abbreviations

AOC3	Amine oxidase, copper containing-3
DMEM	Dulbecco's modified Eagle medium
FACS	Fluorescence-activated cell sorting
FBS	Fetal bovine serum
IL	Interleukin
KO	Knockout
KPi	Potassium phosphate
MSC	Mesenchymal stem cells
NCS	Newborn calf serum
NEAA	Non-essential amino acid
PBS	Phosphate buffered saline
PF1	Peroxyfluor-1
P/S	Penicillin/ Streptomycin
s2	Schneider 2 *Drosophila* cells
shAOC3	soluble human AOC3
TC	Tissue culture
TPQ	2,4,5 trihydroxyphenylalanine quinone
WGA	Wheat germ agglutinin
WT	Wild-type

Abstract

In search of a physiological role for amine oxidase,copper containing-3 (AOC3) in adipocytes

by

Sam Hsien-i Shen

Doctor of Philosophy in Chemistry

University of California, Berkeley

Professor Judith P. Klinman, Chair

In search of a physiological role for amine oxidase,copper containing-3 (AOC3) in adipocytes
The function of adipocytes was initially thought to be fat storage, thermal insulation, and organ protection. With the discovery of adipokine, cytokine, and chemokine production by adipocytes, they are now considered to have endocrine function with a major role in homeostasis and energy balance. Amine oxidase, copper containing 3 (AOC3) is a major ectoenzyme expressed by adipocytes and catalyzes the oxidative deamination of amines to produce hydrogen peroxide, ammonia, and aldehyde. The physiological function of AOC3 in adipocytes and its endogenous substrate(s) are currently unknown. First, a signaling role for the hydrogen peroxide product was investigated. Using an intracellular probe specific for H_2O_2, it was found that the plasma membrane of adipocytes is permeable to H_2O_2 introduced exogenously. However, it was not possible to detect an increase in intracellular H_2O_2 even after long incubation times with AOC3 substrates. Adipocytes were found to produce extracellular H_2O_2 at an approximate rate of 0.078 uM/min/well upon incubation with AOC3 substrate from whole cell kinetic studies. Due to this slow rate of H_2O_2 production, the probe may not be sensitive enough to show an increase in intracellular H_2O_2 originating from AOC3 turnover. Adipocytes may have an immune function, with possible involvement in chemokine production. Using chemotaxis assays, the migration of RAW264.7 macrophages was found to be independent of media components released by adipocytes incubated with isoamylamine, suggesting an absence or ineffectively low concentration of macrophage-specific chemokine release by adipocytes. However, these experiments used unactivated macrophages, which subsequently were reported by others to have chemotactic characteristics that are distinct from activated macrophages; the latter will be the subject of future studies. In addition to the chemotaxis assay, release of the chemokines by adipocytes was investigated using ELISA. It was found that release of monocyte chemoattractant protein-1 (MCP-1) by adipocytes was dependent on both concentration of H_2O_2 exposure and incubation time, with adipocytes also capable of constitutive MCP-1 release. However, the release of MCP-1, as well as other cytokines (including IL-6, KC, and IP-10), was found to have little correlation with AOC3 turnover. On the other hand, release of IL-13, a

1

cytokine correlated with populations of alternatively activated macrophages, was shown to be dependent on AOC3 turnover, though the increase was low with no correlation to H_2O_2. To find adipocyte response(s) to AOC3 turnover, it is important to characterize the enzyme's kinetic profile, since the endogenous substrate(s) of AOC3 is currently unknown. With this goal in mind, the human AOC3 enzyme was expressed and purified using a new expression system and purification protocol. Using the purified enzyme, a substrate kinetic profile was determined. It was found that both cyclic and noncyclic alkylamines, arylamines, and branched chain amines are all substrates for AOC3 with k_{cat}/K_m values ranging from 2.05 - 4.05 x 10^4 $s^{-1}M^{-1}$. Substrate hydrophobicity did not seem to affect the catalytic efficiency. It is noted that branched chain aliphatic amines are among the best substrates for AOC3, despite the fact that these amines are not metabolic products in mammals. Finally, the generation of an AOC3 knockout cell line (derived from AOC3 knockout mice) was pursued, providing a potential alternative to the use of AOC3 inhibitors in cell-based assays. Bone marrow derived mesenchymal stem cells (MSC) are multi-potent with the ability to differentiate into adipocytes. Using two techniques to enrich murine MSC, it was possible to reach an adipocyte yield of 1 -2 % of the total cell population.

Chapter 1:

Introduction

The global epidemic of obesity will be a major cause of morbidity and mortality in the future. In the United States alone, approximately 300,000 adults die of complications arising from obesity each year [1]. There are an estimated 400 million adults worldwide who can be classified as clinically obese, increasing to 700 million by 2015, according to the World Health Organization. The United States accounts for greater than 30% of the global clinically obese cases. In 2000, 19.8% of adults in the United States were clinically obese, a 61% increase from 1991 [2]. Childhood obesity is also on the rise, with an estimated 20 million cases worldwide. Obesity can lead to life-threatening chronic diseases such as type 2 diabetes, hypertension, dyslipidemia, stroke, cancer, and cardiovascular disease. The World Health Organization estimates 154 million adult diabetic cases worldwide in 2000, rising to 300 million by 2025 [3]. In fact, for every one kilogram increase in weight, the risk of diabetes increases by 4.5% [4].

Obesity is characterized by adipocyte hypertrophy and hyperplasia. Adipocytes are a major component of adipose tissue, in addition to collagen fibers, blood vessels, fibroblasts, and immune cells. Adipocytes are adept at storing triacylglycerol during caloric excess and making available the energy reserve during times when available stores do not meet the body's requirement. Unlike other organs, white adipose tissue is distributed in various parts of the body, broadly categorized as subcutaneous and visceral, as well as other organs such as lymph nodes and skeletal muscle. Until the discovery of leptin in 1994 [5], adipose tissue was thought to be a passive organ primarily involved in the simple function of fat storage, thermal insulation, and organ protection. Now, adipose tissue is known to be involved in a complex network of endocrine, paracrine, and autocrine signals that influences the functions of many tissues, including hypothalamus, pancreas, liver, skeletal muscle, and the immune system [6]. In fact, white adipose tissue is now thought to be the largest endocrine organ in most humans. In lean individuals with a body mass index between 22 – 23, approximately 10 - 20% of total body weight is adipose tissue. Excess adipose tissue has been shown to increase the risk of coronary heart disease, hypertension, Type 2 diabetes, and even cancer. In fact, adipocytes seem to be at the crossroads of homeostasis, playing a key role in energy balance. When normal adipocytes become engorged with lipids, this can lead to lipid accumulation in other tissues, such a muscle, reducing their ability to function properly, leading to aforementioned diseased states [7].

Within the secretome of adipose tissue, the net release of fatty acids during energy balance deficits is most widely recognized. In recent years, a catalogue of cytokines and chemokines has been discovered, collectively known as adipokines. As of 2007, more than 50 adipokines have been reported [8]. The adipokine that has received the most attention is leptin, once thought to be a possible anti-obesity treatment. Leptin functions as an endocrine signaling molecule between adipose tissue and the hypothalamus, conveying the status of energy stores in the body to the central nervous system [9-10]. Leptin has since been found to have pleiotropic effects, involved in modulating the action of insulin in human hepatic cells [11], reproduction [12], hematopoiesis [13], bone formation [14], blood pressure [15], angiogenesis [16], and immunity [17-18].

Though leptin is not expressed exclusively by adipose tissue, another adipokine, adiponectin, was found to be produced only by adipose tissue [19-20]. Adiponectin has insulin-sensitizing effects by lowering the triglyceride content in the muscle and liver of obese mice [21]. Interestingly, plasma concentrations of adiponectin in obese patients were significantly lower

than non-obese patients [22].   With the characterization of leptin and adipokine, a host of adipokines has since been discovered and characterized including apelin, visfatin, zinc-α2-glycoprotein, retinol binding protein-4, resistin, and adipsin to name a few [23-28]. Many of the adipokines were found to have either an insulin-sensitizing or insulin-desensitizing effect. In addition to these adipokines, adipose tissue has also been found to produce traditional cytokines and chemokines such as plasminogen activator inhibitor-1, tumor necrosis factor – α (TNF-α), interleukin-6 (IL-6), IL-1β, IL-8, IL-10, transforming growth factor - β, angiotensinogen, nerve growth factor, macrophage migration inhibitory factor, and monocyte chemoattractant protein-1 [29-31]. In fact, cytokines such as TNF-α and IL-6 are known to be pro-inflammatory. Recently, obesity has been linked with chronic low-grade inflammation of adipose tissue as circulating levels of two inflammatory markers, C-reactive protein (CRP) and fibrinogen, was increased in obese patients. CRP is strongly correlated with body mass index, waist circumference, and adipose body mass [32-33]. This chronic inflammation in adipose tissue has been shown to be associated with insulin resistance [34].

Amine oxidase, copper containing 3 (AOC3) in adipocytes is expressed on the outer surface of the cell membrane, possessing a single-pass transmembrane domain [35]. AOC3 is found as homodimers of between 70 – 90 kDa per subunit that contain two cofactors per subunit, a Cu(II) metal center and a novel redox cofactor. AOC3 catalyzes the oxidative deamination of primary aromatic and aliphatic amines to form hydrogen peroxide, ammonia, and the corresponding aldehyde as shown below:
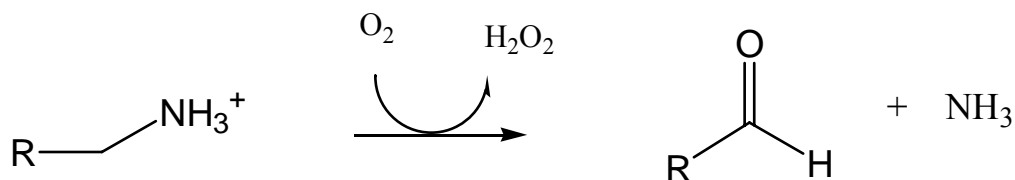
The classes of amine oxidases (AO) were discovered in the 1920's, initially classified by their substrate specificity [36]. This classification scheme proved untenable as amine oxidases were found to have broad substrate specificities, including primary monoamines, diamines, and polyamines.   Two broad groups for classifying AO were later elucidated based on susceptibility to carbonyl reagents (e.g. phenylhydrazine and semicarbazide). Those enzymes that were not susceptible to the carbonyl reagents were later found to contain a flavin coenzyme [37]. The flavin-containing monoamine oxidases exist in two forms, MAO-A and MAO-B, both found in the outer mitochondrial membrane with different substrate specificities [38]. The optimal substrates for MAO-A were found to be neurotransmitters, including serotonin and norepinephrine. MAO-B preferentially oxidized benzylamine, phenylethylamine, and surprisingly the tertiary amine, 1-methyl4-phenyl-1,2,3,6-tetrahydropyridine (MPTP) [39-40].

A novel cofactor for the copper containing amine oxidases susceptible to carbonyl reagents was identified in 1990 to be a post-translationally modified tyrosine, forming a quinonoid structure [41].   The tyrosine was found in the consensus sequence T-X-X-N-**Y**-D/E [42]. With the discovery of topaquinone, the quinone form of 2,4,5-trihidroxyphenylalanine, a new class of redox cofactors derived from post-translational modifications involving tyrosines, lysines, cysteines, and tryptophans have since been identified. The quinone cofactor of methylamine dehydrogenase, an enzyme found in many methylotrophic soil bacteria, was identified to be

tryptophanyltryptophan-quinone (TTQ) in 1991 [43]. The quinone cofactor of lysyl oxidase was found to be derived from a crosslinked lysine and tyrosine (LTQ) in 1996 [44]. In 2001, another member of these novel redox cofactors was found in a novel amine dehydrogenase found in the bacteria, *Pseudomonas putida*. The quinohemoprotein amine dehydrogenase (QH-AmDH) was found to contain two heme groups in addition to the interchain linkage between a cysteine and tryptophanylquinone (CTQ) [45]. These redox cofactors are all involved in the oxidative deamination of amines to produce the corresponding aldehyde, though the fate of the electrons in the case of the dehydrogenases is to reduce a cognate electron acceptor rather than to reduce O_2 to H_2O_2.

The mechanism of amine substrate oxidation by AOC3 and the class of amine oxidases with the TPQ cofactor has been mostly elucidated [46]. TPQ-containing AO display a ping-pong enzymatic mechanism, in which the first product, the aldehyde, is generally released before the second substrate, dioxygen, is added [47]. In the consensus mechanism for the reductive half reaction, the primary amine substrate is oxidized to the corresponding aldehyde and released, generating the reduced aminoquinol form of TPQ. The substrate initially attacks the C-5 position of TPQ through a nucleophilic addition reaction, as opposed to the C-2 and C-4 positions that are resonance stabilized with resulting decrease in electrophilicity [48]. This reaction forms the first stable intermediate, the substrate Schiff base, after the intermediate carbinolamine loses a water through the acquisition of a proton from a protonated active site base. X-ray crystallographic studies of human AOC3 reveal an active site base, aspartate 386, which is involved in a proton abstraction at the substrate C-α position, leading to conversion from substrate Schiff base to product Schiff base [35, 49]. The formation of the product Schiff base involves the transfer of two electrons from the substrate amine to TPQ_{ox}. Finally, hydrolysis of the product Schiff base leads to the release of the aldehyde product and the formation of the aminoquinol and TPQ_{red} as shown in Scheme 1 on the next page.

The mechanism of TPQ_{ox} regeneration to yield the active form of AOC3 in the oxidative half reaction is not as well understood. Overall, O_2 is reduced to hydrogen peroxide via the transfer of two electrons from TPQ_{red}, resulting in the formation of the cofactor iminoquinone. TPQ_{ox} is then recovered after a hydrolysis reaction, resulting in the release of ammonia. Interestingly, the iminoquinone has been shown to be the preferred form of the TPQ_{ox} cofactor in the addition of substrate amine in model systems [50]. The source of debate in the mechanism of the oxidative half reaction involves the nature of the first electron transfer to O_2 [51]. In one possible pathway, the first electron is transferred from TPQ_{red} to Cu(II), forming the semiquinone radical form of TPQ and Cu(I). Dioxygen then rapidly combine with Cu(I), forming Cu(II) superoxide before the second electron is transferred with two protons, producing H_2O_2 [52]. In an alternate mechanism, O_2 binds to a hydrophobic pocket within the enzyme, adjacent to the copper metal center. An electron is directly transferred from TPQ to O_2, with the copper center serving to stabilize the superoxide to form the same Cu (II) superoxide intermediate [53-54]. The six electron oxidation of tyrosine to TPQ relying exclusively on O_2 and a Cu(II) metal center without the need of another enzyme is also another area of active research [55]. Interestingly, the Cu metal center is involved in both the biogenesis of TPQ and the oxidative half reaction though its role in these two reactions may be quite distinct.

Though the enzymatic mechanism of AOC3 has been well characterized, its physiological role in mammals, notably humans, is still currently unknown. AOC3 is found in all living aerobic organisms including bacteria, yeast, plants, and animals with few exceptions such as *Saccharomyces cerevisiae*. In bacteria and yeast, AOC3 is thought to be involved in providing a

4

Scheme 1: Reductive half reaction of AOC3
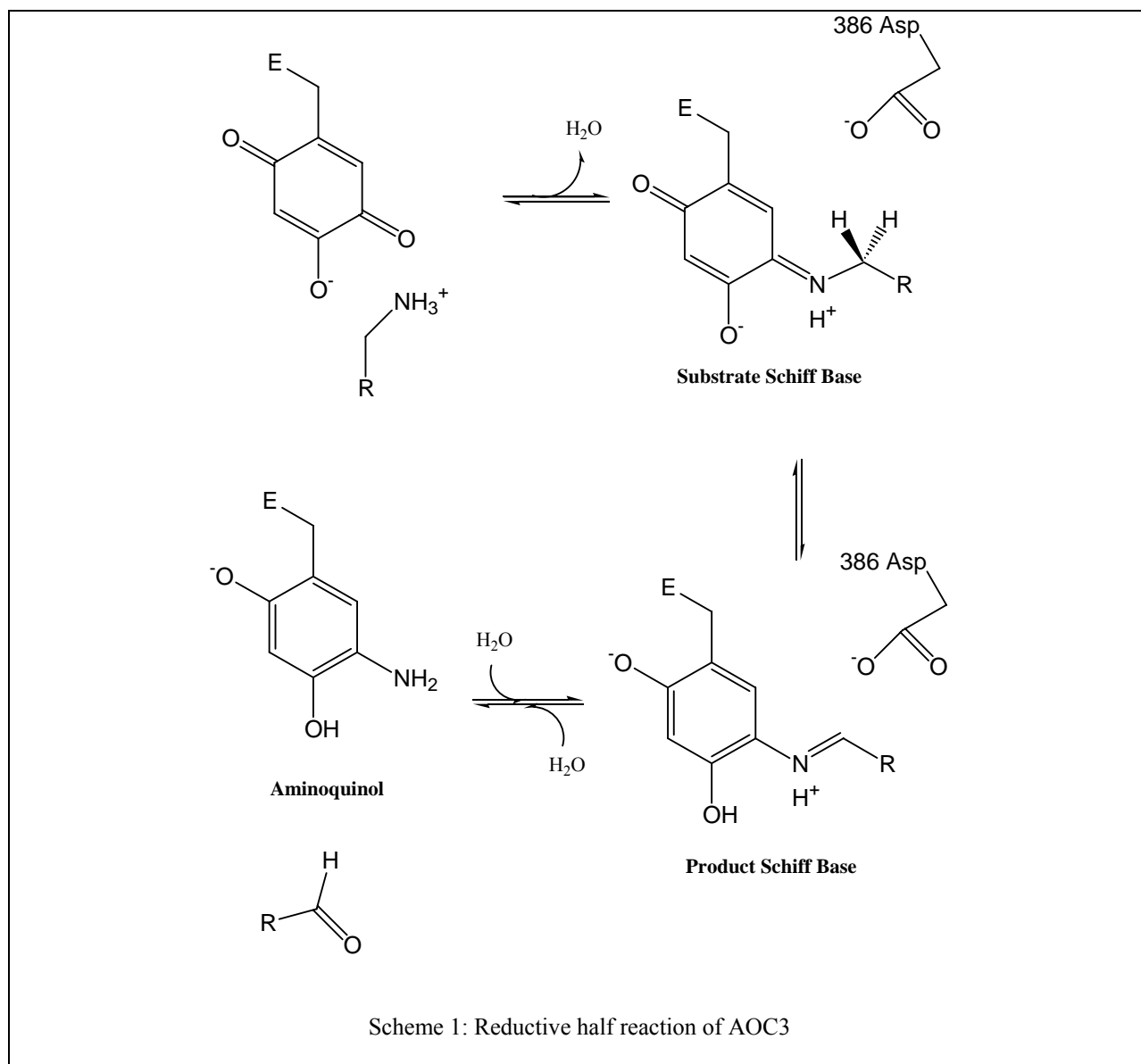
nitrogen and carbon source for the microbes. AOC3 is the most abundant soluble protein found in the extracellular fluids of pea, lentil, and chickpea seedlings [56]. Upon wounding, AOC3 mRNA levels have been found to rapidly increase and thought to be involved in the repair process after injury [57]. In addition, the H_2O_2 formed by AOC3 is thought to be involved in cross-linking structural proteins in the cell wall to strengthen the plant's defenses after mechanical damage or pathogen challenge [58]. Notably another amine oxidase, lysyl oxidase (LO), an enzyme with the LTQ cofactor, is expressed extracellularly and is also involved in a cross-linking reaction. The human LO enzyme is involved in the stabilization of collagen and elastin in the extracellular space by oxidizing specific lysine residues to peptidyl α-aminoadipic-δ-semialdehyde (AAS). These aldehyde groups can then form covalent cross-links with another peptidyl aldehyde group or the ε-amino group of lysine [59-60]. LO does differ from plant AOC3 in that the cross-linking is a direct result of the enzymatic reaction, where the cross-linking in plants is indirect, through the production of H_2O_2.

In mammals, the physiological role of AOC3 was initially thought to be involved in the metabolism of xenobiotic and endogenously produced amines. However, the natural substrate(s) for AOC3 *in vivo* is still currently unknown. The distribution of AOC3 in mammals is also wide-ranging with the first demonstrated site of high enzymatic activity being in bovine and rabbit aorta [61]. The localization of AOC3 in the vasculature has since been extended to humans. The AOC3 in vasculature was thought to be predominantly in smooth muscle cells, though there is also expression in endothelial cells [62]. In human tissues, the specific activity of AOC3, correcting for MAO contribution, was highest in aorta (338 pmol/min/mg). Lung, duodenum, and vena cava also showed activity (86-133 pmol/min/mg), though at a lower level, while the kidney, adrenal, heart, liver, pancreas, spleen, and thyroid were found to have much less activity (< 54 pmol/min/mg) [63]. From a cellular perspective in mammals, AOC3 was found to be highly expressed in vascular and nonvascular smooth muscle cells, adipocytes, endothelial cells, and dendritic cells [64]. In fact, AOC3 has been shown to comprise of up to 2.3% of the total plasma membrane proteins in rat adipocytes [65]. In contrast, AOC3 appears to be absent in leukocytes, epithelial, fibroblasts, and nerve cells. To complicate the matter further, AOC3 is not only localized to the plasma membrane of cells, known as membrane-bound AOC3, but also exists as a soluble enzyme in plasma. Membrane-bound and plasma AOC3 most likely have different physiological roles, with the plasma portion contributing to vascular endothelial damage leading to cardiac diseases and congestive heart failure [66-67], both type 1 and type 2 diabetes [68], Alzheimer's [69], and liver disorders [70]. Recently, the membrane-bound AOC3 has been implicated in the enhancement of tumor growth by supporting neoangiogenesis [71]. The origin of plasma AOC3 is thought to be exclusively derived from a membrane-bound source though the exact cellular or tissue source could be endothelium and/or adipocytes [72-73]. With such a wide tissue distribution in mammals, it is unknown whether a common physiological role will be found for AOC3. It is more likely that AOC3 has disparate roles in each cellular and tissue context. For example, AOC3 expressed in smooth muscle and adipocytes do not bind lymphocytes, whereas endothelial AOC3 has been shown to be involved in adhesion [74]. Surprisingly, the size of AOC3 in these cell types has also been shown to differ though the cDNA is the same. A trimeric form of AOC3 (~250kDa) has been shown to be expressed in smooth muscle cells [75]. Mammalian AOC3 is heavily glycosylated with three putative O-linked and six potential N-linked glycosylation sites per monomer. Differences in glycosylation in each cell type could explain the disparate physiological roles of AOC3. In X-ray crystallographic studies of the human AOC3 expressed in human embryonic kidney (HEK293) cells, carbohydrate moieties were found at five of the six N-glycosylation sites [49]. Carbohydrates attached to Asn232 were found to flank the active site, possibly affecting substrate specificity. In contrast, all six N-linked glycosylation sites were filled in rat endothelial Ax cells.

One possible role of AOC3 expressed on endothelial cells is its involvement in the extravasation of leukocytes into inflamed tissue [76]. The immune system must produce a population of lymphocytes able to recognize foreign antigens anywhere in the body. In order to patrol the body for infection, lymphocytes recirculate continuously from blood to tissue and vice versa, often several times a day. This recirculation is not random and depends on an array of adhesion molecules expressed on lymphocytes and vascular endothelial cells, chemokines, and cytokines. During cases of tissue inflammation, lymphocytes and cells of the innate immune system, such as monocytes and polymorphonuclear leukocytes, rapidly accumulate. The active recruitment of leukocytes into inflamed tissue has been separated into five possibly

overlapping steps, tethering, rolling, activation, firm adhesion, and transmigration [77]. The kinetics of each step can vary from seconds, as in the case of activation, to minutes, as in the case of firm adhesion [78]. By producing monoclonal antibodies to human synovial vessels, Salmi and Jalkenen found that one of the antibodies strongly stained endothelial venules in immunohistological studies and also inhibited lymphocyte binding [75]. This monoclonal antibody was found to recognize AOC3. In addition, induction of AOC3 expression and translocation to the luminal surface of blood vessels occurred under inflammatory conditions [79-80]. Interestingly, in cases when AOC3 enzymatic activity is abolished either by inhibitor or by site-directed mutagenesis of catalytically important tyrosine to phenylalanine, the recruitment of leukocytes was impaired in *in vitro* flow chamber assays using human umbilical vein endothelial cells [81]. Therefore, the enzymatic activity of AOC3 seems to be vital in its adhesive properties. In an important study of the role of AOC3 in leukocyte recruitment, an AOC3 knockout mouse was generated. The knockout mice were found to be healthy, maintained normal body weight, fertile, and had normal life spans when grown in a specific pathogen free environment [76]. The absolute number of leukocytes was also similar to wildtype, though lymphocyte numbers in lymphoid organs were decreased in the knockout. In the knockout mouse, the rolling velocity of polymorphonuclear leukocytes (PMN) was found to be about five times faster compared to wildtype, although the aggregate number of rolling PMNs remained the same. The efficiency of firm adhesion was also found to be 3.2 times higher in wildtype vs. knockout [76]. AOC3 seems to be involved in the rolling and firm adhesion of leukocyte recruitment into inflamed tissue, with possible involvement in transmigration, as efficiency of transmigration was reduced by 47% in knockout mice though this could be due in part to fewer leukocytes firmly adhered to the vascular endothelium. Further studies suggest that AOC3 may also be involved in the normal redistribution of immune cells between tissue and blood. Finally, knockout mice challenged with virulent *Yersinia enterocolitica* serotype O:8 by inoculation intragastrically were not more prone to death in comparison with wildtype, suggesting absence of AOC3 did not impair response to microbial infection. However, with the evidence of AOC3 involvement in leukocyte recruitment, there is no evidence that it has the same function in adipocytes.

A complicating factor to the AOC3 knockout studies is the existence of four copper containing amine oxidases that may compensate for the deletion of AOC3 through genetic redundancy [82-83]. There are four known isomers of copper containing amine oxidases, AOC1 – AOC4. AOC1, also known as diamine oxidase, was originally named histaminase due to its ability to clear histamine [84], a possible function of the enzyme. In humans, AOC1 contains a predicted signal peptide at the N-terminus for the classical secretory pathway and was found to be strongly expressed in the placenta [85], kidney [86], and the gut [87]. AOC1 has broad substrate specificity, involving mostly diamines such as cadaverine, putrescine, and spermidine, but showing very little activity for AOC3 substrates like benzylamine and methylamine [88]. Human AOC2 is a retina-specific amine oxidase, and expression was restricted to retinal ganglion cell layer, containing the optic nerve, suggesting a possible involvement in ocular disorders [89]. AOC4 exhibits high plasma amine oxidase activity in mammals expressing functional enzyme, however both humans and rodents lack a functional AOC4 [90]. Human AOC4 contains a nonsense mutation at position 225, resulting in the nonfunctional enzyme [91]. AOC3 was found to have approximately 38% amino acid identity with AOC1 and a higher 65% identity with AOC2 [92]. AOC3 shares 81% similarity with AOC4 [93]. AOC1 is not thought to be expressed by adipocytes and it is unknown whether AOC2 and AOC4 are expressed by

7

adipocytes, though humans lack a functional AOC4 gene. Unfortunately, the function of AOC2 is also currently unknown.

Since adipose tissue play an important part in energy balance and ultimately homeostasis, a possible role of AOC3 may be an involvement in insulin signaling. Insulin is the major hormone involved in energy balance and storage, regulating the level of glucose available to other organs and optimizing the uptake and storage of "fuels" in circulation [94]. Insulin signaling involves a complicated series of protein kinase cascades, including phosphorylation of insulin receptor substrates (IRS) and activation of lipid kinases, such as phosphatidyl inositol-2 kinase [95]. The resulting secondary signaling molecules are then involved in a diversification of the insulin signal through the activation of a cascade of serine/threonine protein kinases, ultimately leading to the translocation of GLUT4 glucose transporter to the cell membrane, facilitating the uptake of glucose [96]. In addition to skeletal muscle and liver, adipose tissue is also insulin sensitive, with adipocytes expressing the insulin receptor. Insulin has been shown to stimulate the tethering and fusion of GLUT4 vesicles to the plasma membrane of adipocytes [97]. With obesity and both adult- and juvenile-onset diabetes on the rise worldwide, the evidence that insulin resistance is actually initiated in adipose tissue [98] suggests that elucidation of the mechanism behind impaired insulin signaling will be crucial. With reports of the importance of H_2O_2 in the activation of the distal insulin signaling cascade in adipocytes [99], a possible link to AOC3 may have been found. It has been found that insulin exposure elicits a rapid production of H_2O_2, which is thought to enhance insulin signaling by oxidation of the active site cysteine in protein tyrosine phosphatases [100]. Protein tyrosine phosphatases (PTP) are involved in the regulation of the reversible tyrosine phosphorylation in insulin signaling. By inactivating PTPs, insulin signaling is prolonged, allowing key components of the signaling pathway to be in the phosphorylated and active state.

Hydrogen peroxide, as a product of amine oxidation, is a possible link between insulin signaling and AOC3. In fact, acute *in vivo* administration of amine substrates improves glucose tolerance in rats, mice, and rabbits, while long term treatment of diabetic rats with benzylamine or methylamine and vanadate conferred resistance to hyperglycemia. When diabetic rats, exhibiting hyperinsulinemia and hyperglycemia, were administered benzylamine and vanadate intravenously, they showed improvement in glucose tolerance, resembling non-diabetic controls [101-102]. In addition, the presence of catalase along with AOC3 substrates effectively abolished the insulin-sensitizing effects, further implicating the importance of H_2O_2 [103]. Furthermore, if the rats were treated with the AOC3 inhibitor, semicarbazide, both glucose uptake and lipolysis inhibition were found to be impaired [104]. On the other hand, substrates of AOC3 failed to have an insulin-like effect on adipocytes from AOC3 knockout mice [105]. Interestingly, long term exposure of obese rats to the AOC3 inhibitor, semicarbazide, was found to decrease fat deposition due most likely to enhanced lipolysis, though decreased food intake was also observed [106]. It should be noted that, with mounting evidence that H_2O_2 produced upon amine oxidation contributes to insulin signaling, vanadate (not normally present physiologically) is necessary for benzylamine and methylamine to exert their effect, presumably by inhibiting the protein tyrosine phosphatase. In addition, there have been no other reports with regards to how AOC3 may be involved in the insulin signaling cascade. H_2O_2 has increasingly gained recognition as a possible cellular signaling molecule. It is thought to play an important role in cell proliferation, differentiation, migration, and apoptosis [107]. Though AOC3 could be involved in insulin signaling through H_2O_2, other biological responses could also be possible and require investigation. .

Recently, adipose tissue has been found to produce a host of traditional cytokines and chemokines, including TNF-α, IL-6, IL-1β, IL-8, IL-10, TGF-β, MIF, and MCP-1, prompting its designation as an endocrine organ. Cytokines are small signaling proteins that are released by activated cells of the immune system to help regulate both an immune response to infection and inflammation. For example, IL-6 [108], IL-1β [109], and TNF-α [110] are pro-inflammatory cytokines, responsible for inducing a set of genes involved in inflammation, innate and adaptive immunity, as well as cell death and survival. On the other hand, TGF-β and IL-10 are thought to have anti-inflammatory effects by inhibiting release of TNF-α, and other pro-inflammatory signals [111]. In addition, MIF and MCP-1 are chemokines, a family of chemotactic factors that control leukocyte function and trafficking [112-114]. Inappropriate activation by chemokines has been implicated in cardiovascular disease, neuroinflammation, cancer, and inflammation due to allergic reactions [115]. With increasing evidence of a leukocyte adhesion and trafficking role for AOC3 in endothelial cells, an investigation into whether AOC3 could also be involved in an immune function in adipocytes was initiated. Interestingly, a direct immune response to infection by an obligate intracellular protozoan, *Toxoplasma gondii*, in 3T3-L1 adipocytes was found to be derived from the formaldehyde and hydrogen peroxide products of AOC3-catalyzed methylamine oxidation [116]. Based on previous experiments in our lab, addition of AOC3 substrates to adipocytes elicited an increase in MCP-1 production, with a correlation to the H_2O_2 product.

Monocyte chemoattractant protein 1, also known as C-C motif ligand 2 (CCL2), is a member of a family of chemokines with two adjacent cysteines located at the N-terminus, acting as a potent chemotactic factor for monocytes [117]. There are four members of this class of chemokines (MCP-1, MCP-2, MCP-3, and MCP-4), with each member able to bind the receptors of at least two members of this family, affecting a different set of target cells, and displaying some overlapping and novel functions *in vitro* [118]. MCP-1 is the best characterized of the group and is produced by a variety of cells, either constitutively or upon induction. It is involved in the recruitment of monocytes into areas of inflammation and is thought to be the main chemokine responsible for monocyte recruitment [119]. Previously, MCP-1 has been implicated in upregulating cell surface expression of adhesion molecules on monocytes [120], providing a link to the adhesive properties of AOC3 in endothelial cells. More recently, obesity has been associated with increased macrophage infiltration into adipose tissue with a concomitant elevation in MCP-1 levels in the plasma of mice [121], as well as the alteration of adipocyte function by MCP-1, leading to insulin resistance [122].

With new insights into adipocyte function, finding the function of a highly expressed ecto-enzyme, AOC3, could help in the understanding of the evolving role that adipose tissue plays in homeostasis, energy balance, and immunity. AOC3 catalyzes the oxidative deamination of primary amines to form the corresponding aldehyde, ammonia, and H_2O_2. One focus is the possible signaling role that the H_2O_2 product may have in adipocytes. However, since AOC3 is expressed on the extracellular surface of adipocytes, in order for H_2O_2 to have an intracellular signaling role, it most likely must first pass through the cell membrane, though other signaling routes may be possible such as oxidation of extracellular lipids. The ability for H_2O_2 to pass through the cell membrane of adipocytes was explored using a sensitive fluorescent intracellular probe. Currently, the endogenous substrate(s) of AOC3 is also unknown and a complete substrate kinetic profile has yet to be published. Finding the k_{cat} and K_m of various substrates, ranging from aliphatic to aromatic amines and including peptide-based amines, could provide insight into the characteristics of the endogenous substrate(s). To pursue this, a new purification

method for human AOC3 was developed, and substrate kinetics were determined by measuring oxygen consumption using an O_2 electrode. With a possible link to immunity, a role of AOC3 in cytokine release by adipocytes, mediated through H_2O_2 production, was also investigated using cell-based assays, enzyme-linked immunosorbent assay (ELISA), and chemotaxis assays. These cell-based assays are complicated by the need to introduce inhibitors of AOC3 as a control. Bone marrow mesenchymal stem cells (MSC) can be differentiated into cartilage, bone, and adipocytes [123]. With enrichment of MSC from AOC3 knockout mice, it would be possible to differentiate these stem cells into adipocytes that do not express AOC3, eliminating the need for inhibitor controls. It is hoped that these approaches will provide a clue to the role of the highly expressed ectoenzyme, AOC3, found in adipocytes.

References

1. Allison, D.B., et al., *Annual deaths attributable to obesity in the United States.* JAMA, 1999. **282**(16): p. 1530-8.
2. Mokdad, A.H., et al., *The spread of the obesity epidemic in the United States, 1991-1998.* JAMA, 1999. **282**(16): p. 1519-22.
3. Kumanyika, S., et al., *Obesity prevention: the case for action.* Int J Obes Relat Metab Disord, 2002. **26**(3): p. 425-36.
4. Ford, E.S., D.F. Williamson, and S. Liu, *Weight change and diabetes incidence: findings from a national cohort of US adults.* Am J Epidemiol, 1997. **146**(3): p. 214-22.
5. Zhang, Y., et al., *Positional cloning of the mouse obese gene and its human homologue.* Nature, 1994. **372**(6505): p. 425-32.
6. Fruhbeck, G., et al., *The adipocyte: a model for integration of endocrine and metabolic signaling in energy metabolism regulation.* Am J Physiol Endocrinol Metab, 2001. **280**(6): p. E827-47.
7. Rajala, M.W. and P.E. Scherer, *Minireview: The adipocyte - At the crossroads of energy homeostasis, inflammation, and atherosclerosis.* Endocrinology, 2003. **144**(9): p. 3765-3773.
8. Trayhurn, P. and I.S. Wood, *Adipokines: inflammation and the pleiotropic role of white adipose tissue.* Br J Nutr, 2004. **92**(3): p. 347-55.
9. Margetic, S., et al., *Leptin: a review of its peripheral actions and interactions.* Int J Obes Relat Metab Disord, 2002. **26**(11): p. 1407-33.
10. Friedman, J.M. and J.L. Halaas, *Leptin and the regulation of body weight in mammals.* Nature, 1998. **395**(6704): p. 763-70.
11. Cohen, B., D. Novick, and M. Rubinstein, *Modulation of insulin activities by leptin.* Science, 1996. **274**(5290): p. 1185-8.
12. Chehab, F.F., M.E. Lim, and R. Lu, *Correction of the sterility defect in homozygous obese female mice by treatment with the human recombinant leptin.* Nat Genet, 1996. **12**(3): p. 318-20.
13. Cioffi, J.A., et al., *Novel B219/OB receptor isoforms: possible role of leptin in hematopoiesis and reproduction.* Nat Med, 1996. **2**(5): p. 585-9.
14. Ducy, P., et al., *Leptin inhibits bone formation through a hypothalamic relay: A central control of bone mass.* Cell, 2000. **100**(2): p. 197-207.
15. Fruhbeck, G., *Pivotal role of nitric oxide in the control of blood pressure after leptin administration.* Diabetes, 1999. **48**(4): p. 903-908.
16. Sierra-Honigmann, M.R., et al., *Biological action of leptin as an angiogenic factor.* Science, 1998. **281**(5383): p. 1683-1686.
17. Lord, G.M., et al., *Leptin modulates the T-cell immune response and reverses starvation-induced immunosuppression.* Nature, 1998. **394**(6696): p. 897-901.
18. Matarese, G., S. Moschos, and C.S. Mantzoros, *Leptin in immunology.* J Immunol, 2005. **174**(6): p. 3137-42.
19. Hu, E., P. Liang, and B.M. Spiegelman, *AdipoQ is a novel adipose-specific gene dysregulated in obesity.* Journal of Biological Chemistry, 1996. **271**(18): p. 10697-10703.
20. Scherer, P.E., et al., *A Novel Serum-Protein Similar to C1q, Produced Exclusively in Adipocytes.* Journal of Biological Chemistry, 1995. **270**(45): p. 26746-26749.
21. Yamauchi, T., et al., *The fat-derived hormone adiponectin reverses insulin resistance associated with both lipoatrophy and obesity.* Nature Medicine, 2001. **7**(8): p. 941-946.
22. Arita, Y., et al., *Paradoxical decrease of an adipose-specific protein, adiponectin, in obesity.* Biochemical and Biophysical Research Communications, 1999. **257**(1): p. 79-83.
23. Boucher, J., et al., *Apelin, a newly identified adipokine up-regulated by insulin and obesity.* Endocrinology, 2005. **146**(4): p. 1764-1771.
24. Fukuhara, A., et al., *Visfatin: A protein secreted by visceral fat that mimics the effects of insulin (Retracted article, see vol 318, pg 565, 2007).* Science, 2005. **307**(5708): p. 426-430.
25. Sanchez, L.M., A.J. Chirino, and P.J. Bjorkman, *Crystal structure of human ZAG, a fat-depleting factor related to MHC molecules.* Science, 1999. **283**(5409): p. 1914-1919.
26. Yang, Q., et al., *Serum retinol binding protein 4 contributes to insulin resistance in obesity and type 2 diabetes.* Nature, 2005. **436**(7049): p. 356-362.
27. Steppan, C.M., et al., *The hormone resistin links obesity to diabetes.* Nature, 2001. **409**(6818): p. 307-312.

28. White, R.T., et al., *Human Adipsin Is Identical to Complement Factor-D and Is Expressed at High-Levels in Adipose-Tissue.* Journal of Biological Chemistry, 1992. **267**(13): p. 9210-9213.

29. Mohamed-Ali, V., J.H. Pinkney, and S.W. Coppack, *Adipose tissue as an endocrine and paracrine organ.* International Journal of Obesity, 1998. **22**(12): p. 1145-1158.

30. Ahima, R.S. and J.S. Flier, *Adipose tissue as an endocrine organ.* Trends in Endocrinology and Metabolism, 2000. **11**(8): p. 327-332.

31. Trayhurn, P., *Endocrine and signalling role of adipose tissue: new perspectives on fat.* Acta Physiologica Scandinavica, 2005. **184**(4): p. 285-293.

32. Festa, A., et al., *The relation of body fat mass and distribution to markers of chronic inflammation.* Int J Obes Relat Metab Disord, 2001. **25**(10): p. 1407-15.

33. Yudkin, J.S., et al., *C-reactive protein in healthy subjects: associations with obesity, insulin resistance, and endothelial dysfunction: a potential role for cytokines originating from adipose tissue?* Arterioscler Thromb Vasc Biol, 1999. **19**(4): p. 972-8.

34. Xu, H., et al., *Chronic inflammation in fat plays a crucial role in the development of obesity-related insulin resistance.* J Clin Invest, 2003. **112**(12): p. 1821-30.

35. Airenne, T.T., et al., *Crystal structure of the human vascular adhesion protein-1: unique structural features with functional implications.* Protein Sci, 2005. **14**(8): p. 1964-74.

36. Roulet, F. and E.A. Zeller, *Uber Die Diamin-Oxydase Der Smegmabazillen.* Helvetica Chimica Acta, 1945. **28**(6): p. 1326-1342.

37. Kapeller-Adler, R., *Amine oxidases and methods for their study.* 1970, New York,: Wiley-Interscience. xi, 319 p.

38. Singer, T.P. and R.R. Ramsay, *Flauoprotein structure and mechanism 2. Monoamine oxidases: old friends hold many surprises.* Faseb Journal, 1995. **9**(8): p. 605-10.

39. Chiba, K., A. Trevor, and N. Castagnoli, Jr., *Metabolism of the neurotoxic tertiary amine, MPTP, by brain monoamine oxidase.* Biochem Biophys Res Commun, 1984. **120**(2): p. 574-8.

40. Salach, J.I., et al., *Oxidation of the neurotoxic amine 1-methyl-4-phenyl-1,2,3,6-tetrahydropyridine (MPTP) by monoamine oxidases A and B and suicide inactivation of the enzymes by MPTP.* Biochem Biophys Res Commun, 1984. **125**(2): p. 831-5.

41. Janes, S.M., et al., *A new redox cofactor in eukaryotic enzymes: 6-hydroxydopa at the active site of bovine serum amine oxidase.* Science, 1990. **248**(4958): p. 981-7.

42. Janes, S.M., et al., *Identification of topaquinone and its consensus sequence in copper amine oxidases.* Biochemistry, 1992. **31**(48): p. 12147-54.

43. McIntire, W.S., et al., *A new cofactor in a prokaryotic enzyme: tryptophan tryptophylquinone as the redox prosthetic group in methylamine dehydrogenase.* Science, 1991. **252**(5007): p. 817-24.

44. Wang, S.X., et al., *A crosslinked cofactor in lysyl oxidase: redox function for amino acid side chains.* Science, 1996. **273**(5278): p. 1078-84.

45. Vandenberghe, I., et al., *The covalent structure of the small subunit from Pseudomonas putida amine dehydrogenase reveals the presence of three novel types of internal cross-linkages, all involving cysteine in a thioether bond.* Journal of Biological Chemistry, 2001. **276**(46): p. 42923-31.

46. Mure, M., S.A. Mills, and J.P. Klinman, *Catalytic mechanism of the topa quinone containing copper amine oxidases.* Biochemistry, 2002. **41**(30): p. 9269-78.

47. Taylor, C.E., et al., *A catalytic mechanism for the enzyme benzylamine oxidase from pig plasma.* Biochem J, 1972. **130**(3): p. 713-28.

48. Wilmot, C.M., et al., *Catalytic mechanism of the quinoenzyme amine oxidase from Escherichia coli: exploring the reductive half-reaction.* Biochemistry, 1997. **36**(7): p. 1608-20.

49. Jakobsson, E., et al., *Structure of human semicarbazide-sensitive amine oxidase/vascular adhesion protein-1.* Acta Crystallogr D Biol Crystallogr, 2005. **61**(Pt 11): p. 1550-62.

50. Mure, M. and J.P. Klinman, *Model Studies of Topaquinone-Dependent Amine Oxidases .2. Characterization of Reaction Intermediates and Mechanism.* Journal of the American Chemical Society, 1995. **117**(34): p. 8707-8718.

51. Welford, R.W.D., et al., *Partial conversion of Hansenula polymorpha amine oxidase into a "Plant" amine oxidase: Implications for copper chemistry and mechanism.* Biochemistry, 2007. **46**(38): p. 10817-10827.

52. Dooley, D.M., et al., *A Cu(I)-Semiquinone State in Substrate-Reduced Amine Oxidases.* Nature, 1991. **349**(6306): p. 262-264.

53. Goto, Y. and J.P. Klinman, *Binding of dioxygen to non-metal sites in proteins: exploration of the importance of binding site size versus hydrophobicity in the copper amine oxidase from Hansenula polymorpha.* Biochemistry, 2002. **41**(46): p. 13637-43.

54. Su, Q. and J.P. Klinman, *Probing the mechanism of proton coupled electron transfer to dioxygen: the oxidative half-reaction of bovine serum amine oxidase.* Biochemistry, 1998. **37**(36): p. 12513-25.

55. Dooley, D.M., *Structure and biogenesis of topaquinone and related cofactors.* J Biol Inorg Chem, 1999. **4**(1): p. 1-11.

56. Slocum, R.D. and H.E. Flores, *Biochemistry and physiology of polyamines in plants.* 1991, Boca Raton: CRC Press. 264 p.

57. Rea, G., et al., *Developmentally and wound-regulated expression of the gene encoding a cell wall copper amine oxidase in chickpea seedlings.* Febs Letters, 1998. **437**(3): p. 177-182.

58. Mehdy, M.C., *Active Oxygen Species in Plant Defense against Pathogens.* Plant Physiol, 1994. **105**(2): p. 467-472.

59. Kagan, H.M. and W. Li, *Lysyl oxidase: properties, specificity, and biological roles inside and outside of the cell.* Journal of Cellular Biochemistry, 2003. **88**(4): p. 660-72.

60. Lucero, H.A. and H.M. Kagan, *Lysyl oxidase: an oxidative enzyme and effector of cell function.* Cell Mol Life Sci, 2006. **63**(19-20): p. 2304-16.

61. Rucker, R.B. and B.L. O'Dell, *Connective tissue amine oxidase. I. Purification of bovine aorta amine oxidase and its comparison with plasma amine oxidase.* Biochim Biophys Acta, 1971. **235**(1): p. 32-43.

62. Lyles, G.A. and I. Singh, *Vascular smooth muscle cells: a major source of the semicarbazide-sensitive amine oxidase of the rat aorta.* J Pharm Pharmacol, 1985. **37**(9): p. 637-43.

63. Andres, N., et al., *Tissue activity and cellular localization of human semicarbazide-sensitive amine oxidase.* J Histochem Cytochem, 2001. **49**(2): p. 209-17.

64. Jalkanen, S. and M. Salmi, *Cell surface monoamine oxidases: enzymes in search of a function.* EMBO J, 2001. **20**(15): p. 3893-901.

65. Morris, N.J., et al., *Membrane amine oxidase cloning and identification as a major protein in the adipocyte plasma membrane.* Journal of Biological Chemistry, 1997. **272**(14): p. 9388-92.

66. Boomsma, F., et al., *Plasma semicarbazide-sensitive amine oxidase (SSAO) is an independent prognostic marker for mortality in chronic heart failure.* Eur Heart J, 2000. **21**(22): p. 1859-63.

67. Boomsma, F., et al., *Plasma semicarbazide-sensitive amine oxidase is elevated in patients with congestive heart failure.* Cardiovascular Research, 1997. **33**(2): p. 387-391.

68. Boomsma, F., et al., *Circulating semicarbazide-sensitive amine oxidase is raised both in Type I (insulin-dependent), in Type II (non-insulin-dependent) diabetes mellitus and even in childhood Type I diabetes at first clinical diagnosis.* Diabetologia, 1999. **42**(2): p. 233-237.

69. Ferrer, I., et al., *Overexpression of semicarbazide sensitive amine oxidase in the cerebral blood vessels in patients with Alzheimer's disease and cerebral autosomal dominant arteriopathy with subcortical infarcts and leukoencephalopathy.* Neuroscience Letters, 2002. **321**(1-2): p. 21-24.

70. Kurkijarvi, R., et al., *Circulating form of human vascular adhesion protein-1 (VAP-1): Increased serum levels in inflammatory liver diseases.* Journal of Immunology, 1998. **161**(3): p. 1549-1557.

71. Marttila-Ichihara, F., et al., *Vascular Adhesion Protein-1 Enhances Tumor Growth by Supporting Recruitment of Gr-1(+)CD11b(+) Myeloid Cells into Tumors.* Cancer Research, 2009. **69**(19): p. 7875-7883.

72. Stolen, C.M., et al., *Origins of serum semicarbazide-sensitive amine oxidase.* Circulation Research, 2004. **95**(1): p. 50-57.

73. Abella, A., et al., *Adipocytes release a soluble form of VAP-1/SSAO by a metalloprotease-dependent process and in a regulated manner.* Diabetologia, 2004. **47**(3): p. 429-438.

74. Maula, S.M., et al., *Carbohydrates located on the top of the "cap" contribute to the adhesive and enzymatic functions of vascular adhesion protein-1.* European Journal of Immunology, 2005. **35**(9): p. 2718-2727.

75. Jaakkola, K., et al., *Human vascular adhesion protein-1 in smooth muscle cells.* American Journal of Pathology, 1999. **155**(6): p. 1953-1965.

76. Salmi, M. and S. Jalkanen, *A 90-Kilodalton Endothelial-Cell Molecule Mediating Lymphocyte Binding in Humans.* Science, 1992. **257**(5075): p. 1407-1409.

77. Stolen, C.M., et al., *Absence of the endothelial oxidase AOC3 leads to abnormal leukocyte traffic in vivo.* Immunity, 2005. **22**(1): p. 105-115.

78. Butcher, E.C. and L.J. Picker, *Lymphocyte homing and homeostasis.* Science, 1996. **272**(5258): p. 60-66.

79. Salmi, M., K. Kalimo, and S. Jalkanen, *Induction and Function of Vascular Adhesion Protein-1 at Sites of Inflammation.* Journal of Experimental Medicine, 1993. **178**(6): p. 2255-2260.

80. Jaakkola, K., et al., *In vivo detection of vascular adhesion protein-1 in experimental inflammation.* American Journal of Pathology, 2000. **157**(2): p. 463-471.

81. Koskinen, K., et al., *Granulocyte transmigration through the endothelium is regulated by the oxidase activity of vascular adhesion protein-1 (VAP-1).* Blood, 2004. **103**(9): p. 3388-3395.

82. Perez, P., S.A. Lira, and R. Bravo, *Overexpression of Rela in Transgenic Mouse Thymocytes - Specific Increase in Levels of the Inhibitor Protein I-Kappa-B-Alpha.* Molecular and Cellular Biology, 1995. **15**(7): p. 3523-3530.

83. Kafri, R., M. Springer, and Y. Pilpel, *Genetic Redundancy: New Tricks for Old Genes.* Cell, 2009. **136**(3): p. 389-392.

84. Best, C.H. and E.W. McHenry, *The inactivation of histamine.* Journal of Physiology-London, 1930. **70**(4): p. 349-372.

85. Elmore, B.O., J.A. Bollinger, and D.M. Dooley, *Human kidney diamine oxidase: heterologous expression, purification, and characterization.* Journal of Biological Inorganic Chemistry, 2002. **7**(6): p. 565-579.

86. Chassande, O., et al., *Human Gene for Diamine Oxidase, an Amiloride Binding-Protein - Molecular-Cloning, Sequencing, and Characterization of the Promoter.* Journal of Biological Chemistry, 1994. **269**(20): p. 14484-14489.

87. Bieganski, T., et al., *Distribution and Properties of Human Intestinal Diamine Oxidase and Its Relevance for the Histamine Catabolism.* Biochimica Et Biophysica Acta, 1983. **756**(2): p. 196-203.

88. McGrath, A.P., et al., *Structure and Inhibition of Human Diamine Oxidase.* Biochemistry, 2009. **48**(41): p. 9810-9822.

89. Imamura, Y., et al., *Human retina-specific amine oxidase: Genomic structure of the gene (AOC2), alternatively spliced variant, and mRNA expression in retina.* Genomics, 1998. **51**(2): p. 293-298.

90. Schwelberger, H.G., *The origin of mammalian plasma amine oxidases.* Journal of Neural Transmission, 2007. **114**(6): p. 757-762.

91. McGrath, A.P., et al., *A new crystal form of human diamine oxidase.* Acta Crystallographica Section F-Structural Biology and Crystallization Communications, 2010. **66**: p. 137-142.

92. Zhang, Q., et al., *Characterization of AOC2 gene encoding a copper-binding amine oxidase expressed specifically in retina.* Gene, 2003. **318**: p. 45-53.

93. Cronin, C.N., et al., *cDNA cloning of two splice variants of a human copper-containing monoamine oxidase pseudogene containing a dimeric Alu repeat sequence.* Gene, 1998. **220**(1-2): p. 71-76.

94. Avruch, J., *Insulin signal transduction through protein kinase cascades.* Molecular and Cellular Biochemistry, 1998. **182**(1-2): p. 31-48.

95. White, M.F. and C.R. Kahn, *The Insulin Signaling System.* Journal of Biological Chemistry, 1994. **269**(1): p. 1-4.

96. Chang, L., S.H. Chiang, and A.R. Saltiel, *Insulin signaling and the regulation of glucose transport.* Molecular Medicine, 2004. **10**(7-12): p. 65-71.

97. Lizunov, V.A., et al., *Insulin stimulates the halting, tethering, and fusion of mobile GLUT4 vesicles in rat adipose cells.* Journal of Cell Biology, 2005. **169**(3): p. 481-489.

98. Smith, U., *Impaired ('diabetic') insulin signaling and action occur in fat cells long before glucose intolerance - is insulin resistance initiated in the adipose tissue?* International Journal of Obesity, 2002. **26**(7): p. 897-904.

99. Mahadev, K., et al., *Hydrogen peroxide generated during cellular insulin stimulation is integral to activation of the distal insulin signaling cascade in 3T3-L1 adipocytes.* Journal of Biological Chemistry, 2001. **276**(52): p. 48662-48669.

100. Wu, X.D., et al., *Hyperglycemia potentiates H2O2 production in adipocytes and enhances insulin signal transduction: Potential role for oxidative inhibition of thiol-sensitive protein-tyro sine phosphatases.* Antioxidants & Redox Signaling, 2005. **7**(5-6): p. 526-537.

101. Carpene, C., et al., *Amine oxidase substrates for impaired glucose tolerance correction.* Journal of Physiology and Biochemistry, 2005. **61**(2): p. 405-419.

102. Iglesias-Osma, M.C., et al., *Methylamine but not mafenide mimics insulin-like activity of the semicarbazide-sensitive amine oxidase-substrate benzylamine on glucose tolerance and on human adipocyte metabolism.* Pharmacological Research, 2005. **52**(6): p. 475-484.

103. Zorzano, A., et al., *Semicarbazide-sensitive amine oxidase activity exerts insulin-like effects on glucose metabolism and insulin-signaling pathways in adipose cells.* Biochimica Et Biophysica Acta-Proteins and Proteomics, 2003. **1647**(1-2): p. 3-9.

104. Visentin, V., et al., *Glucose handling in streptozotocin-induced diabetic rats is improved by tyramine but not by the amine oxidase inhibitor semicarbazide.* European Journal of Pharmacology, 2005. **522**(1-3): p. 139-146.

105. Bour, S., et al., *Semicarbazide-sensitive amine oxidase substrates fail to induce insulin-like effects in fat cells from AOC3 knockout mice.* Journal of Neural Transmission, 2007. **114**(6): p. 829-833.

106. Carpene, C., et al., *Reduction of fat deposition by combined inhibition of monoamine oxidases and semicarbazide-sensitive amine oxidases in obese Zucker rats.* Pharmacological Research, 2007. **56**(6): p. 522-530.

107. Veal, E.A., A.M. Day, and B.A. Morgan, *Hydrogen peroxide sensing and signaling.* Mol Cell, 2007. **26**(1): p. 1-14.

108. Heinrich, P.C., et al., *Principles of interleukin (IL)-6-type cytokine signalling and its regulation.* Biochemical Journal, 2003. **374**: p. 1-20.

109. Kampf, C., et al., *Effects of TNF-alpha, IFN-gamma and IL-beta on normal human bronchial epithelial cells.* European Respiratory Journal, 1999. **14**(1): p. 84-91.

110. Kataoka, T., *Chemical biology of inflammatory cytokine signaling.* Journal of Antibiotics, 2009. **62**(12): p. 655-667.

111. Tsunawaki, S., et al., *Deactivation of Macrophages by Transforming Growth Factor-Beta.* Nature, 1988. **334**(6179): p. 260-262.

112. Rollins, B.J., *Chemokines.* Blood, 1997. **90**(3): p. 909-928.

113. Luster, A.D., *Chemokines - Chemotactic cytokines that mediate inflammation.* New England Journal of Medicine, 1998. **338**(7): p. 436-445.

114. Mackay, C.R., *Chemokines: immunology's high impact factors.* Nature Immunology, 2001. **2**(2): p. 95-101.

115. Gerard, C. and B.J. Rollins, *Chemokines and disease.* Nature Immunology, 2001. **2**(2): p. 108-115.

116. Zhu, S., et al., *Toxicity of derivatives from semicarbazide-sensitive amine oxidase-mediated deamination of methylamine against Toxoplasma gondii after infection of differentiated 3T3-L1 cells.* Toxicol In Vitro. **24**(3): p. 809-14.

117. Deshmane, S.L., et al., *Monocyte Chemoattractant Protein-1 (MCP-1): An Overview.* Journal of Interferon and Cytokine Research, 2009. **29**(6): p. 313-326.

118. Van Coillie, E., J. Van Damme, and G. Opdenakker, *The MCP eotaxin subfamily of CC chemokines.* Cytokine & Growth Factor Reviews, 1999. **10**(1): p. 61-86.

119. Ajuebor, M.N., et al., *Endogenous monocyte chemoattractant protein-1 recruits monocytes in the zymosan peritonitis model.* Journal of Leukocyte Biology, 1998. **63**(1): p. 108-116.

120. Jiang, Y.L., et al., *Monocyte Chemoattractant Protein-1 Regulates Adhesion Molecule Expression and Cytokine Production in Human Monocytes.* Journal of Immunology, 1992. **148**(8): p. 2423-2428.

121. Takahashi, K., et al., *Adiposity elevates plasma MCP-1 levels leading to the increased CD11b-positive monocytes in mice.* Journal of Biological Chemistry, 2003. **278**(47): p. 46654-46660.

122. Sartipy, P. and D.J. Loskutoff, *Monocyte chemoattractant protein 1 in obesity and insulin resistance.* Proceedings of the National Academy of Sciences of the United States of America, 2003. **100**(12): p. 7265-7270.

123. Caplan, A.I., *Mesenchymal stem cells.* J Orthop Res, 1991. **9**(5): p. 641-50.

Chapter 2:

Entry of Exogenously Produced H_2O_2 by AOC3 into 3T3-L1 Adipocytes

Introduction

Since the discovery that the reactive nitrogen species (RNS), $NO^{\cdot}$, can activate guanylate cyclase to produce cGMP [1] , investigations have shown reactive oxygen species (ROS) and other RNS play a role in cell signaling. ROS are oxygen species which are more reactive than molecular oxygen, including O_2^{-}, H_2O_2, singlet oxygen, and hydroxyl radical, $OH^{\cdot}$. In addition to $NO^{\cdot}$, RNS includes peroxynitrite ($OONO^{-}$), $NO_2^{\cdot}$, and nitrosil (NO^{+}). Rather than an exclusive involvement in pathological processes, ROS and RNS have steadily become understood to be critical in processes necessary for life. For example, cyclooxygenases require ROS derived hydroperoxides to produce prostaglandins [2], extracellularly generated O_2^{-} can trigger calcium release in endothelial cells [3], and protein tyrosine phosphatases can be irreversibly inactivated by peroxynitrite [4]. In fact, low concentrations of H_2O_2 have been shown to be necessary for cellular proliferation [5].

The production, duration, and termination of signaling molecules must be regulated. Additionally, the signaling molecule must also be specific for its intracellular target. H_2O_2 is one of the byproducts of the oxidation of primary amines by AOC3. Interestingly, from the list of possible ROS generated by the processes of life, H_2O_2 is thought to be the ROS most likely to act as a signaling molecule [6-7] due to its regulated production, for example by NADPH oxidase [8] through the spontaneous or enzyme-catalyzed dismutation of O_2^{-}. The duration and termination of H_2O_2 signaling is also regulated by a vast network of enzymes, including catalases [9], glutathione peroxidases [10], and peroxiredoxins [11-12], which are all involved in H_2O_2 catabolism [13]. Since H_2O_2 is a normal byproduct of aerobic respiration, it is likely found in most or all human cells [14] and this network of enzymes have evolved to regulate its presence. In terms of specificity, the oxidizing potential of H_2O_2 can be exploited in a two-electron nucleophilic substitution reaction with the thiol side chain of cysteines as shown:

$$\text{Cys-RS}^{-} + H_2O_2 \rightarrow \text{Cys-RSOH} + OH^{-} \quad (1)$$

The thiol side chain of cysteine is oxidized to the sulfenic acid. This cysteine sulfenic acid derivative can be formed more favorably if a proton donating group in close proximity allows the hydroxyl group to leave as water and the stabilization of the thiolate by conserved basic residues. Once formed, the oxidized cysteine can be longer lived when protected in an apolar environment, away from reactive molecules, such as proximal Cys-SH groups [15]. In fact, the oxidized cysteine has been detected in cells using antibodies [16] and fluorescent probes [17]. Upon cysteine oxidation by H_2O_2 at the active site, the activity of protein tyrosine phosphatases (PTP) can be inhibited, prolonging protein tyrosine kinase (PTK) signaling [18-20], which is necessary in the initiation of growth factor and insulin signaling. Transcription factor activation or inhibition is usually the end result of signal transduction. Interestingly, there is evidence that transcription factors can be directly activated [21] or inhibited [22] by H_2O_2-induced formation of cysteine sulfenic acid.

One possible physiological function of AOC3 in adipocytes may be the production H_2O_2 as a signaling molecule, serving as a proxy for an amine signal generated extracellularly in the periphery of adipocytes. Primary aliphatic amines are the preferred substrates for mouse and

human AOC3, though primary aromatic amines such as benzylamine and phenethylamine can also be substrates, with benzylamine being one of the best substrates in terms of K_m and k_{cat}/K_m. Methylamine and aminoacetone are also substrates with both present endogenously as a byproduct of amino acid metabolism. Given that the endogenous substrate(s) is/are currently unknown, an extensive study of the substrate profile of human AOC3 will be described in Chapter 3.

In order to have an intracellular signaling role, the H_2O_2 produced by AOC3 in the extracellular space must enter the adipocyte. H_2O_2 was thought to be freely diffusable across the lipid bilayers of cellular membranes since it is a small, uncharged molecule [23]. However, recent reports show that the lipid composition of the membrane is one of the determinants in the permeability of the membrane [24-25]. In fact, H_2O_2 was not found to be freely diffusable in growing *E. coli* [26], mammalian cells [27], and *S. cerevisiae* in stationary phase [28]. These observations imply that the entry of H_2O_2 into cells may be regulated either by the lipid composition of the membrane and/or by the presence or absence of channel proteins allowing diffusion. With the discovery of aquaporins, channel proteins for water which at one time was also thought to diffuse freely across cell membranes, the presence of a H_2O_2 channel protein in cells is also possible. In fact, in addition to water, aquaporins have also been shown to conduct glycerol and other small solutes [29-30]. H_2O_2 possesses almost the same dipole moment, dielectric properties, capacity to form hydrogen bonds as water, and meets certain size restrictions to be able to pass through aquaporins [31]. Specifically for adipocytes, aquaporin 7 was found to conduct glycerol in mice and knockouts exhibited impaired glycerol release upon triglyceride hydrolysis and developed obesity and insulin resistance [32].

Since transport of H_2O_2 across the adipocyte cell membrane is not a foregone conclusion, it is necessary to investigate the membrane permeability of H_2O_2 produced by turnover of amine substrate by AOC3. There have been many studies of intracellular H_2O_2 concentration using a variety of methods, including both fluorescent and chemiluminescent probes offering high detection sensitivity [33-34]. In addition to these chemical probes, a genetically encoded H_2O_2 probe constructed from the regulatory domain of *E. coli* OxyR was found to have a detection limit in HeLa cells of 5 uM H_2O_2 though published results used 50 uM [35]. The maximal extracellular concentration of H_2O_2 generated during signaling is thought to be in the $2-4$ uM range [36]. However due to limited diffusibility and the intracellular consumption of H_2O_2, a peroxide gradient is generated upon external H_2O_2 formation or addition, leading to the observation of an intracellular $[H_2O_2]$ that is one-seventh of a 50 uM bolus added to Jurkat T-cells [37]. For signaling purposes, that would indicate an effective intracellular $[H_2O_2]$ of around 0.5 uM [38], making the detection limit one of the most important characteristics of a H_2O_2 signaling probe.

Due to the poor detection efficiency of the genetic probe and complexity of introducing the probe into cells, an approach involving chemical probes was sought, preferably with detection of very low $[H_2O_2]$ and desirable properties for live cell analysis, including ease of use, high sensitivity, simplicity in data collection, and high spatial resolution using microscopic imaging techniques. Dichlorodihydrofluorescein (DCFH) is one of the most popular probes used to detect H_2O_2. However, DCFH is a member of a family of reduced redox probes, including dihydro-rhodamines, Amplex Red, and hydroethidine, that have been shown to be either photo-oxidizable [39] or photo-reducible [40] without being specific for H_2O_2 [41]. In addition, the oxidation of Amplex Red requires the presence of horseradish peroxidase, making it unfeasible in an intracellular application. Other probes include europium-based luminescent probes with a

detection limit of 1.8 uM [42], diphenylphosphine-based fluorophores [43], and alternatives to reduced probes that exploit the nucleophilic character of H_2O_2. For example, a coumarin-based reporter with a H_2O_2-cleavable protecting group was able to detect H_2O_2 in the 0.1- 5 uM range though at a pH slightly outside of the physiological range (pH 8.3) [44] but with unknown cellular properties such as possible efflux of activated probe from the cell. Another probe relying on deprotection of pentafluorobenzenesulfonyl fluoresceins did not exhibit high specificity for H_2O_2, showing more sensitivity toward O_2^- [45]. These chemical probes suffer from a lack of specificity for H_2O_2 vs. other ROS or RNS, insolubility in aqueous media that makes it incompatible with live cell experiments, the need for excitation in the UV region that can induce cell damage, and unknown intracellular probe loading characteristics.

In addition to the above mentioned characteristics that would make a chemical probe favorable in the detection of H_2O_2, special considerations must be made for live adipocyte experiments. These include facile cellular loading of the probe and prevention of probe leakage from the cell after activation, high reactivity at low H_2O_2 concentrations, nontoxicity, and absence of unwanted metabolism. Peroxyfluor-1 (PF1) is a water-soluble and specific H_2O_2 probe based on deprotection of arylboronates to phenols by H_2O_2 to generate the fluorescent fluorescein product and has been evaluated in live HEK293T cells [46]. Fluorescein (and its derivatives) is one of the most commonly used fluorescent probes applied to live cell imaging experiments [47]. It has high molar absorptivity at 488 nm, large fluorescent quantum yield, and photo-stability, making it readily detected in live cells using a confocal microscope with an argon laser. PF1 also exhibits a greater than 500-fold higher response to H_2O_2 vs. other ROS and RNS. Additionally, its use in live cell experiments has demonstrated favorable cellular loading without killing the cells, as well as the dominance of the anionic and dianionic fluorescein species at physiological pH (pKa = 4.31, 6.43 [48]), hindering membrane permeability and leakage of activated probe. With these favorable characteristics, PF1 was applied to live adipocytes to detect intracellular H_2O_2 upon incubation with various AOC3 amine substrates.

Methods

Cell Culture of Adipocytes. The differentiation protocol started with a 100 mm tissue culture dish of murine 3T3-L1 fibroblasts obtained from American Type Cell Culture. Cells were grown to confluence 7 days after initial plating. Once confluent, cellular differentiation was induced using insulin, dexamethasone, and methylisobutylxanthine as previously described [49]. Cells were cultured in Dulbecco's Modified Eagle Medium (DMEM) (Invitrogen, Carlsbad, CA) supplemented with 10% Fetal Bovine Serum (FBS) (Hyclone, Waltham, MA). Differentiation takes 8 days. Only passage 1 – 3 differentiated adipocytes were used.

Fluorescence Imaging. Confocal fluorescence imaging was performed on a Zeiss LSM 510 META laser scanning microscopy system containing a Zeiss upright Axioplan microscope and a 63x water-immersion objective at the Berkeley Molecular Imaging Center. Excitation at 488 nm was carried out with an argon laser and emission collected from 500 – 600 nm using META detection system. Excitation at 543 nm was carried out with a HeNe laser and emission collected from 700 – 800 nm using META detection system. Detector gain, amplifier offset, and amplifier gain were normalized so that adipocytes incubated in only PBS buffer resulted in an absence of fluorescence and 100 uM H_2O_2 incubation with PF1 (generously provided by Prof. Christopher Chang, University of California, Berkeley) loading exhibited sharp fluorescence. Prior to imaging experiments involving inhibitor comparisons, cells were washed twice with warm Phosphate Buffered Saline (PBS) (Invitrogen, Carlsbad, CA) and incubated either with or without 100 uM semicarbazide (SC) (Sigma Aldrich, St. Louis, MO) for 30 minutes at 37°C in PBS first. After inhibitor incubation, all adipocytes were incubated with PF1 (5 uM unless stated otherwise in PBS) for 15 minutes to allow intracellular loading at 37°C. Adipocytes were then incubated for at least 2 hours with amine substrates, methylamine , isoamylamine, or benzylamine, (all purchased from Sigma Aldrich, St. Louis, MO) at various concentrations at 37°C before imaging. For images involving exogenous H_2O_2 addition, a bolus of H_2O_2 (2 – 100 uM) was added and incubated at 37°C for 15 minutes prior to imaging. FM464 (Invitrogen, Carlsbad, CA) lipophilic dye was added to adipocytes at 2 ug/mL directly on microscope stage and immediately imaged. For detection of intracellular hydrogen peroxide after exposure to insulin, adipocytes were pretreated with 10 uM DPI (Sigma Aldrich, St. Louis, MO) for 30 minutes at 37°C if NADPH oxidase was inhibited. 100 nM human insulin (Sigma Aldrich, St. Louis, MO) was added to adipocytes and incubated for 5 minutes prior to imaging.

Results

The suitability of PF1 to detect intracellular H_2O_2 in cultured adipocytes was determined by incubating adipocytes with a bolus of various H_2O_2 concentrations. Adipocytes were incubated with H_2O_2 concentrations ranging from 2 uM – 100 uM after preloading the cells with 5 uM PF1 for 15 minutes. In Figure 1A, upon 2 uM H_2O_2 addition, a green fluorescent signal was observed. However, in the overlay with the differential interference contrast (DIC) image on the bottom, the cell with the fluorescent signal does not exhibit the typical adipocyte morphology of lipid laden cells with multiple fat vacuoles. These fluorescent signals were disregarded as the cells may not be fully differentiated adipocytes or adipocytes that were not actively storing lipids and may be in the process of necrosis or apoptosis. Only signals from fully differentiated, lipid laden adipocytes were considered. PF1 does not seem to be able to detect H_2O_2 when 2 uM was introduced exogenously due to the absence of a fluorescent signal inside viable adipocytes. In Figure 1B and 1C, upon 8 uM and 16 uM H_2O_2 incubation respectively, weak fluorescent signals associated with fully differentiated adipocytes can be seen, though this level of fluorescence could be attributed to normal intracellular H_2O_2 production by adipocytes as shown in adipocytes loaded with PF1 but without any exogenous H_2O_2 added (Figure 1F). Upon incubation with 32 uM and 100 uM H_2O_2, noticeable differences in intracellular H_2O_2 can be detected with PF1 as shown in Figure 1D and 1E. It would appear the threshold of detection by PF1 for extracellular H_2O_2 in adipocytes is in the region of 32 uM. This detection limit would not be satisfactory for the detection of intracellular H_2O_2 signaling, which is expected to be below 10 uM. Reactivity of PF1 with H_2O_2 was found to have a pseudo first order rate constant of 5.4×10^{-4} s^{-1}, taking about 90 minutes for 1 uM PF1 to be fully deprotected by 1 mM H_2O_2 [50]. This low reactivity will make the competition for H_2O_2 between PF1 and intracellular peroxidases an important consideration.

Due to slow rate of reaction between PF1 and H_2O_2, adipocytes were incubated with 32 uM H_2O_2 for approximately 3.5 hours to see whether the increase in time will allow the added PF1 to fully react, thus integrating the fluorescent signal over a longer time period. In Figure 2A, images of adipocytes incubated for 3 hours 37 minutes with 32 uM H_2O_2 after 5 uM PF1 preloading show increased fluorescence vs. both adipocytes with only 15 minute of 32 uM H_2O_2 incubation and adipocytes loaded with PF1 without exogenous H_2O_2 addition and incubated for 3 hours 43 minutes (Figure 2B). From the DIC image, there also does not seem to be more adipocyte death due to the longer incubation time. This longer incubation time does seem to allow PF1 to integrate the fluorescent signal, possibly circumventing the detection limit problem, though effectively eliminating detection of signaling as a time-specific event. However, the ability of AOC3-derived H_2O_2 to enter the adipocyte could still be demonstrated using the longer incubation time.

The ability to collect light selectively from only a thin optical slice of the specimen is one of the advantages of confocal microscopy. Since each image arises from the same z-plane of the adipocyte, it is assumed that the PF1 fluorescent signal surrounded by adipocyte cell membrane is intracellular. In an effort to demonstrate this experimentally, FM464, a lipophilic dye selectively labeling plasma membrane, was used to see if the fluorescence from activated PF1 can be shown to be internal to the FM464-labeled plasma membrane. FM464 is water-soluble, nontoxic to cells, and non-fluorescent in aqueous media. The dye is believed to insert into the outer leaflet of the surface membrane where it becomes intensely fluorescent. However, one

drawback is the rapid rate in which the dye is endocytosed, typically within 10 minutes of introduction, thus the need for immediate imaging once the dye is added. Therefore, FM464 dye was always added to cells on the microscope stage with quick gentle mixing after the long incubations. Figure 3A and 3C show the fluorescence images from FM464 and activated PF1 respectively. Figure 3B is a DIC image of the adipocytes, showing that the cells are intact. In Figure 3D, the three images were overlayed, showing that the green fluorescence of activated PF1 is internal to the FM464 labeled plasma membrane. This is a good indication that the activated PF1 is intracellular, within the plasma membrane of the adipocytes and that the exogenously introduced H_2O_2 was able to enter the cell. With this result, it is possible to assume that the fluorescence within the cell arises from PF1 reaction with intracellular H_2O_2.

The ability of the H_2O_2 produced by AOC3 to enter adipocytes was then investigated using the longer incubation time. Isoamylamine, a relatively good substrate of murine AOC3 with K_m = 148 uM and k_{cat}/K_m = 4.9 x 10^3 $M^{-1}s^{-1}$, was added at a concentration of 10 K_m (1.48 mM) to adipocytes. The resulting images were compared to adipocytes that had first been pretreated with 100 uM semicarbazide (SC), an irreversible inhibitor of AOC3 [51] and adipocytes preloaded with PF1 without any amine addition. In comparing Figure 4A and 4B, there does not seem to be a noticeable difference between intracellular H_2O_2 in adipocytes with and without SC addition with substrate incubation for approximately 3 hours. Figure 4C show that there was an observable endogenous level of naturally occurring H_2O_2, though it was lower in intensity than either Figure 4A or 4B. In an effort to reproduce these results using a new set of adipocytes with similar incubation time, comparison between SC-treated and non-SC treated cells resulted in a fluorescence difference as shown in Figure 5A and 5B. In this case, an increase in intracellular H_2O_2 was found in the non-SC adipocytes compared to that of SC-treated adipocytes, though the level of increase was faint. However, this result was very difficult to reproduce and the fluorescence intensity difference does not show a definitive increase in intracellular H_2O_2 due specifically to AOC3 turnover, as naturally occurring H_2O_2 was again observable (Figure 5C), though resulting in low fluorescence intensity.

With addition of isoamylamine, AOC3 expressed by adipocytes produces H_2O_2 continuously vs. the initial characterization studies involving a bolus addition of H_2O_2. Therefore the rate of intracellular H_2O_2 accumulation will depend on the rate of AOC3 turnover, the rate of two deprotections of the PF1 probe by H_2O_2, and the rate H_2O_2 passage through the plasma membrane of the adipocyte. Additional incubation time may allow PF1 to integrate the fluorescent signal as more AOC3-derived H_2O_2 is formed. Therefore, a longer substrate incubation time of approximately 4.5 hours was undertaken. Looking at the DIC images in Figure 6, there do not seem to be more nonviable cells due to the longer incubation time. Comparing Figure 6A and 6B, there appears to be an increase in fluorescence intensity in the cells without SC addition, similar to Figure 5. However, as before, the increase was very difficult to reproduce. Figure 6C does show a slight increase in naturally occurring H_2O_2 vs. the previous sets of cells though apparently lower than the fluorescence seen in Figure 6A. Therefore, even with a longer incubation time, it is not possible to conclude definitively with PF1 that an increase in intracellular H_2O_2 occurs upon AOC3 substrate addition. Unfortunately, incubation times past 4.5 hours resulted in more adipocyte death and imaging experiments couldn't be carried out.

Due to difficulty of seeing an increase in intracellular H_2O_2 in adipocytes even after long substrate incubation times, two other strategies were undertaken. First, an increased PF1 concentration was used. Adipocytes were preloaded with 10 uM instead of 5 uM PF1 and

incubated with an alternate amine substrate, methylamine. Methylamine is produced in physiological settings and is thought to be a possible natural substrate for AOC3. However, methylamine is not as good of a substrate as isoamylamine, with $K_m = 795$ uM and $k_{cat}/K_m = 7.2 \times 10^2 M^{-1} s^{-1}$. Adipocytes were incubated with methylamine for approximately 3.5 hours with either 1.59 mM methylamine (Figure 7A) or 7.95 mM methylamine (Figure 7B). Both images show a dramatic increase in fluorescence as expected. However, this increase was also seen in background fluorescence, when no substrate was added (Figure 7C). Imaging at a higher PF1 concentration resulted in an ability to observe the level of naturally occurring intracellular H_2O_2, but unfortunately this level of H_2O_2 overwhelmed the production of H_2O_2 by AOC3, resulting in high background noise.

In an effort to synthesize a more sensitive probe with a lower detection limit, a second generation PF1 probe was designed to detect endogenous H_2O_2 signaling in which the fluorescein is attached to only one boronated protecting group [52]. The rate of probe (PF2) deprotection is expected to be faster, though its kinetic characteristics are not published, allowing for a more sensitive detection of low intracellular H_2O_2. Treating adipocytes with low levels of exogenous H_2O_2 after PF2 loading, it was difficult to distinguish an increase in fluorescence in adipocytes treated with a bolus of 4 uM H_2O_2 (Figure 8B) vs. background fluorescence of adipocytes loaded with PF2 without H_2O_2 addition (Figure 8A). However, the level of fluorescence was definitely more apparent than adipocytes loaded with PF1 and treated to similar levels of H_2O_2. Upon addition of 8 uM H_2O_2, there does seem to be an increase in fluorescence when compared to both the background and addition of 4 uM H_2O_2 (Figure 8C). This result suggests that it may be possible to detect changes in intracellular H_2O_2 with sub-10 uM sensitivity in adipocytes using PF2. Comparing images after incubating adipocytes with 1.48 mM isoamylamine, the fluorescence intensity between substrate incubation without SC addition (Figure 9A) and with SC addition (Figure 9B) for approximately 3 hours was found to be indistinguishable though there was a high level of intracellular fluorescence. Again, PF2 was able to pick up a significant amount of background fluorescence which overwhelms the signal from AOC3-produced H_2O_2. The same result was found when adipocytes were incubated with 7.95 mM methylamine for approximately 2.5 hours (Figure 10A vs. 10B). PF2 has higher sensitivity toward intracellular H_2O_2. However due to higher level of background fluorescence, the contribution of AOC3-generated H_2O_2 was indistinguishable.

One possible signaling role of H_2O_2 produced by AOC3 turnover expressed by adipocytes is the inhibition of protein tyrosine phosphatases (PTP) that are involved in insulin signaling. Insulin signaling in adipose-like cells was shown to cause a rapid formation of intracellular H_2O_2 and decreased PTP1B activity, a tyrosine phosphatase thought to reverse the phosphorylation of insulin receptor (IR) and insulin receptor substrate (IRS) [53]. Phosphorylation of IR and IRS occur upon binding of insulin to IR. Though it's unknown whether AOC3 and IR co-locate within lipid domains known as caveolae [54], it has been shown that the H_2O_2 produced during insulin stimulation in 3T3-L1 adipocytes is essential to the activation of the insulin signaling cascade [55]. As an attempt to determine whether PF1 is able to detect intracellular H_2O_2 upon insulin receptor stimulation, adipocytes were incubated with 5 uM PF1 for 15 minutes prior to addition of insulin. The H_2O_2 produced during insulin stimulation is a product of NADPH oxidase activation, which can be inhibited with diphenyleneiodonium chloride (DPI) [56]. Adipocytes pretreated with 10 uM DPI for 30 minutes prior to introduction of 100 nM insulin exhibited a lower fluorescence intensity (Figure 11A) vs. adipocytes without DPI pretreatment (Figure 11B red arrow), showing that PF1 is able to detect an increase in intracellular H_2O_2 upon

23

introduction of insulin, though again the increase in intensity was low. However, when adipocytes were supplemented with both insulin and primary amine (either 1.48 mM isoamylamine or 7.95 mM methylamine), there was no significant increase in intracellular H_2O_2 compared to addition of insulin alone after cells were preloaded with PF1 as shown in Figure 11C (red arrow) and 11D.

Discussion

Two different probes were used to investigate whether H_2O_2 produced by adipocytes during AOC3 turnover could act as an intracellular signaling molecule. Both PF1 and PF2 were known to be specific for H_2O_2 vs. other ROS and RNS, soluble in aqueous media, nontoxic to cells, and exhibited intracellular adipocyte loading, as seen from the H_2O_2 incubation studies. Upon characterization with exogenous H_2O_2 addition, PF1 was found to have a detection limit around 32 uM while PF2 was found to have a detection limit around 8 uM in adipocytes. From whole cell kinetic studies in Chapter 3, the adipocytes, saturated with amine substrate, would be able to generate 15.6 uM / hour. With incubation times from 2 to 4 hours, that would result in a production of 31.2 uM – 62.4 uM H_2O_2, easily within the detection limit of both PF1 and PF2. Unfortunately this continuous production of H_2O_2 may be more prone to catabolism by the anti-oxidant network within the adipocytes, while the bolus addition may be able to over-whelm this network and thus produce an observable difference in probe activation. Interestingly, fluorescence was never detected within the lipid vacuoles of adipocytes.

After the fluorescence from probe activation was shown to be intracellular, while comparisons of activated probe within adipocytes treated with and without semicarbazide inhibitor did not exhibit a very large difference in intracellular H_2O_2, even after the long incubation time of 4.5 hours. A slight increase in intracellular fluorescence could be seen in adipocytes incubated only with amine substrate without SC pretreatment, but was difficult to reproduce in experiments involving different sets of cultured 3T3-L1 adipocytes. Doubling the concentration of PF1 and using a more sensitive H_2O_2 probe with only one boronated protecting group (PF2) increased the background fluorescence of normal intracellular H_2O_2 production, making it difficult to observe any significant increase in intracellular H_2O_2 due to AOC3 turnover. Additionally, insulin signaling is known to require an increase in intracellular H_2O_2. PF1 was able to detect an increase in intracellular H_2O_2 vs. when NADPH oxidase is inhibited. However upon addition of both insulin and AOC3 amine substrate, a difference in intracellular H_2O_2 was not observed when compared to just insulin alone. From the above studies, it is not possible to conclude the entry into adipocytes of extracellularly produced H_2O_2 by AOC3 to act as a participant in intracellular signaling.

References

1. Arnold, W.P., et al., *Nitric oxide activates guanylate cyclase and increases guanosine 3':5'-cyclic monophosphate levels in various tissue preparations.* Proc Natl Acad Sci U S A, 1977. **74**(8): p. 3203-7.
2. Hemler, M.E. and W.E. Lands, *Evidence for a peroxide-initiated free radical mechanism of prostaglandin biosynthesis.* J Biol Chem, 1980. **255**(13): p. 6253-61.
3. Hawkins, B.J., et al., *Superoxide flux in endothelial cells via the chloride channel-3 mediates intracellular signaling.* Mol Biol Cell, 2007. **18**(6): p. 2002-12.
4. Takakura, K., et al., *Rapid and irreversible inactivation of protein tyrosine phosphatases PTP1B, CD45, and LAR by peroxynitrite.* Arch Biochem Biophys, 1999. **369**(2): p. 197-207.
5. Burdon, R.H., *Superoxide and hydrogen peroxide in relation to mammalian cell proliferation.* Free Radic Biol Med, 1995. **18**(4): p. 775-94.
6. Hancock, J.T., R. Desikan, and S.J. Neill, *Role of reactive oxygen species in cell signalling pathways.* Biochem Soc Trans, 2001. **29**(Pt 2): p. 345-50.
7. Forman, H.J., M. Maiorino, and F. Ursini, *Signaling functions of reactive oxygen species.* Biochemistry, 2010. **49**(5): p. 835-42.
8. Babior, B.M., *NADPH oxidase: an update.* Blood, 1999. **93**(5): p. 1464-76.
9. Nicholls, P., F. I., and P.C. Loewen, *Enzymology and Structure of Catalases.* Adv Inorg Chem, 2000. **51**: p. 51-106.
10. Toppo, S., et al., *Catalytic mechanisms and specificities of glutathione peroxidases: variations of a basic scheme.* Biochim Biophys Acta, 2009. **1790**(11): p. 1486-500.
11. Wood, Z.A., L.B. Poole, and P.A. Karplus, *Peroxiredoxin evolution and the regulation of hydrogen peroxide signaling.* Science, 2003. **300**(5619): p. 650-3.
12. Wood, Z.A., et al., *Structure, mechanism and regulation of peroxiredoxins.* Trends Biochem Sci, 2003. **28**(1): p. 32-40.
13. Forman, H.J., M. Torres, and J. Fukuto, *Redox signaling.* Mol Cell Biochem, 2002. **234-235**(1-2): p. 49-62.
14. Halliwell, B., M.V. Clement, and L.H. Long, *Hydrogen peroxide in the human body.* FEBS Lett, 2000. **486**(1): p. 10-3.
15. Claiborne, A., et al., *Protein-sulfenic acids: Diverse roles for an unlikely player in enzyme catalysis and redox regulation.* Biochemistry, 1999. **38**(47): p. 15407-15416.
16. Seo, Y.H. and K.S. Carroll, *Profiling protein thiol oxidation in tumor cells using sulfenic acid-specific antibodies.* Proc Natl Acad Sci U S A, 2009. **106**(38): p. 16163-8.
17. Poole, L.B., et al., *Fluorescent and affinity-based tools to detect cysteine sulfenic acid formation in proteins.* Bioconjug Chem, 2007. **18**(6): p. 2004-17.
18. Lee, S.R., et al., *Reversible inactivation of protein-tyrosine phosphatase 1B in A431 cells stimulated with epidermal growth factor.* J Biol Chem, 1998. **273**(25): p. 15366-72.
19. Meng, T.C., T. Fukada, and N.K. Tonks, *Reversible oxidation and inactivation of protein tyrosine phosphatases in vivo.* Mol Cell, 2002. **9**(2): p. 387-99.
20. Rhee, S.G., et al., *Intracellular messenger function of hydrogen peroxide and its regulation by peroxiredoxins.* Curr Opin Cell Biol, 2005. **17**(2): p. 183-9.
21. Zheng, M., F. Aslund, and G. Storz, *Activation of the OxyR transcription factor by reversible disulfide bond formation.* Science, 1998. **279**(5357): p. 1718-21.
22. Abate, C., et al., *Redox regulation of fos and jun DNA-binding activity in vitro.* Science, 1990. **249**(4973): p. 1157-61.
23. Halliwell, B. and J.M.C. Gutteridge, *Free radicals in biology and medicine.* 4th ed. 2007, Oxford ; New York: Oxford University Press.
24. Mizoguchi, H. and S. Hara, *Effect of fatty acid saturation in membrane lipid bilayers on simple diffusion in the presence of ethanol at high concentrations.* Journal of Fermentation and Bioengineering, 1996. **81**(5): p. 406-411.
25. Toh, T.H., et al., *Implications of FPS1 deletion and membrane ergosterol content for glycerol efflux from Saccharomyces cerevisiae.* Fems Yeast Research, 2001. **1**(3): p. 205-211.
26. Seaver, L.C. and J.A. Imlay, *Hydrogen peroxide fluxes and compartmentalization inside growing Escherichia coli.* Journal of Bacteriology, 2001. **183**(24): p. 7182-7189.

27. Makino, N., et al., *A metabolic model describing the H2O2 elimination by mammalian cells including H2O2 permeation through cytoplasmic and peroxisomal membranes: comparison with experimental data.* Biochimica Et Biophysica Acta-General Subjects, 2004. **1673**(3): p. 149-159.

28. Sousa-Lopes, A., et al., *Decreased cellular permeability to H2O2 protects Saccharomyces cerevisiae cells in stationary phase against oxidative stress.* Febs Letters, 2004. **578**(1-2): p. 152-156.

29. Agre, P., et al., *Aquaporin water channels--from atomic structure to clinical medicine.* J Physiol, 2002. **542**(Pt 1): p. 3-16.

30. Yasui, M., *Molecular mechanisms and drug development in aquaporin water channel diseases: structure and function of aquaporins.* J Pharmacol Sci, 2004. **96**(3): p. 260-3.

31. Bienert, G.P., J.K. Schjoerring, and T.P. Jahn, *Membrane transport of hydrogen peroxide.* Biochim Biophys Acta, 2006. **1758**(8): p. 994-1003.

32. Hibuse, T., et al., *Aquaporin 7 deficiency is associated with development of obesity through activation of adipose glycerol kinase.* Proc Natl Acad Sci U S A, 2005. **102**(31): p. 10993-8.

33. Wardman, P., *Fluorescent and luminescent probes for measurement of oxidative and nitrosative species in cells and tissues: progress, pitfalls, and prospects.* Free Radic Biol Med, 2007. **43**(7): p. 995-1022.

34. Gomes, A., E. Fernandes, and J.L.F.C. Lima, *Fluorescence probes used for detection of reactive oxygen species.* Journal of Biochemical and Biophysical Methods, 2005. **65**(2-3): p. 45-80.

35. Belousov, V.V., et al., *Genetically encoded fluorescent indicator for intracellular hydrogen peroxide.* Nature Methods, 2006. **3**(4): p. 281-286.

36. Kulagina, N.V. and A.C. Michael, *Monitoring hydrogen peroxide in the extracellular space of the brain with amperometric microsensors.* Analytical Chemistry, 2003. **75**(18): p. 4875-4881.

37. Antunes, F. and E. Cadenas, *Estimation of H2O2 gradients across biomembranes.* Febs Letters, 2000. **475**(2): p. 121-126.

38. Stone, J.R., *An assessment of proposed mechanisms for sensing hydrogen peroxide in mammalian systems.* Arch Biochem Biophys, 2004. **422**(2): p. 119-24.

39. Setsukinai, K., et al., *Development of novel fluorescence probes that can reliably detect reactive oxygen species and distinguish specific species.* J Biol Chem, 2003. **278**(5): p. 3170-5.

40. Chignell, C.F. and R.H. Sik, *A photochemical study of cells loaded with 2 ',7 '-dichlorofluorescin: Implications for the detection of reactive oxygen species generated during UVA irradiation.* Free Radical Biology and Medicine, 2003. **34**(8): p. 1029-1034.

41. Crow, J.P., *Dichlorodihydrofluorescein and dihydrorhodamine 123 are sensitive indicators of peroxynitrite in vitro: Implications for intracellular measurement of reactive nitrogen and oxygen species.* Nitric Oxide-Biology and Chemistry, 1997. **1**(2): p. 145-157.

42. Wolfbeis, O.S., et al., *A europium-ion-based luminescent sensing probe for hydrogen peroxide.* Angew Chem Int Ed Engl, 2002. **41**(23): p. 4495-8.

43. Onoda, M., et al., *First fluorescent photoinduced electron transfer (PET) reagent for hydroperoxides.* Org Lett, 2003. **5**(9): p. 1459-61.

44. Lo, L.C. and C.Y. Chu, *Development of highly selective and sensitive probes for hydrogen peroxide.* Chemical Communications, 2003(21): p. 2728-2729.

45. Maeda, H., et al., *Fluorescent probes for hydrogen peroxide based on a non-oxidative mechanism.* Angewandte Chemie-International Edition, 2004. **43**(18): p. 2389-2391.

46. Chang, M.C., et al., *A selective, cell-permeable optical probe for hydrogen peroxide in living cells.* J Am Chem Soc, 2004. **126**(47): p. 15392-3.

47. Urano, Y., et al., *Evolution of fluorescein as a platform for finely tunable fluorescence probes.* J Am Chem Soc, 2005. **127**(13): p. 4888-94.

48. Sjoback, R., J. Nygren, and M. Kubista, *Absorption and Fluorescence Properties of Fluorescein.* Spectrochimica Acta Part a-Molecular and Biomolecular Spectroscopy, 1995. **51**(6): p. L7-L21.

49. Stephens, J.M., J. Lee, and P.F. Pilch, *Tumor necrosis factor-alpha-induced insulin resistance in 3T3-L1 adipocytes is accompanied by a loss of insulin receptor substrate-1 and GLUT4 expression without a loss of insulin receptor-mediated signal transduction.* Journal of Biological Chemistry, 1997. **272**(2): p. 971-976.

50. Miller, E.W., et al., *Boronate-based fluorescent probes for imaging cellular hydrogen peroxide.* J Am Chem Soc, 2005. **127**(47): p. 16652-9.

51. Jalkanen, S. and M. Salmi, *Cell surface monoamine oxidases: enzymes in search of a function.* EMBO J, 2001. **20**(15): p. 3893-901.

52. Miller, E.W., et al., *Molecular imaging of hydrogen peroxide produced for cell signaling.* Nat Chem Biol, 2007. **3**(5): p. 263-7.

53. Mahadev, K., et al., *Insulin-stimulated hydrogen peroxide reversibly inhibits protein-tyrosine phosphatase 1B in vivo and enhances the early insulin action cascade.* Journal of Biological Chemistry, 2001. **276**(24): p. 21938-21942.

54. Cohen, A.W., et al., *Role of caveolin and caveolae in insulin signaling and diabetes.* American Journal of Physiology-Endocrinology and Metabolism, 2003. **285**(6): p. E1151-E1160.

55. Mahadev, K., et al., *Integration of multiple downstream signals determines the net effect of insulin on MAP kinase vs. PI 3 '-kinase activation: potential role of insulin-stimulated H2O2.* Cellular Signalling, 2004. **16**(3): p. 323-331.

56. Mahadev, K., et al., *Hydrogen peroxide generated during cellular insulin stimulation is integral to activation of the distal insulin signaling cascade in 3T3-L1 adipocytes.* Journal of Biological Chemistry, 2001. **276**(52): p. 48662-48669.
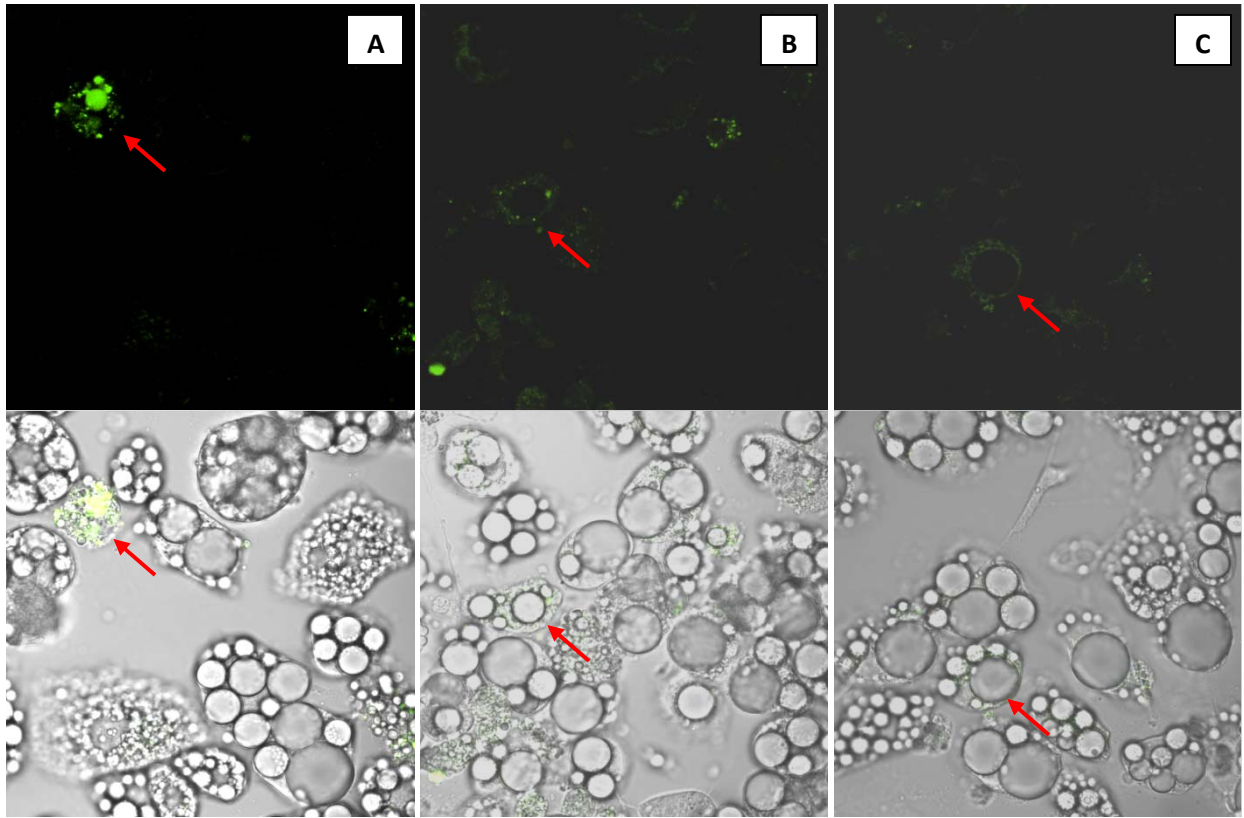
Figure 2.1- Confocal microscopy images of adipocytes treated with various concentrations of exogenous H_2O_2. In each image, the top image is the fluorescent emission signal (green) from activated PF1 detected between 500 – 600 nm. The bottom image is the merged image of both the differential interference contrast (DIC) image and the fluorescent emission signal. A – 2 uM exogenous H_2O_2 added. Red arrow points at fluorescent signal in top image and the DIC fluorescent merged image in bottom image B – 8 uM exogenous H_2O_2 added. C – 16 uM exogenous H_2O_2 added. Red arrows in B and C correspond to fluorescent signal in fully differentiated lipid laden adipocytes.
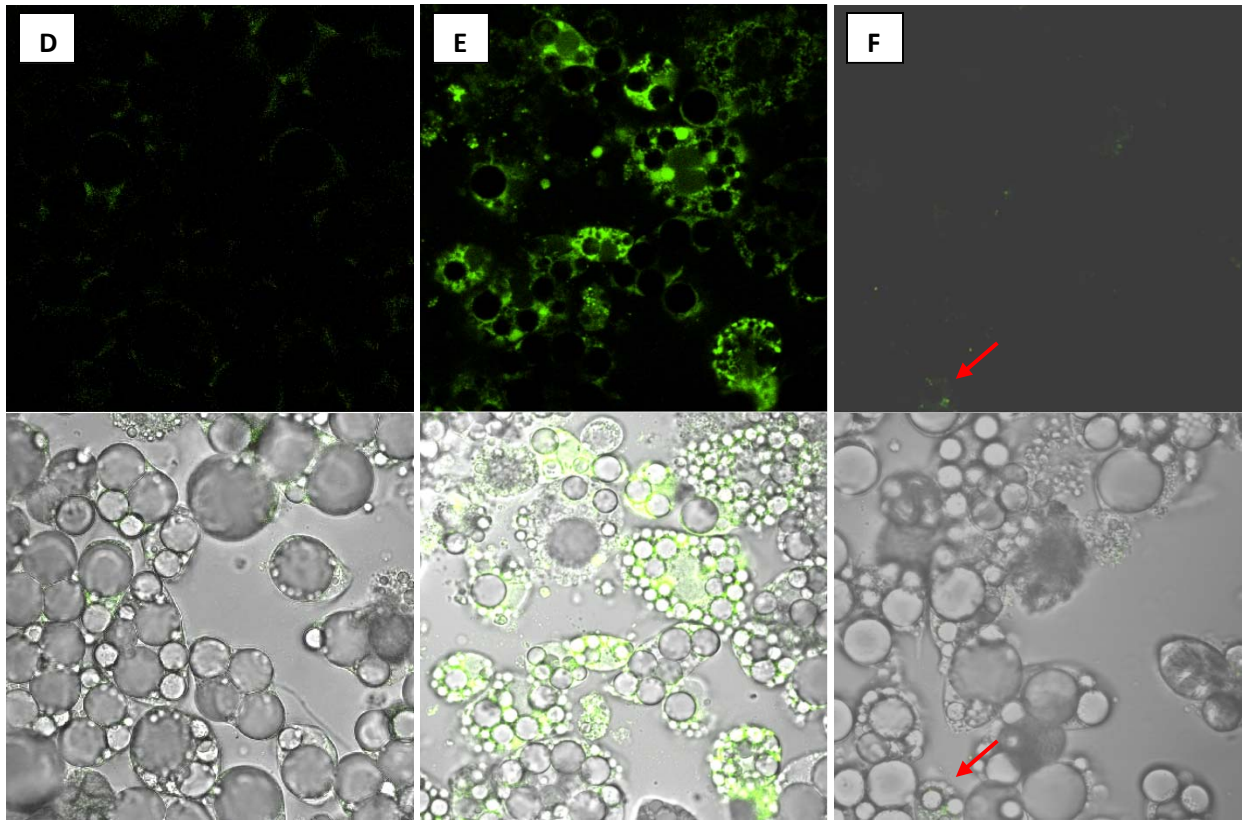
Figure 2.1- (cont.) D – 32 uM exogenous H_2O_2 added. E – 100 uM exogenous H_2O_2 added. F – 0 uM exogenous H_2O_2 added, just 5 uM PF1.
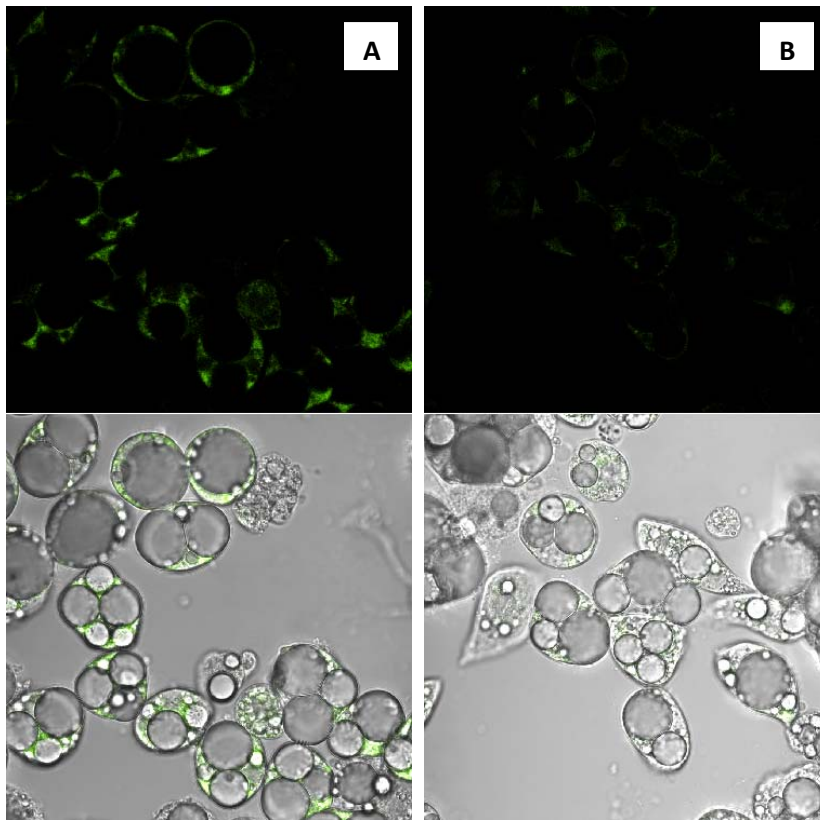
Figure 2.2- Confocal microscopy images of adipocytes treated with or without 32 uM H_2O_2 after 5 uM PF1 intracellular loading and imaged after 3.5 hours at 37°C in PBS. A – 32 uM exogenous H_2O_2 added and adipocytes incubated for 3 hours 37 minutes prior to imaging. B – 0 uM exogenous H_2O_2 added and adipocytes incubated for 3 hours 43 minutes prior to imaging.
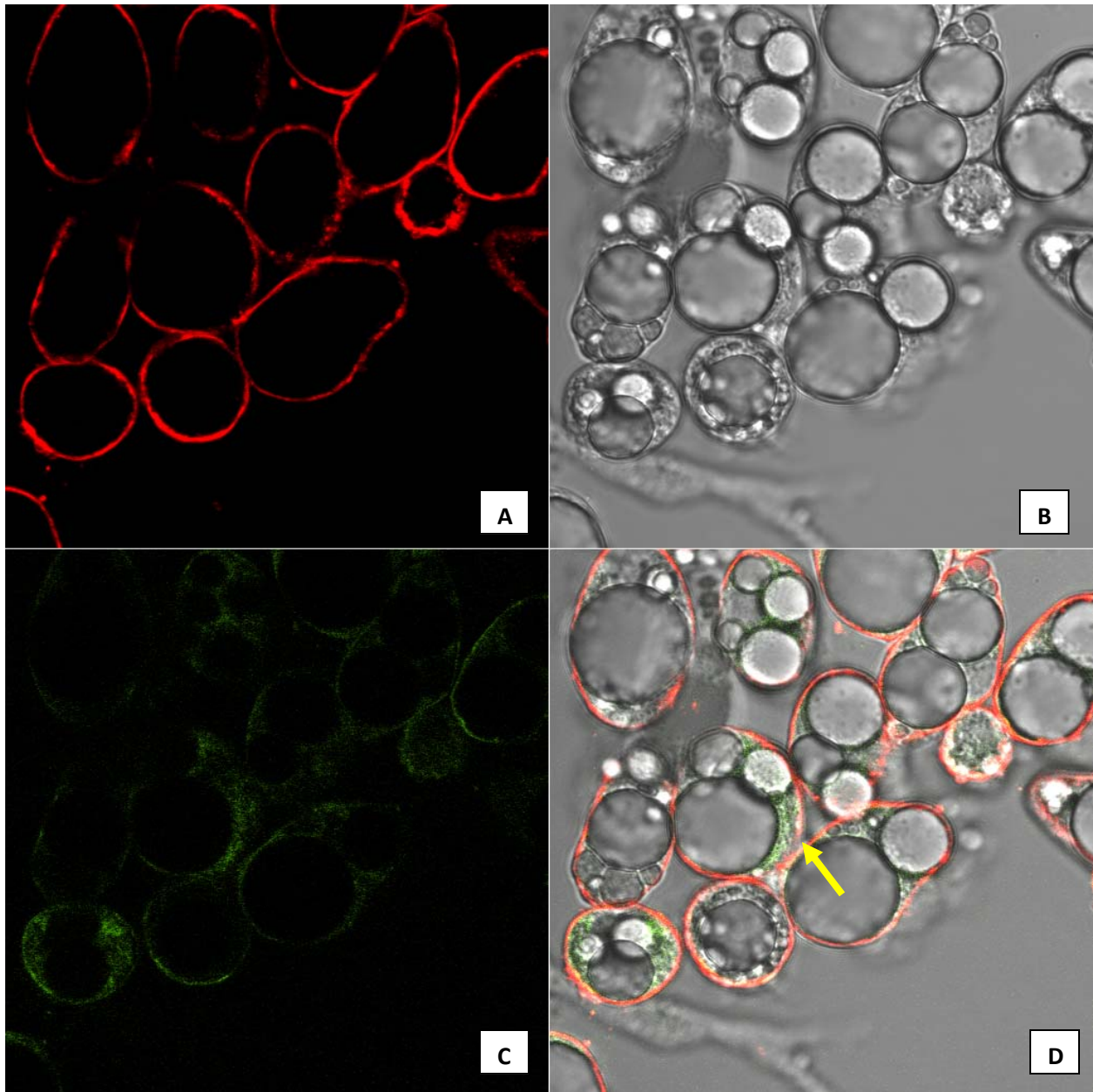
Figure 2.3- Adipocytes were treated with 100 uM H_2O_2 for 15 minutes after PF1 loading. Prior to imaging, FM464 lipophilic dye was added at 2 ug/mL. The images were taken from the same field in series using HeNe and argon lasers. A – Fluorescence emission for FM464 (red) detected between 700 – 800 nm. B – DIC image of adipocyte. C – Fluorescent emission signal (green) from activated PF1 detected between 500 – 600 nm. D. Composite of A, B, and C. Yellow arrow shows green fluorescence surrounded by red fluorescence.
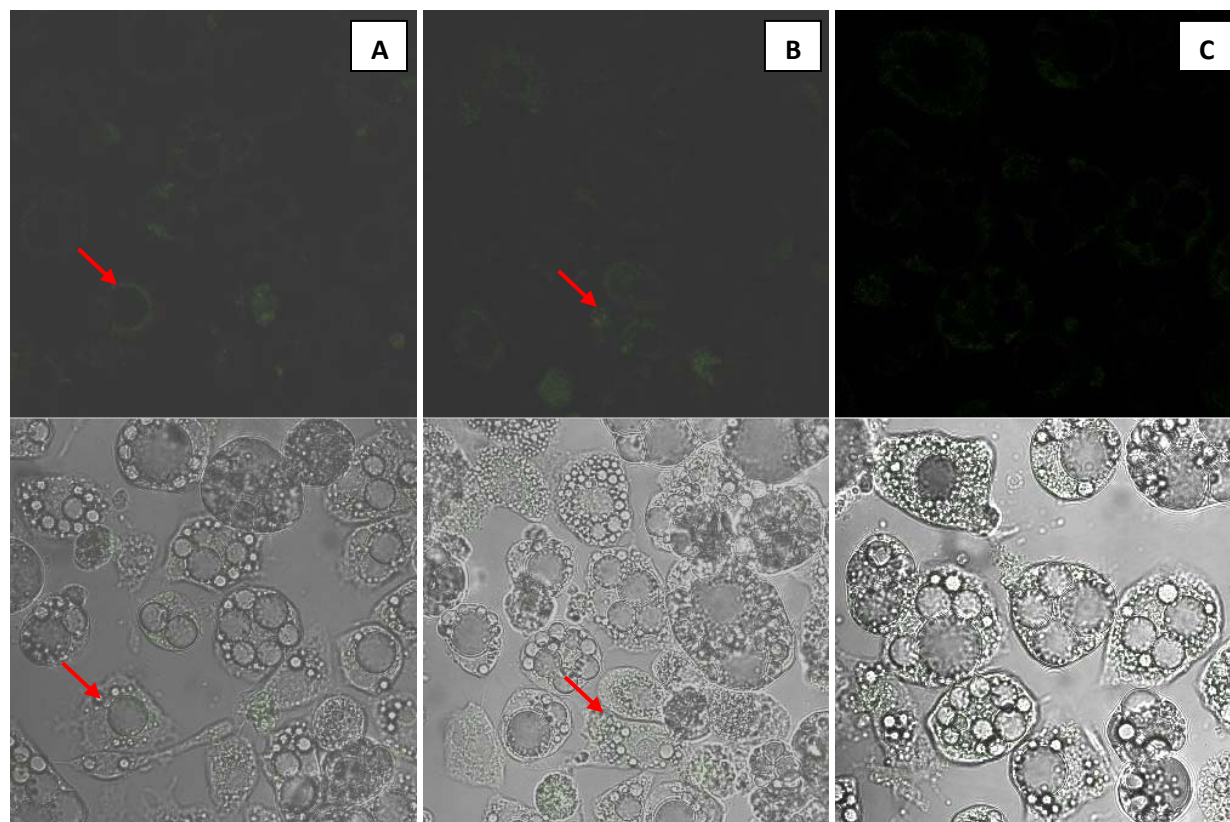
Figure 2.4- Adipocytes were incubated with 1.48 mM isoamylamine, with or without 100 uM semicarbazide inhibitor pretreatment for 30 minutes. All adipocytes were first preloaded with 5 uM PF1 for 15 minutes prior to addition of amine substrate. Adipocytes were incubated at 37°C for over 2.5 hours prior to imaging. A - 1.48 mM isoamylamine incubation for 2 hours 51 minutes. B. Semicarbazide pretreatment for 30 minutes prior to 1.48 mM isoamylamine introduction and incubated for 2 hours 40 minutes. C. PF1 probe incubation with no addition of isoamylamine or semicarbazide for 2 hours 55 minutes. Red arrows point to fluorescence in viable adipocytes.
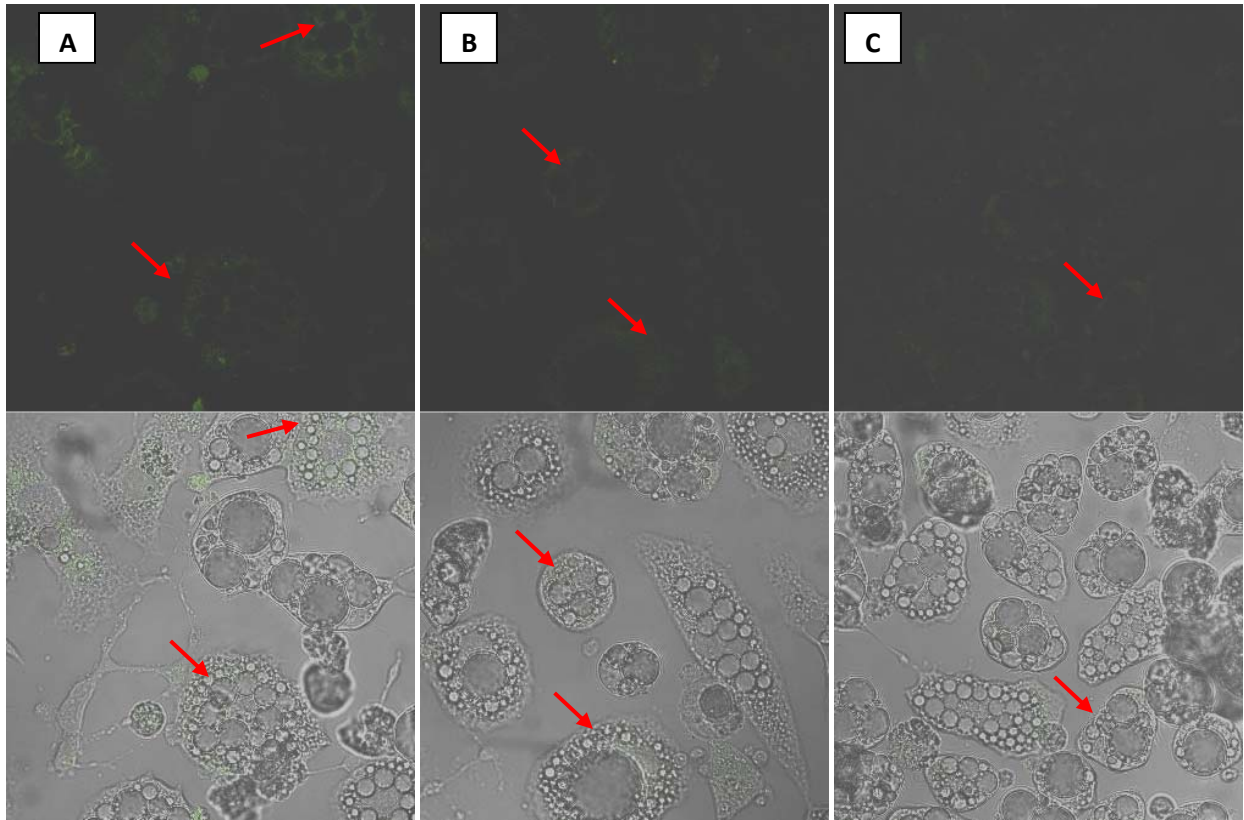
Figure 2.5- Adipocytes were incubated with 1.48 mM isoamylamine, with or without 100 uM semicarbazide inhibitor pretreatment for 30 minutes. All adipocytes were first preloaded with 5 uM PF1 for 15 minutes. Adipocytes were incubated at 37°C for over 3 hours prior to imaging. A - 1.48 mM isoamylamine incubation for 3 hours 11 minutes. B. Semicarbazide pretreatment for 30 minutes prior to 1.48 mM isoamylamine introduction and incubated for 3 hours 6 minutes. C. PF1 probe incubation with no addition of isoamylamine or semicarbazide for 3 hours 17 minutes. Red arrows point to fluorescence in viable adipocytes.
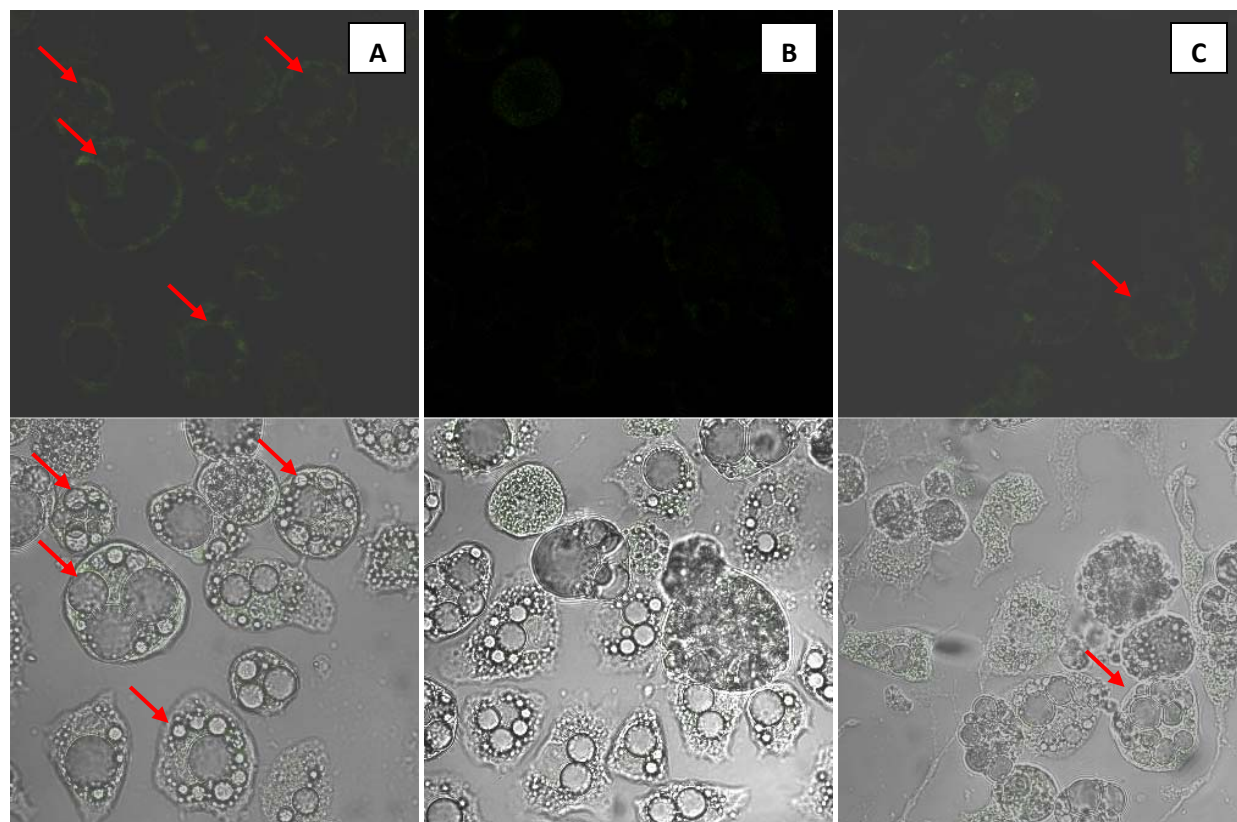
Figure 2.6- Adipocytes were incubated with 1.48 mM isoamylamine, with or without 100 uM semicarbazide inhibitor pretreatment for 30 minutes. All adipocytes were first preloaded with 5 uM PF1 for 15 minutes. Adipocytes were incubated at 37°C for over 4 hours prior to imaging. A - 1.48 mM isoamylamine incubation for 4 hours 20 minutes. B. Semicarbazide pretreatment for 30 minutes prior to 1.48 mM isoamylamine introduction and incubated for 4 hours 6 minutes. C. PF1 probe incubation with no addition of isoamylamine or semicarbazide for 4 hours 1 minutes. Red arrows point to fluorescence in viable adipocytes.
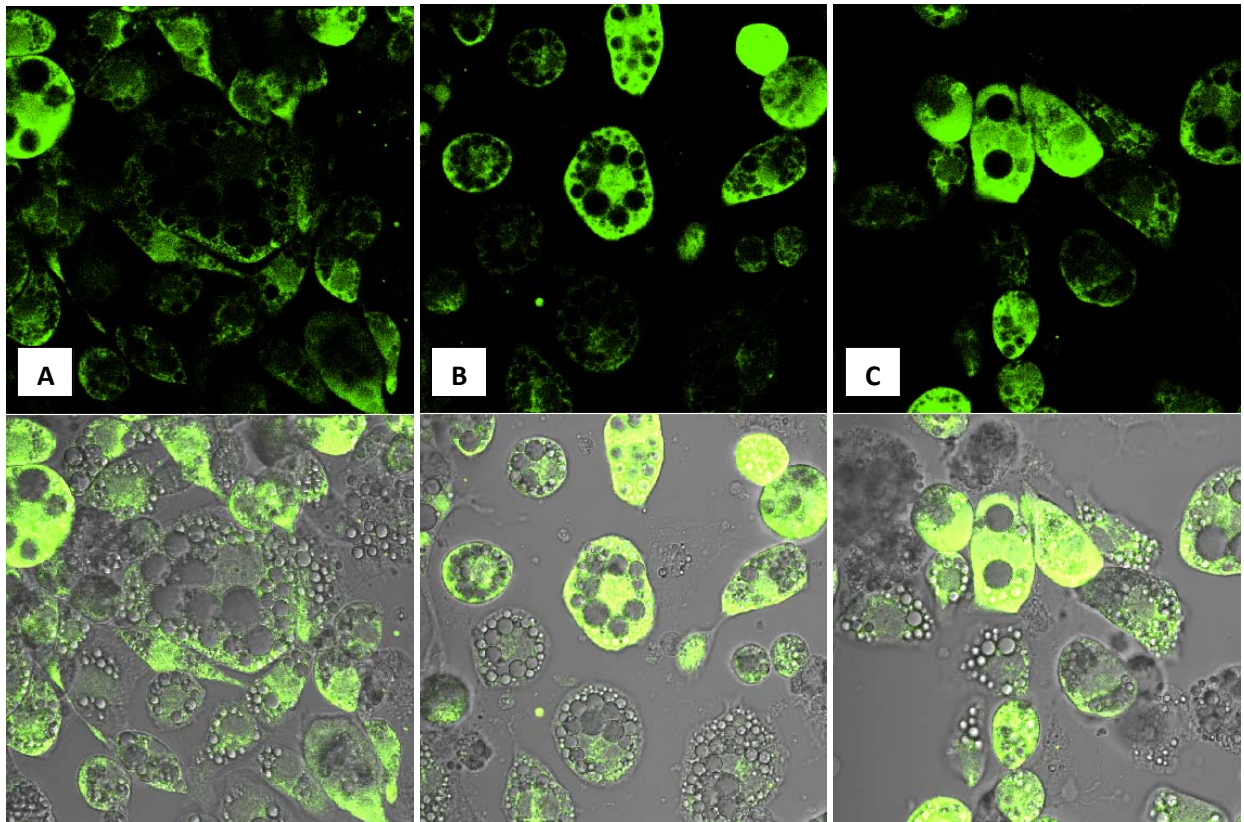
Figure 2.7- Adipocytes were incubated with different concentrations of methylamine for approximately 3.5 hours at 37°C prior to imaging. All adipocytes were first preloaded with 10 uM PF1 for 15 minutes prior to addition of amine substrate. A – Incubation with 1.59 mM methylamine and imaged after 3 hours 27 minutes incubation. B – Incubation with 7.95 mM methylamine and imaged after 3 hours 12 minutes. C – PF1 probe incubation with no addition of methylamine for 3 hours 32 minutes.
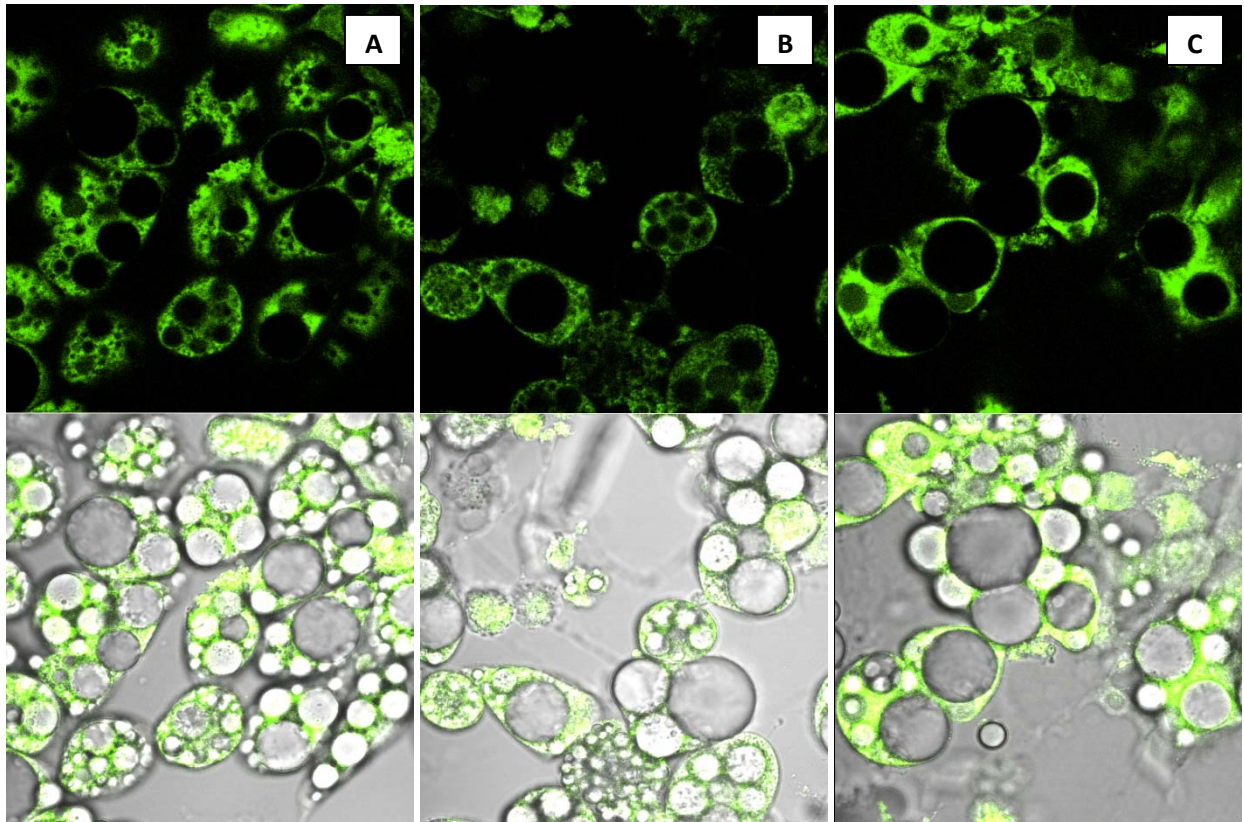
Figure 2.8- All adipocytes were first preloaded with 5 uM PF2 for 15 minutes prior to addition of H_2O_2. All cells incubated with H_2O_2 for 15 minutes prior to imaging. A – Incubation with only PF2, no H_2O_2 added. B – Incubation with 4 uM H_2O_2. C – Incubation with 8 uM H_2O_2.
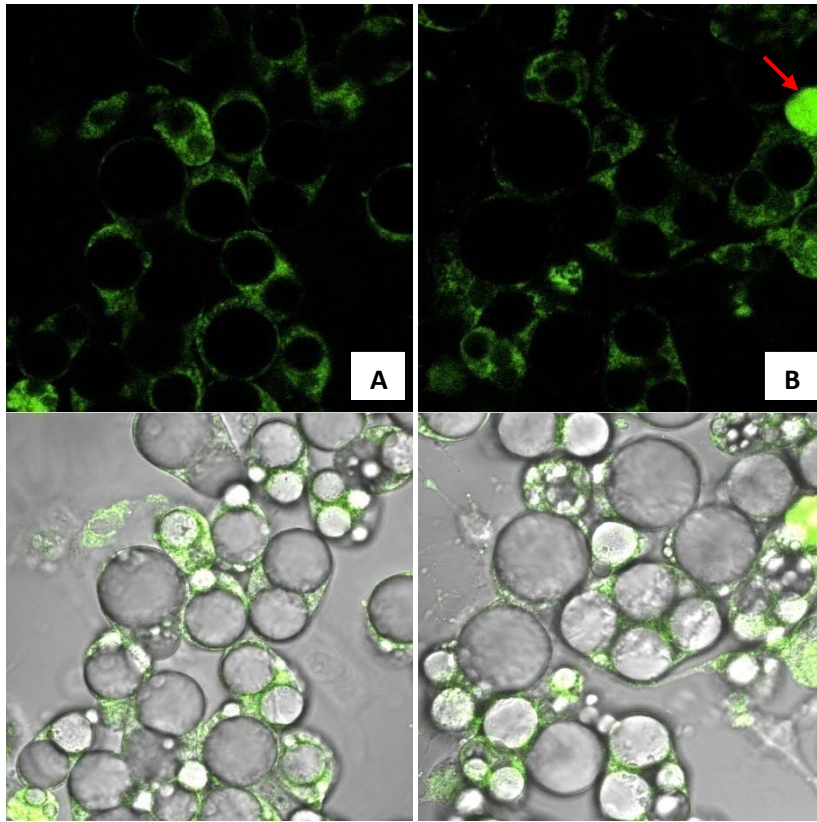
Figure 2.9- All adipocytes were first preloaded with 5 uM PF2 for 15 minutes prior to addition of isoamylamine. Adipocytes were incubated with 1.48 mM isoamylamine for approximately 3 hours at 37°C prior to imaging. A – Incubation with 1.48 mM isoamylamine and imaged after 3 hours. B – Incubation with 100 uM SC for 30 mintues and then 1.48 mM isoamylamine and imaged after 2 hours 50 minutes.   The red arrow points at fluorescence that should be disregarded due to lack of adipocyte morphology in the DIC image.
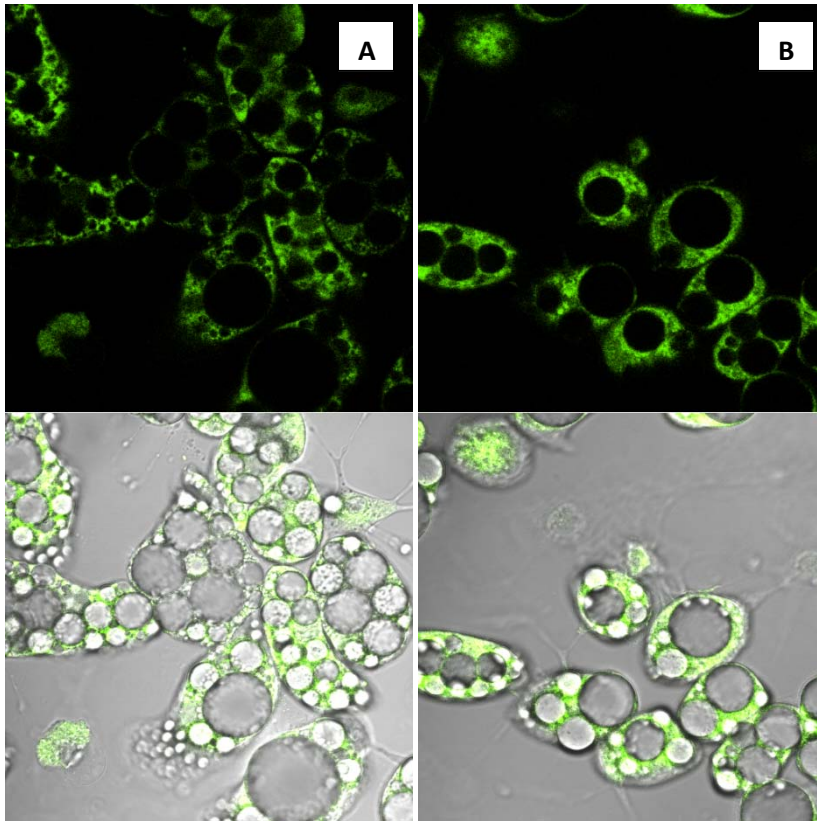
Figure 2.10- All adipocytes were first preloaded with 5 uM PF2 for 15 minutes prior to addition of methylamine. Adipocytes were incubated with 7.95 mM mM methylamine for approximately 2.5 hours at 37°C prior to imaging. A – Incubation with 7.95 mM methylamine and imaged after 2 hours 40 minutes. B – Incubation with 100 uM SC for 30 mintues and then 7.95 mM methylamine and imaged after 2 hours 30 minutes.
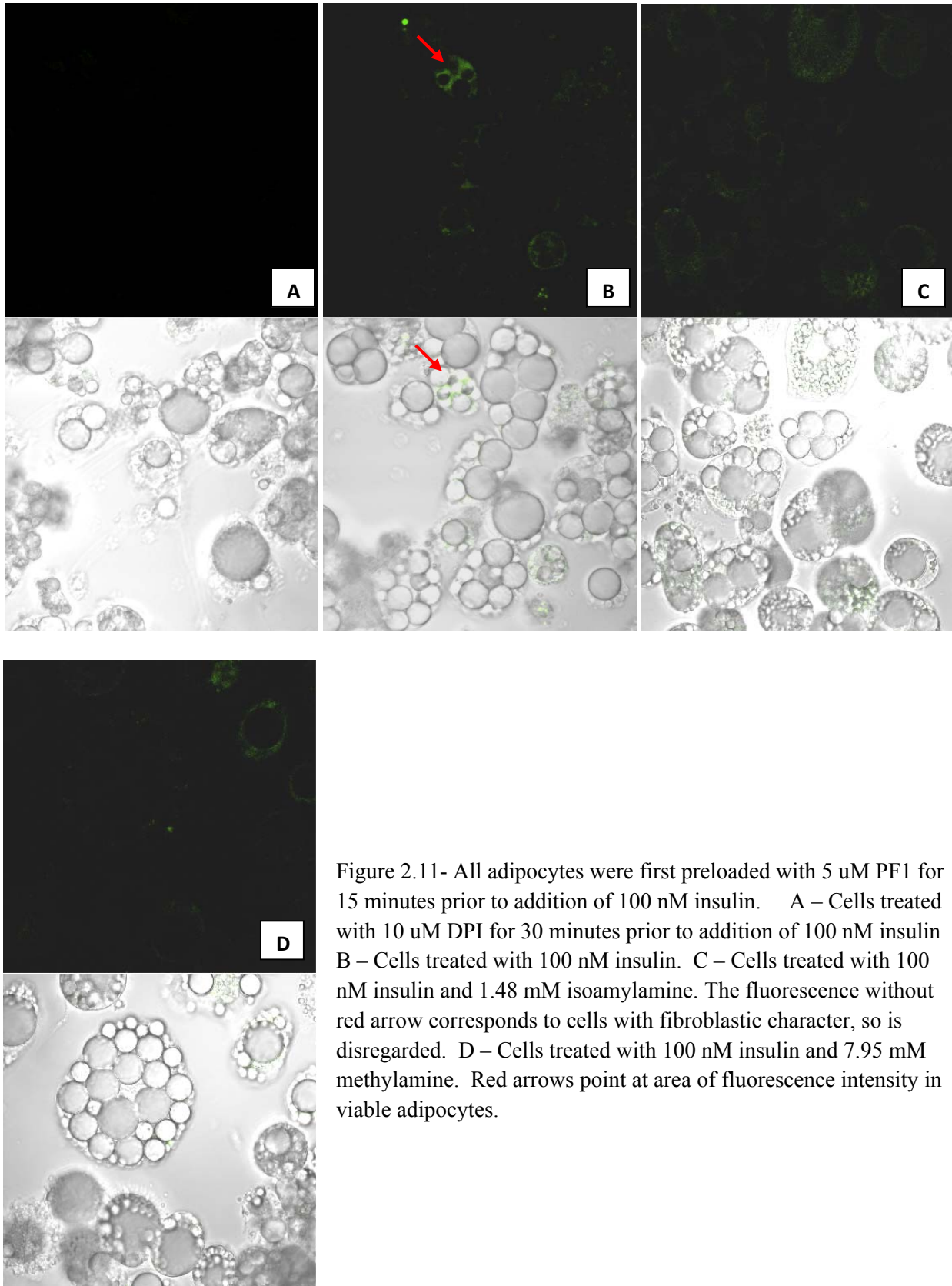
Figure 2.11- All adipocytes were first preloaded with 5 uM PF1 for 15 minutes prior to addition of 100 nM insulin. A – Cells treated with 10 uM DPI for 30 minutes prior to addition of 100 nM insulin B – Cells treated with 100 nM insulin. C – Cells treated with 100 nM insulin and 1.48 mM isoamylamine. The fluorescence without red arrow corresponds to cells with fibroblastic character, so is disregarded. D – Cells treated with 100 nM insulin and 7.95 mM methylamine. Red arrows point at area of fluorescence intensity in viable adipocytes.

Chapter 3:

Substrate Kinetic Profile of Human AOC-3

Introduction

The endogenous substrate(s) of human AOC3 is/are currently unknown. Knowing the endogenous substrate(s) would provide an invaluable clue to the physiological role of AOC3. Two primary amines produced endogenously in humans most commonly cited as AOC3 substrates are methylamine and aminoacetone. Methylamine can be produced *in vivo* by metabolism of sarcosine, creatine [1] and epinephrine [2], both shown experimentally in rats. Studies in human umbilical arteries show that methylamine (MA) deamination occurs primarily by AOC3 [3]. Benzylamine is a xenobiotic amine found to have high AOC3 activity. Aminoacetone is formed by the metabolism of threonine [4] and glycine and was found to be a substrate of AOC3 in human umbilical arteries [5].

In addition to methylamine and aminoacetone, there has been speculation that other primary amines could be possible substrates of human AOC3 [6], including two catecholamine hormones, norepinephrine and dopamine, histamine [7], serotonin, tyramine, tryptamine, phenethylamine, and L-lysine [8], all of which are known hormones or neurotransmitters found endogenously. However, there has been no published report of whether these primary amines are possible substrates of human AOC3. In addition, metabolites of the hormone thyroxine, 3-iodo-thyronamine and 3,3',5-triiodothyronamine, could also be possible substrates as the oxidized byproducts 3-iodothyroacetic acid and 3,3',5-triiodothyroacetic acid were found in both human and rat serum [9]. In addition, with reports that AOC3 activity has been shown to be an insulin mimetic [10], a search for more efficient substrates as possible diabetes drugs has taken place using computational methods. Using computational docking studies, both 4-fluoro-benzylamine ($k_{cat}/K_m = 3.4 \times 10^3 \text{ s}^{-1}\text{M}^{-1}$) and 4-phenylbutylamine ($k_{cat}/K_m = 2.9 \times 10^3 \text{ s}^{-1}\text{M}^{-1}$) [11], 1,12-diaminododecane ($K_m = 10 - 30$ uM) [12] were found to be better substrates for human AOC3 than benzylamine. In addition, the bulkiness of para substitutions on the benzylamine ring can improve or harm substrate affinity [13]. Peptide-based substrates have also been hypothesized. For example, the catalytic activity of AOC3 was found to be necessary in its putative role as a vascular adhesion molecule in endothelial cells [14]. A possible endothelial cell-leukocyte interaction involves a peptide-bound lysine on the surface of leukocytes acting as a substrate of AOC3, temporarily crosslinking the two cells through the formation of a Schiff base. It was shown through molecular modeling that the peptide GGGGKGGGG was able to fit into the active site of AOC3. Recently, using phage display, a leukocyte-expressed ligand, Siglec-10 (sialic acid-binding immunoglobulin-like lectin-10), which may be involved in cell-cell recognition, was also found to be a substrate of AOC3 [15].

The distribution of mammalian AOC3 *in vivo* may also provide a clue to its function. Looking at AOC3 activity in the plasma and tissue of pigs, rats, and humans, it was found that all tissues exhibited amine oxidase activity sensitive to semicarbazide, with all three species exhibiting high activity in the vasculature and in fat tissues [16]. Other tissues with significant AOC3 activity include lung, ileum, gall bladder, and umbilical cord, though these may all be due to contamination by the vasculature. By direct tissue comparison, there was more AOC3 activity in humans than in rats and pigs. Interestingly, there was more AOC3 activity found in the adipose tissue of pigs than in humans. Rather than looking at AOC3 activity, immunohisto-chemical assays using a polyclonal antibody revealed similar tissue distribution in humans. For example, in lung tissue, AOC3 was found to be localized to bronchiolar cells and in all pneumocytes of alveoli while in duodenum, AOC3 was present mostly in the membrane of

42

enterocytes of villi [17]. In the same paper, fibroblasts, cells that maintain structural integrity of extracellular matrix, found surrounding systemic arteries, were also found to express AOC3 and human tissues completely devoid of AOC3 include both the thyroid gland and exocrine pancreas. Though AOC3 is widely distributed, major sources of the enzyme have been shown to be from adipocytes, endothelial cells, and smooth muscle cells [18]. With the expression of AOC3 found almost ubiquitously in humans, the enzyme may be responsible for the oxidation of more than one primary substrate.

Due to the importance of a complete substrate profile for the human AOC3, it is surprising most kinetic studies have involved the tissue-bound enzyme, rather than with its purified form [19],[20]. Since AOC3 is a cell-surface enzyme with an extracellular catalytic domain, it was possible to use whole cells to measure substrate kinetics [21]. For example, studies of the presence of semicarbazide sensitive amine oxidase activity have involved tissue from rat aorta [22], human umbilical artery [23], bovine lung [24], porcine dental pulp [25], and even catfish [26] to name a few. Studies using the tissue-bound form of AOC3 are complicated by the necessity to inhibit known amine oxidases, such as MAO-A and MAO-B and the need to control for the effect of the inhibitors. A substrate profile based on the purified form of human AOC3 would enhance the search for its physiological role. For example, knowing that epinephrine is not a substrate of AOC3 would eliminate its involvement in the regulation of epinephrine signaling.

To pursue a substrate profile, human AOC3 needs to be obtained in its purified form. There are three published protocols involving the purification of human AOC3. Two of the protocols involve using a glutathione-S-transferase (GST)-tagged fusion protein. In both protocols, a truncated GST-AOC3 without the transmembrane domain was expressed in stably transfected human embryonic kidney (HEK) -293T cells. HEK293T cells require fetal bovine serum, which can complicate the purification process of untagged proteins due to variable protein components, most notably serum albumin. In addition, in one purification procedure, expressed GST-AOC3 was secreted into a total of 90 liters of raw media collected over 10 days, which can be burdensome to handle and breakdown of enzyme can occur during storage as media was harvested after 3 and 7 days [27]. In the other GST-tagged AOC3 purification protocol, the breakdown during storage of multiple harvests and the use of serum are still issues. However, the protocol is complicated by the design of several mutated GST tags and the recovery of 383 ug purified protein /L of cells is not a great yield [28]. In both protocols, the GST tag is cleaved after purification. In the third purification scheme, full length human AOC3 was expressed in Chinese hamster ovary (CHO) cells [29]. However, affinity chromatography using monoclonal anti-AOC3 antibody was the main purification step and unfortunately, the antibody is not commercially available.

Previously, in our lab, the mouse AOC3 was purified without using a tag and expressed using Schneider 2 (s2) *Drosophila* cells. Each human AOC3 monomer is heavily sialylated with six potential N-linked and 3 O-linked glycosylation sites, which have been found to be important in activity [30]. Due to the importance of post-translational modifications, expression in *E. coli* was restricted and previously, difficulty was experienced with expression in *S. cerevisiae*. s2 cells are easy to maintain and are only slightly adherent to tissue culture flasks. They can be maintained at approximately room temperature (27°C) without the need of 5% CO_2, only using serum free media to culture, and expressed protein levels can reach 50 mg/L [31]. In addition, it is relatively quick to get protein expression, generating protein of interest in approximately 3 – 4 weeks after co-transfection with a plasmid containing a gene conferring resistance to

hygromycin. There have been many examples of mammalian protein expression with s2 cells [32], and s2 cells expressed human ADAM33 transmembrane protein with 10-fold greater expression than other insect cell lines, Sf9 and Hi5 cells [33]. In addition, s2 cells were able to express glycosylated heterologous human enzymes [34], [35] with reports that insect cells are capable of complex glycosylations [36]. An expression plasmid containing an inducible metallothionein (MT) promoter and BiP secretion signal were used. The MT promoter allows protein expression to be induced with metal ions, including $CuSO_4$, while the BiP signal tags the protein for secretion into the cell growth media, which can be simply collected rather than having to lyse the cells to obtain expressed protein. With these considerations, expression of human AOC3 was undertaken in hopes of better yields and more facile protocol than previous published purifications.

Methods

Construction of expression vector for producing soluble human AOC3. The soluble portion of human AOC3 (shAOC3) (GenBank Accession No. NM_003734) from residues 28 – 763 was cloned by PCR from VAP-1 cDNA-clone plasmid (generously supplied by Prof. Sirpa Jalkanen) containing the complete coding sequence of human AOC3. Amplification was performed using 5' primer 5'-TATCAG **GAATTC**AT GCAGGGGTGGAGATGGGGGTGA-3' with EcoRI restriction site introduced upstream of the N-terminus. The 3' primer was 5'-TATCAG-**CTCGAG**TTACTAGTTGTGAGAGAAGCCC CCGTG-3' with XhoI restriction site introduced after two stop codons. PCR (Expand High Fidelity PCR System, Roche and Pfu Ultra DNA Polymerase, Stratagene) was carried out 30 cycles with 1 minute denaturing at 95°C, 1 minute annealing at 60°C, and 2 minutes 15 seconds elongation at 72°C (MJ Research PTC-200 Peltier Thermal Cycler) The PCR product was digested with EcoRI and XhoI and ligated (Rapid DNA Ligation Kit, Roche) into the expression vector pMT/BiP/V5-His B (Invitrogen). The expression plasmid was sequenced at the DNA Sequencing Facility at University of California, Berkeley.

Construction of expression vector for producing soluble human His-tagged AOC3.
Residues 29 – 763 were cloned by PCR as previously described with a different set of PCR primers, 5' primer 5'-TATCAG-**GAATTC**TGGTGGAGATGGGGGTGAACCC and 3' primer was 5'- TATCAG**CTCGAG**GTTGTGA-GAGAAGCCCCCGTG. Expression plasmid was produced as previously described with exception that expression vector pMT/BiP/V5-His A (Invitrogen) was used.

Transfection of Schneider 2 (s2) Drosophila cells and selection of stable cell line. s2 cells were grown to 2-4 x 10^6 cells/ mL in serum free Excel 420 (JRH, Lenexa, KS) and co-transfected with pMT/BiP/V5-His B-AOC3 plasmid and pCoHygro selection vector using Calcium Phosphate Transfection kit (Invitrogen). All s2 cells were grown at 27°C. The suggested transfection procedure provided by manufacturer (Invitrogen) was followed with exception that addition of calcium chloride solution and phosphate solution were added 10 uL at a time with ample mixing. After 24 hours, s2 cells were washed twice with Excel-420 and 10% FBS (Hyclone, Thermo Fisher) and incubated for 2 days. After 2 days, s2 cells were washed twice and resuspended in Excel-420 and 10% FBS (complete media) with 300 ug/mL hygromycin. s2 cells were washed and complete media replenished every 3-4 days. After one week, in addition to complete media, 600 ug/mL hygromycin was added and selection continued for 2 more weeks. After 2 weeks, resistant cells were scaled up to 500 mL and induced with 600 uM $CuSO_4$ (EMD Chemicals, Gibbstown, NJ) and detection of soluble human AOC3 (shAOC3) was done by Western blot. s2 cell line expressing shAOC3 were snap frozen and stored in liquid nitrogen. Cellfectin was purchased from Invitrogen and suggested transfection protocol of manufacturer was followed.

Western Blotting of shAOC3. 10 uL of samples was mixed with equal volume Laemmli Sample Buffer (Bio-rad Laboratories, Hercules, CA) + 5% β-mercaptoethanol for electrophoresis. Before loading on a 10% acrylamide gel, samples were boiled for 7 minutes at 100°C. The resolved proteins were transferred to nitrocellulose membrane (Bio-rad Laboratories, Hercules, CA) using a Mini-PROTEAN II (Bio-rad Laboratories, Hercules, CA) system kept on ice. Effectiveness of protein transfer was determined using Precision Plus Protein Standards Kaleidoscope (Bio-rad). Blocking was performed with TBS (2.42 g Tris base, 8 g NaCl, adjusted to pH 7.6 with HCl), 5% nonfat dry milk (Carnation, Nestle), and 0.1% Tween-20 for 1 hour at room temperature. After washing 3 times with TBS/T (TBS buffer, 0.1% Tween-20), membrane was incubated with a 1:2400 dilution of primary anti-hAOC3 antibody (generously provided by Prof. Sirpa Jalkanen, University of Turku, Finland) in blocking buffer with gentle agitation overnight (approximately 14 - 16 hours) at 4°C. Membrane was then washed 3 times with TBS/T buffer and the membrane incubated in 1:1000 dilution of secondary antibody, horseradish peroxidase conjugated anti-mouse IGG (Cell Signaling Technology, Danvers, MA) with gentle agitation for 1 hour at room temperature. After washing the membrane 3 times, shAOC3 was detected using ECL Plus Western Blotting Detection System (GE Healthcare, Buckinghamshire, UK)

Production of shAOC3 by s2 cells. s2 cells were scaled-up from 5 mL at 2×10^6 cells/mL in T-25 flasks to $20 – 25 \times 10^6$ cells/mL in both T-75 flasks (approximately15 mL total volume) and T-150 flasks (approximately 30 mL total volume). Cells were counted using Brightline hemacytometer (Hausser Scientific, Horsham, PA) disregarding nonviable cells using 0.4% Trypan Blue (Sigma Aldrich, St. Louis, MO). s2 cells were grown in serum free Insect-Xpress (Lonza, Basel, Switzerland) with 600 ug/mL hygromycin (Invitrogen, Carlsbad, CA). A starter culture consisting of 200 mL and 100 mL were both seeded at 2×10^6 cells/mL in two 2L disposable Erlenmeyer flasks and one 1L disposable Erlenmeyer flask respectively. For scale-up, only serum-free Insect-Xpress media, without hygromycin or FBS, were used. s2 cells were grown on a shaker platform rotating at 98 rpm for 2 days. With a doubling time of approximately 24 hours, the cell density should be approximately 8×10^6 cells/mL. Afterwards, each flask was diluted three fold by adding 400 mL and 200 mL media and the shaker brought to 105 rpm and allowed to propagate for 24 hours. After 24 hours, expression was induced with 600 uM $CuSO_4$ for approximately 3 days. Final cell count after 3 days should be above 22×10^6 cells/mL.

Purification of shAOC3 using Cation Exchange. Starting with 1.5L raw expression media, the s2 cells were first spun down at 4000 rpm for 15 minutes at 4°C. The supernatant was isolated and concentrated by ultra-filtration (Amicon, Millipore) to approximately 700 mL using a Millipore membrane (MWCO 50 kDa) at 4°C. The concentrated media was then dialyzed in 12L of 10 mM potassium phosphate (Fisher) buffer, pH 6.5 for at least 4 hours, after which buffer was replaced with fresh dialysis buffer and dialysis was allowed to occur overnight for

approximately 15 hours. The first purification step involved cation exchange chromatography using 75 mL of SP Sepharose Fast Flow (Sigma, St. Louis) equilibrated with 10 mM potassium phosphate (KPi) buffer, pH 6.5. The dialyzed concentrated media was loaded onto the cation exchange column and eluted off the column with 1L buffer gradient (500 mL 10 mM KPi pH 6.5 and 500 mL 10 mM KPi pH 6.5/ 250 mM NaCl) into approximately 8 mL fractions. The fractions were run on a SDS-PAGE gel and the fractions corresponding to the mass of shAOC3 were collected. The fractions were concentrated to approximately 10 mL by ultra-filtration (Amicon, Millipore) using a Millipore membrane (MWCO 50 kDa) and diluted with10 mL 10 mM KPi buffer, pH 6.5, 20% glycerol to make a final 20 mL 10% glycerol solution to stabilize protein and minimize precipitation. The 20 mL partially purified protein was further concentrated down to 1 – 2 mL. The concentrate was then loaded onto a gel filtration column, charged with 290 mL Sephacryl S-200 HR (Amersham Biosciences, Piscataway, NJ) equilibrated with 50 mM KPi, pH 6.5. A pump was connected to the gel filtration column with flow regulator and 1 mL fractions were collected with equilibrating buffer over 16-20 minutes. Fractions were run on a SDS-PAGE gel and fractions with purified shAOC3 were collected and concentrated to approximately 100 – 200 uL (Microcon Ultracel YM-50, Millipore). Purified protein was snap frozen in 50 mM KPi, pH 6.5 buffer and stored at -20°C. All purification steps were performed at 4°C.

Purification of shAOC3 using Anion Exchange. This method was adapted from the purification of the mouse AOC3 (Diana Wertz), which involved DEAE anion exchange and S-200 gel filtration. After overnight dialysis of concentrated raw cell media, DEAE Sepharose Fast Flow (Amersham Biosciences, Piscataway, NJ), equilibrated with 5 mM KPi, pH 7.2, was eluted with two 1L buffer gradients composed of either equal volumes of 5 mM KPi, pH 7.2 and 100 mM KPi, pH 7.2 or 100 mM KPi, pH 7.2 and 300 mM KPi, pH 7.2. Most human AOC3 was expected to elute off the anion exchange column after the 5 mM/100 mM gradient. The fractions containing shAOC3 were collected, concentrated to 1 – 3 mL and loaded onto a Sephacryl S-200 gel filtration column as previously described. When using Q-Sepharose Fast Flow (Amersham, Piscataway, NJ) anion exchange after failure to purify with DEAE Sepharose, an identical procedure was used in preparation of raw cell media and elution conditions. For batch binding, raw media containing hAOC3 was diluted to 4L with 5 mM KPi, pH7.2 and incubated with 100 mL DEAE Sepharose Fast Flow for 30 minutes at 4°C with stirring. After 30 minutes, the buffer was siphoned off after allowing the resin to settle and the resin poured into a column for protein elution.

Purification of His-tagged shAOC3 using TALON column. Procedure identical to that used for cation exchange purification was followed. DEAE Sepharose Fast Flow anion exchange column was equilibrated using 5 mM KPi, pH 7.2 and media loaded onto column and washed with 0.5M EDTA 5 mM KPi, pH 7.2 buffer in order to wash away excess Cu in the raw media that may interfere with TALON immobilized metal ion affinity chromatography. Protein was

eluted off the DEAE anion exchange column using 500 mM NaCl, 5 mM KPi, pH 7.2 buffer and loaded onto a TALON (Clontech, Mountain View, CA) metal ion affinity column. Column was washed with 5 mM KPi, pH 7.2 buffer before elution of shAOC3 using 150mM imidazole, 5 mM KPi, pH 7.2 buffer. Fractions were run on a 10% acrylamide SDS-PAGE gel for identification of those containing shAOC3.

Determination of TPQ Content. The TPQ content of shAOC3 was determined using phenylhydrazine in 50 mM KPi, pH 6.5 [37], at room temperature by measurement of the change in absorbance at $\lambda = 448$ nm with and without phenylhydrazine using $\varepsilon = 40500$ $M^{-1}cm^{-1}$. This extinction coefficient was determined for copper amine oxidase expressed by the yeast, *Hansenula polymorpha* [cf. 37]. The concentration of enzyme monomer was determined by Bradford assay (Bio-rad Protein Assay) using bovine albumin, fraction V (Pierce, Rockford, IL) standard and MW per monomer of 84622.

Purified soluble human AOC3 benzylamine activity. The benzylamine substrate was dissolved in 50 mM KPi, pH 6.5 at a concentration of 2 mM. Substrate was blanked in a Cary 50 Bio UV Vis spectrophotometer (Varian, Palo Alto, CA) before addition of either 3 uL or 6 uL purified protein to initiate reaction. Total substrate buffer volume was 110 uL. Benzaldehyde product formation was monitored at absorbance $\lambda = 250$ nm ($\varepsilon = 13800$ $M^{-1}cm^{-1}$ [38]) for one minute.

Steady-State Kinetics. Steady-state kinetic measurements were carried out by monitoring oxygen consumption using a Clark electrode and YSI Model 5300 Biological Oxygen Monitor. A final volume of 1 mL 500 mM KPi, pH 7.4 at 37°C containing variable amounts of substrate, with reaction initiated by addition of shAOC3. For determination of k_{cat} and K_m, the oxygen concentration was kept constant at 211 uM. Data were fitted to Michaelis-Menten equation, and k_{cat} was calculated using the active protein concentration as determined by phenylhydrazine assay.

Whole cell 3T3-L1 adipocytes kinetics. 3T3-L1 adipocytes were cultured (as previously described) in 24-well plates. Kinetic experiments were performed on Day 8 – 10 differentiated adipocytes either passage 1 or 2. Prior to the experiment, cells were washed twice with warmed PBS and once with warmed DMEM + 10% FBS. Only wells fully populated by adipocytes were used. Adipocytes were then incubated in 500 uL DMEM + 10%FBS and all cells treated with 0.33 mM clorgyline (Sigma) and 3.33 mM L-deprenyl (Sigma). In the set of control experiments, adipocytes were also treated with 1 mM semicarbazide. Cells were incubated with inhibitors for 30 minutes at 37°C and 5% CO_2. After incubation, cells were washed twice with warmed Krebs Ringer Phosphate (KRP) buffer (145 mM NaCl, 5.7 mM sodium phosphate, 4.86 mM KCl, 0.54 mM $CaCl_2$, 1.22 mM $MgSO_4$, 5.5 mM glucose, pH 7.35). A coupled enzymatic reaction involving horseradish peroxidase (HRP) and Amplex Red was used to detect H_2O_2 produced upon substrate turnover. Upon final addition of 500 uL KRP buffer containing 50 uM

Amplex Red reagent and 0.1 U/mL HRP, isoamylamine (from 125 uM – 8 mM) was added to wells pre-incubated either with or without SC inhibitor. All procedures involving Amplex Red was performed in the dark as it is photo-oxidizable. Envision Multilabel Reader with a 570nm optical filter (Perkin Elmer, Waltham, MA) was used to determine the absorbance of oxidized Amplex Red. Measurements were taken every 3 minutes for 30 minutes at 37°C. A H_2O_2 standard curve was performed in KRP using $0 - 32$ uM stabilized H_2O_2 provided with the Amplex Red kit.

Results

Untagged soluble mouse AOC3 (mAOC3) was previously expressed in our lab using s2 Drosophila cell expression system. Comparing mouse and human AOC3 amino acid sequences show that they are 82.9% identical, 90.8% similar, with almost identical pI.   This suggests that human AOC3 may be purified by the same procedure. The soluble portion of mouse AOC3 (without residues $1 - 27$ corresponding to the transmembrane domain) was purified by two column chromatography steps, DEAE anion exchange followed by gel-filtration. The soluble portion of human AOC3 (residues $28 - 763$) was cloned into an inducible s2 expression plasmid and co-transfected with pCoHygro selection plasmid into s2 cells. Ratios by weight of expression and selection plasmids were tested for optimal yield of stable co-transfectants. Expression plasmid to selection plasmid ratios of 30:1, 25:1, and 19:1 were tested, with 19:1 found to work most efficiently. Stable s2 cells lines can contain multiple copies of the introduced genes, with more than $500 - 1000$ copies in a head to tail fashion [39]. However, expressed protein levels were low as determined by gel electrophoresis, so a more facile co-transfection system involving Cellfectin, a cationic-lipid formulation designed for insect cell transfections, was tested, though yields were actually worse.

The expression plasmid contains a 5' BiP secretion signal which allows the expressed protein to be secreted into the cell media upon induction. s2 cells were induced with $CuSO_4$ ranging from 100 uM – 1 mM, with 600 uM found to be optimal [40] over the induction period. Other metals, including cadmium, were used to determine if expressed protein yield could be higher. However, 10 uM $CdCl_2$ [41] did not result in an increased yield compared to 600 uM $CuSO_4$. Cell counts were taken prior to and after induction with 600 uM $CuSO_4$ to determine whether the relatively large metal concentration would be toxic to the cells. Doubling time over the induction period of 3 days were found to be consistent with that found during normal culture condition, without a concomitant increase in dead cells, as determined by Trypan blue.

Prior to secretion of expressed hAOC3, the BiP secretion signal is cleaved [42]. AOC3 can thus be purified from the cell culture media, with the s2 cells discarded after each induction. After the media was concentrated and dialyzed, the media was loaded either by direct application onto a DEAE anion exchange column or by batch binding. Batch binding combines both dialysis (by equilibrating pH and ion concentrations of the raw cell media to the loading buffer) and binding of proteins to the anion exchange resin. However, batch binding was not found to be effective due to the low level of expressed AOC3 in the starting raw media.

A SDS-PAGE gel of individual fractions collected after direct application of raw media to a DEAE anion exchange column is shown in Figure 1. Lanes $2 - 9$ show bands corresponding to where hAOC3 monomer would be expected, at approximately 90 kDa. Fractions corresponding to these lanes were collected, concentrated, and loaded onto a gel filtration column, with a gel of the resulting fractions shown in Figure 2. Lanes $2 - 5$ show bands corresponding to hAOC3, with a prominent band in Lane 4, though with significant contamination particularly at approximately 116 kDa. In order to assess whether these expected bands correspond to hAOC3, an immunoblot of fractions suspected of containing hAOC3 from the DEAE and gel filtration columns was run with a monoclonal antibody against hAOC3. The results are shown in Figure 3. Lanes $1 - 5$ correspond to fractions from the gel filtration column while Lanes $7 - 11$ correspond to fractions from DEAE anion exchange, confirming that the band at approximately 90 kDa is in fact hAOC3. Fractions from DEAE anion exchange show a much higher signal for

hAOC3 due to the 10 – 15 fold concentration of fractions while fractions from gel filtration were not concentrated. Unfortunately, at this early stage of purification, experiments to determine enzyme activity specific to AOC3 were found to be inconclusive. The purification protocol was reproduced several times with the same result, signaling that purification of hAOC3 could not be accomplished simply by following the protocol for purification of mouse AOC3.

Rather than use DEAE anion exchange, a stronger anion exchanger, Q-Sepharose, was pursued next with resulting fractions shown in Figure 4. Lanes 9 – 15 show bands corresponding to hAOC3. However the contaminant at 116 kDa remains quite prominent and inseparable by gel filtration. The pH of the running buffer was increased from pH 7.2 to pH 8.0 in hopes that a more anionic character of hAOC3 would result without a commensurate change in the protein contaminants, allowing for stronger interaction with the anion exchange resin. This condition was used for both the Q-Sepharose and DEAE anion exchange columns, with results for the latter shown in Figure 5. The increase in pH did not seem to affect hAOC3 and the contaminant disproportionately. Higher pH was not investigated in the interest of maintaining hAOC3 stability.

Due to the difficulty of purifying untagged hAOC3, an approach involving the use of a 6x histidine tag at the C-terminus was tried. The soluble portion of hAOC3 was cloned into the s2 expression plasmid, taking advantage of the nucleotide sequence coding for a 6x His-tag already placed at the C-terminus in the expression plasmid. An immunoblot of test expressions from successfully selected stable transfections is shown in Figure 6. Lane 1 corresponds to the empty expression plasmid transfection, while Lanes 2- 4 were from three different stable transfections. Transfectant 4 shows a faint band corresponding to hAOC3 and this transfectant was selected to express His-tagged hAOC3. hAOC3 was expressed and the cell media loaded onto a DEAE anion exchange column in order to wash away residual $CuSO_4$ that could interfere with the metal ion affinity chromatography. Figure 7 show the fractions that came off the DEAE wash, with faint bands corresponding to AOC3 in Lane 12. Fractions suspected of containing hAOC3 were pooled and loaded onto TALON column and protein eluted with 150 mM imidazole; the resulting fractions were run on a protein gel as shown in Figure 8. Lane 1 corresponds to the fractions that were pooled from the EDTA wash and show a faint band corresponding to hAOC3. No hAOC3 eluted off the column during the 5 mM KPi, pH 7.2 wash of the TALON column as shown in Lane 2. However, looking at the fractions collected after elution by imidazole, no fractions seem to contain hAOC3. This result could be due to poor expression of His-tagged hAOC3 by s2 cells and/or the possibility that the His tag is not solvent exposed for proper binding to metal ions.

The original untagged hAOC3 had been shown to be expressed in relatively high quantity by the original stably transfected s2 cells and another approach involving ammonium sulfate precipitation was tried as a possible initial step in the purification. Protein precipitation is one of the four most used approaches to protein purification [43]. Precipitation of raw media secreted from induced s2 cells was initiated by addition of 7.06 – 70.6 g ammonium sulfate/ 100 mL of media. Figure 9 show the results of the precipitation. Lane 1 shows that hAOC3 was expressed by the s2 cells, though there is no appearance of hAOC3 in any of the trial precipitations as seen in Lanes 4 – 17.

An approach to purify untagged hAOC3 using cation exchange, rather than anion exchange, was attempted. The theoretical pI of soluble hAOC3 was calculated to be approximately 6.0 (ExPASy Proteomics Server's Compute pI/MW tool at http://ca.expasy.org/ tools/pi_tool.html) which deterred an initial attempt using cation exchange as buffer pH below 6 could destabilize

the protein. Since actual and theoretical pI may not be similar, initial attempts to purify hAOC3 using cation exchange was attempted at pH 6.5. A series of gradients were used to elute the enzyme ranging from 10 mM KPi, pH 6.5/100 mM NaCl, 10 mM KPi, pH 6.5 gradient to 10 mM KPi, pH 6.5/500 mM NaCl, 10 mM KPi, pH 6.5. Figure 10 shows the results of these gradients in Lanes 4 – 8. In Lane 5, a band corresponding to hAOC3 is prominent without a contaminating band at 116 kDa. Using a 10 mM KPi, pH 6.5/250 mM NaCl, 10 mM KPi, pH 6.5 gradient, after loading raw cell media, fractions eluted off the cation exchange were run on a gel as shown in Figure 11. Lanes 12 – 26 show bands corresponding to hAOC3, with the decision to restrict collection to Lanes 12 – 20, which were collected and concentrated for loading onto the gel filtration column. The fractions eluted from the gel filtration column were run on a gel as shown in Figure 12, with Lanes 6 – 18 all showing hAOC3 bands. Only fractions corresponding to Lanes 9 – 15 were collected and concentrated as pure hAOC3. Using cation exchange rather than anion exchange essentially eliminated contaminating proteins that were inseparable by gel filtration, allowing hAOC3 to be purified.

Purified hAOC3 was first characterized for activity using 2 mM benzylamine as substrate and monitoring for the production of benzaldehyde using UV-Vis spectroscopy at $\lambda = 250$ nm. Since the K_m of benzylamine for mouse AOC3 was found to be 49 uM and with significant homology to human AOC3, 2 mM benzylamine should correspond to roughly 40 K_m, saturating the enzyme without high background absorbance as shown in Figure 13. Doubling the amount of enzyme used to initiate the amine oxidation reaction resulted in an approximate doubling of the rate of reaction. In addition, purified enzyme incubated with 100 uM semicarbazide inhibitor for 5 minutes prior to scanning for activity did not result in an increase of benzaldehyde product when the reaction was initiated by benzylamine rather than enzyme addition. These observations verify that hAOC3 with enzymatic activity has been successfully purified. Using a Bradford assay with serum albumin as the standard, approximately 240 ug – 720 ug of purified hAOC3 was isolated per 1.5L of s2 cells, resulting in a total protein of 160 ug – 480 ug of purified protein per liter of cells, about the same yield as the purification involving HEK293T cells. However, one major advantage of the s2 purification protocol is the ability to purify the protein without using a protein tag and the culturing of s2 cells is relatively easier than HEK293T. The specific activity was determined to be approximately 46.2 nmol/mg of monomer/min, as there are two catalytic subunits per hAOC3 homodimer. The concentration of active monomer was determined using phenylhydrazine assay. The quinone moiety of the AOC3 active site cofactor, 2,4,5-trihydroxyphenylalamine quinone (TPQ) can be derivatized using the carbonyl reagent phenylhydrazine and the resulting hydrazone product formation can be monitored by absorbance at $\lambda = 448$ nm [44]. From the phenylhydrazine assay shown in Figure 14, the percent of active protein was determined to be approximately 6.1%. Correcting for the active portion of total protein purified, the specific activity was found to be approximately 760 nmol/mg of monomer/min. Since the biogenesis of TPQ requires copper [45], spiking the purified protein with sub-stoichiometric amounts of $CuCl_2$ could increase the percent of active protein. However, upon incubation with $CuCl_2$, specific activity actually decreased with precipitation observed.

A complete substrate profile of human AOC3 was undertaken with the purified enzyme. The rate of oxidation of various primary amines was monitored by measuring oxygen consumption at 37°C, pH 7.4 and an ionic strength of 1.4M. A high ionic strength was maintained so that addition of substrates up to 38.4 mM would not have a significant effect on ionic strength. In addition, comparison of kinetic rates for various amine substrates at an ionic

strength of 0.13M vs. 1.4M did not show a significant difference, indicating little impact on rate due to the higher ionic strength. Figure 15 A-H shows the steady state rates of substrate oxidation with data fitted to the Michaelis-Menton equation. The corresponding values of k_{cat} and K_m are shown in Table 1. The best substrate in terms of K_m and k_{cat}/K_m is benzylamine at 84 uM and 4×10^4 $s^{-1}M^{-1}$ respectively. Methylamine, phenethylamine, and L-lysine can be found endogenously but all exhibit high K_m values ranging from 652 uM to 3.4 mM, concentrations that would not be expected to occur physiologically. k_{cat}/K_m for these substrates range from $2.05 - 8.58 \times 10^3$ $s^{-1}M^{-1}$. With regard to alkylamines, as the length of alkane chain increases, K_m tends to increase, with the exception of ethylamine, which has a relatively high K_m of 12.8 mM; once again k_{cat}/K_m decreased, with the exception of ethylamine. In terms of the branched chain amines, both isoamylamine and isobutyamine have relatively high K_m values at 4.5 mM and 3.4 mM, respectively. In terms of K_m and k_{cat}/K_m, isobutylamine is a better substrate than isoamylamine. Isopropylamine was not found to be a substrate of hAOC3.

From the substrate profile, human AOC3 is a relatively promiscuous enzyme, making the search for its endogenous substrate(s) more difficult. Conformational diversity and flexibility of the enzyme play an important role in enzymes' ability to catalyze reactions with multiple substrates [46]. For example, conformational diversity of the active site is thought to be important in the ability of both glutathione S-transferase [47] and cytochrome P450 [48] to exhibit substrate promiscuity. Noncovalent interactions between substrate and enzyme are important factors in the formation of the ES complex and contribute to catalysis. Hydrophobic interactions are one major contributor to enzyme-substrate recognition [49]. Catalytic efficiency of several promiscuous enzymes, such as a microbial lactonase [50], was shown to exhibit a dependence on substrate hydrophobicity. For each amine substrate, log P, the logarithm of the partition coefficient between n-octanol and water (log $\frac{C(octanol)}{C(water)}$), was calculated computationally [51]. A plot of log (k_{cat}/K_m) vs. log P for each substrate is plotted in Figure 16. There does not seem to be a correspondence between catalytic efficiency and hydrophobicity, disregarding the L-lysine outlier. There instead may be a relationship between substrate volume and catalytic efficiency. As shown in Figure 17, as the substrate volume increases, the catalytic efficiency decreases, as expected considering steric hindrance encountered by larger substrates. Since catalytic efficiency drops significantly with L-Lysine, 146 Å^3 may be the upper threshold of substrate volume.

With regard to the possibility of peptide-based substrates as a mediator of endothelial cell and leukocyte adhesion, L-lysine, D-Lysine, and the peptide, GGGGKGGGG, were investigated as possible substrates of hAOC3. While L-lysine is a poor substrate of hAOC3 with K_m = 346 mM and k_{cat}/K_m = 2.05 $s^{-1}M^{-1}$, neither D-lysine nor GGGGKGGGG were oxidized by hAOC3. This result suggests a low likelihood of a peptide-based hAOC3 substrate present on the outer surface of leukocytes, though a scaffolding effect could increase the local concentration of these substrates greatly and allow lysine to be a viable physiological substrate. Substrates not shown in the table were also studied, though they were either very weak substrates or not substrates at all. The two catecholamines, norepinephrine and dopamine, as well as tryptamine and octopamine, were not substrates. Histamine and tyramine were weak substrates with almost undetectable rate of oxidation at substrate concentrations of 38.4 mM. As expected, diamines, such as 1,3 diaminopropane, were not substrates of hAOC3. A comparison of k_{cat}/K_m between human and mouse AOC3 is shown in Figure 18 [data not shown, 54]. The second order rate constant is fairly similar between the two species, with the exception of methylamine, in which

the human enzyme is almost twelve times more efficient as the mouse, and cyclohexanemethylamine, in which the mouse enzyme is almost six times more efficient.

The substrate kinetic profile could be different between *in vitro* purified enzyme and the physiological setting of the enzyme. Therefore, the activity of AOC3 expressed on cultured 3T3-L1 mouse adipocytes was determined with isoamylamine as substrate. For the mouse AOC3, isoamylamine was found to be a good substrate with a K_m of 148 uM and k_{cat}/K_m of 4.9×10^3 s^{-1}M^{-1}. Cells were treated with or without semicarbazide inhibitor for 30 minutes and then incubated with various concentrations of isoamylamine substrate. Rather than oxygen consumption, H_2O_2 product formation was monitored by following the oxidation of Amplex Red dye, a commercially available compound used to quantify H_2O_2. The kinetic profile is shown in Figure 19. K_m, which is independent of enzyme concentration, was found to be approximately 432 uM. This compares favorably with the K_m found using purified mouse AOC3 monitoring oxygen consumption. Importantly, this activity demonstrates the presence of AOC3 on the extracellular surface of 3T3-L1 cultured adipocytes, a transformed cell line that may not exhibit the same protein expression profile as physiological adipocytes, known to express AOC3 highly.

Discussion

The human AOC3 enzyme was purified using a new purification protocol without utilizing GST-tagging or AOC3 monoclonal antibody affinity chromatography. The main advantages of this new protocol is the ability to use off-the-shelf commercial reagents without the need for complicating overhead of GST-tagging, that may not be completely cleaved after use [26]. In addition, the s2 cells are more tractable compared with mammalian cell lines in terms of maintenance and handling for expression without loss of critical posttranslational modifications. For example, passaging of s2 does not require trysinization while HEK293T, an adherent cell line, does. In addition, expression of hAOC3 using s2 cells involves 1.5L of raw cell media with cells growing up to a density of $22 - 25$ x 10^6 cells/mL while the other protocols can involve volumes up to 90L with adherent cells like HEK293T growing up to a density of 5.45 x 10^5 cells/cm^2 that can translate to only 1 x 10^6 cells/mL assuming a media volume height of 2 cm. Total hAOC3 enzyme expressed per unit volume would be expected to be less in HEK293T vs. s2 cells.

The purification of human AOC3 does not conform to the protocol for mouse AOC3 though there is significant homology between the two enzymes. After trying Q-Sepharose, a stronger anion exchanger, at both pH7.2 and pH8.0, there was no noticeable difference in eliminating contaminants that couldn't be separated using gel filtration. Both tagging hAOC3 with a 6x His in order to attempt purification using metal ion affinity chromatography and ammonium sulfate precipitation did not yield viable steps in purifying hAOC3. Finally, using a strong cation exchanger, SP Sepharose, with an elution gradient of 0/250 mM NaCl, 10 mM KPi, pH6.5 resulted in a viable separation that can ultimately be cleaned up after gel filtration. The purified enzyme was found to have benzylamine oxidase activity that depended on enzyme concentration, with activity absent after incubation of enzyme with semicarbazide. Using a phenylhydrazine assay, the percent of active protein was found to be approximately 6.1%. A total of 160 ug – 480 ug of hAOC3 was purified per liter of cells, closely matching but not superior to the 383 ug/L purified using GST-tagging. The specific activity was found to be 46.2 nmol/mg of monomer/min. When corrected for active monomers with TPQ cofactor, specific activity increased to 757.4 nmol/mg of monomer/min, closely agreeing with the specific activity reported in the GST-tagged expression using HEK293T cells of 809 nmol/mg of monomer/min [28]. However, a direct comparison of AOC3 specific activities corrected for active monomers is not possible. While a hydrazine derivatization of TPQ was reported in the GST-tagged purification, the actual percentage of active AOC3 after purification was not disclosed. In addition, though a characterization of the purified human AOC3 was reported, no substrate kinetic profile was reported.

Monitoring oxygen consumption using a Clark oxygen electrode, a substrate kinetic profile was determined for purified hAOC3. Prior experiments relied on enzymes expressed on various tissues or from AOC3-containing cell lysates to determine substrate kinetic profiles for substrates such as methylamine, benzylamine, and phenethylamine. There has not been a published substrate profile of purified human AOC3 with various primary amines ranging from metabolites such as methylamine to hormones and neuro-transmitters, such as epinephrine and dopamine. As shown in the table on the next page, comparing published data obtained from cell lysates containing AOC3, the K_m of methylamine was found to be 670 vs. our finding of 652 uM and the

Substrate	Cell lysate[b,c]	Crude adipocyte membrane[c,d]	Purified[a] human AOC3
Benzylamine	26.94[1]	456 (K_m = 175 uM)[3]	757 (K_m = 84.5 uM)
Methylamine	39 (K_m = 670 uM)[2]	-	K_m = 652 uM
Phenethylamine	17 (K_m = 1940 uM)[2]	-	K_m = 2050 uM

a – Enzyme activities reported in nmol/mg/min based on TPQ titer. Activity monitored by O_2 consumption
b – Enzyme activities reported in nmol H_2O_2/mg cell lysate/hr
c – Enzyme activities measured spectrophotometrically by H_2O_2 product formation
d – Enzyme activities reported in nmol H_2O_2/mg cell membrane/min
1 – Reference [55]
2 – Reference [52]
3 – Reference [53]

K_m of phenethylamine was found to be 1940 uM vs. our finding of 2050 uM [52]. The K_m of benzylamine determined by using crude membranes from human adipose tissue was found to be 175 uM [53] vs. our finding of 84.5 uM. The values of K_m found compares favorably with limited published data. Comparison of kinetic data for methylamine and phenethylamine was complicated by the use of cell lysates. Since AOC3 was not purified, values were reported in rate per mg of cell lysate, which is difficult to compare to our findings using purified enzyme. In addition, the kinetic parameters between the mouse [data not shown, 54] and human AOC3 were found to be similar. Hydrophobicity of the substrate did not seem to affect the catalytic efficiency of AOC3 while a three-fold increase in substrate volume decreased catalytic efficiency by approximately 31 fold. From whole cell kinetic analysis, cultured adipocytes were found to express AOC3 extracellularly with K_m for isoamylamine correlating closely with that found using purified enzyme, 432 uM vs. 148 uM.

References

1. Davis, E.J. and R.S. De Ropp, *Metabolic origin of urinary methylamine in the rat.* Nature, 1961. **190**: p. 636-7.
2. Schayer, R.W., R.L. Smiley, and E.H. Kaplan, *The metabolism of epinephrine containing isotopic carbon. II.* Journal of Biological Chemistry, 1952. **198**(2): p. 545-51.
3. Precious, E., C.E. Gunn, and G.A. Lyles, *Deamination of methylamine by semicarbazide-sensitive amine oxidase in human umbilical artery and rat aorta.* Biochem Pharmacol, 1988. **37**(4): p. 707-13.
4. Green, M.L. and W.H. Elliott, *The enzymic formation of aminoacetone from threonine and its further metabolism.* Biochem J, 1964. **92**(3): p. 537-49.
5. Lyles, G.A. and J. Chalmers, *The metabolism of aminoacetone to methylglyoxal by semicarbazide-sensitive amine oxidase in human umbilical artery.* Biochem Pharmacol, 1992. **43**(7): p. 1409-14.
6. O'Sullivan, J., et al., *Semicarbazide-sensitive amine oxidases: enzymes with quite a lot to do.* Neurotoxicology, 2004. **25**(1-2): p. 303-15.
7. Buffoni, F., *Semicarbazide-sensitive amine oxidases: some biochemical properties and general considerations.* Prog Brain Res, 1995. **106**: p. 323-31.
8. Olivieri, A., K. Tipton, and J. O'Sullivan, *L-lysine as a recognition molecule for the VAP-1 function of SSAO.* Journal of Neural Transmission, 2007. **114**(6): p. 747-749.
9. Wood, W.J.L., et al., *Iodothyronamines are Oxidatively Deaminated to Iodothyroacetic Acids in vivo.* Chembiochem, 2009. **10**(2): p. 361-365.
10. Jalkanen, S. and M. Salmi, *Cell surface monoamine oxidases: enzymes in search of a function.* Embo Journal, 2001. **20**(15): p. 3893-3901.
11. Yraola, F., et al., *New efficient substrates for semicarbazide-sensitive amine oxidase/VAP-1 enzyme: analysis by SARs and computational docking.* J Med Chem, 2006. **49**(21): p. 6197-208.
12. Bonaiuto, E., et al., *A structure-activity study to identify novel and efficient substrates of the human semicarbazide-sensitive amine oxidase/VAP-1 enzyme.* Biochimie, 2010.
13. Yraola, F., et al., *Structure-Activity Relationships of SSAO/VAP-1 Arylalkylamine-Based Substrates.* Chemmedchem, 2009. **4**(4): p. 495-503.
14. Salmi, M., et al., *A cell surface amine oxidase directly controls lymphocyte migration.* Immunity, 2001. **14**(3): p. 265-276.
15. Kivi, E., et al., *Human Siglec-10 can bind to vascular adhesion protein-1 and serves as its substrate.* Blood, 2009. **114**(26): p. 5385-5392.
16. Boomsma, F., et al., *Variation in semicarbazide-sensitive amine oxidase activity in plasma and tissues of mammals.* Comp Biochem Physiol C Toxicol Pharmacol, 2000. **126**(1): p. 69-78.
17. Andres, N., et al., *Tissue activity and cellular localization of human semicarbazide-sensitive amine oxidase.* J Histochem Cytochem, 2001. **49**(2): p. 209-17.
18. Stolen, C.M., et al., *Origins of serum semicarbazide-sensitive amine oxidase.* Circ Res, 2004. **95**(1): p. 50-7.
19. Lyles, G.A., *Substrate-specificity of mammalian tissue-bound semicarbazide-sensitive amine oxidase.* Prog Brain Res, 1995. **106**: p. 293-303.
20. Lyles, G.A., *Mammalian plasma and tissue-bound semicarbazide-sensitive amine oxidases: biochemical, pharmacological and toxicological aspects.* Int J Biochem Cell Biol, 1996. **28**(3): p. 259-74.
21. Salmi, M. and S. Jalkanen, *Cell-surface enzymes in control of leukocyte trafficking.* Nat Rev Immunol, 2005. **5**(10): p. 760-71.
22. Elliott, J., B.A. Callingham, and D.F. Sharman, *Semicarbazide-sensitive amine oxidase (SSAO) of the rat aorta. Interactions with some naturally occurring amines and their structural analogues.* Biochem Pharmacol, 1989. **38**(9): p. 1507-15.
23. Precious, E. and G.A. Lyles, *Properties of a semicarbazide-sensitive amine oxidase in human umbilical artery.* J Pharm Pharmacol, 1988. **40**(9): p. 627-33.
24. Lizcano, J.M., et al., *Several Aspects on the Amine Oxidation by Semicarbazide-Sensitive Amine Oxidase (Ssao) from Bovine Lung.* Journal of Neural Transmission-Supplement, 1994(41): p. 415-420.
25. Norqvist, A., L. Oreland, and C.J. Fowler, *Some Properties of Monoamine-Oxidase and a Semi-Carbazide Sensitive Amine Oxidase Capable of the Deamination of 5-Hydroxytryptamine from Porcine Dental-Pulp.* Biochemical Pharmacology, 1982. **31**(17): p. 2739-2744.

26. Kumazawa, T., H. Seno, and O. Suzuki, *Semicarbazide-Sensitive Amine Oxidase Activity in Catfish Tissues.* Comparative Biochemistry and Physiology B-Biochemistry & Molecular Biology, 1989. **92**(2): p. 347-349.

27. Jakobsson, E., et al., *Crystallization of a truncated soluble human semicarbazide-sensitive amine oxidase.* Acta Crystallographica Section F-Structural Biology and Crystallization Communications, 2005. **61**: p. 274-278.

28. Ohman, J., et al., *Production of a truncated soluble human semicarbazide-sensitive amine oxidase mediated by a GST-fusion protein secreted from HEK293 cells.* Protein Expression and Purification, 2006. **46**(2): p. 321-331.

29. Nymalm, Y., et al., *Crystallization and preliminary X-ray analysis of the human vascular adhesion protein-1.* Acta Crystallographica Section D-Biological Crystallography, 2003. **59**: p. 1288-1290.

30. Maula, S.M., et al., *Carbohydrates located on the top of the "cap" contribute to the adhesive and enzymatic functions of vascular adhesion protein-1.* Eur J Immunol, 2005. **35**(9): p. 2718-27.

31. Booth, R.E., S.A. Misquitta, and R.C. Bateman, Jr., *Human pituitary glutaminyl cyclase: expression in insect cells and dye affinity purification.* Protein Expr Purif, 2003. **32**(1): p. 141-6.

32. Olsen, M.K., et al., *Stable production of an analog of human tissue plasminogen activator from cultured Drosophila cells.* Cytotechnology, 1992. **10**(2): p. 157-67.

33. Prosise, W.W., et al., *Protease domain of human ADAM33 produced by Drosophila S2 cells.* Protein Expr Purif, 2004. **38**(2): p. 292-301.

34. Gardsvoll, H., et al., *Characterization of low-glycosylated forms of soluble human urokinase receptor expressed in Drosophila Schneider 2 cells after deletion of glycosylation-sites.* Protein Expr Purif, 2004. **34**(2): p. 284-95.

35. Percival, M.D., et al., *Investigation of human cyclooxygenase-2 glycosylation heterogeneity and protein expression in insect and mammalian cell expression systems.* Protein Expr Purif, 1997. **9**(3): p. 388-98.

36. Davidson, D.J. and F.J. Castellino, *Asparagine-linked oligosaccharide processing in lepidopteran insect cells. Temporal dependence of the nature of the oligosaccharides assembled on asparagine-289 of recombinant human plasminogen produced in baculovirus vector infected Spodoptera frugiperda (IPLB-SF-21AE) cells.* Biochemistry, 1991. **30**(25): p. 6165-74.

37. Welford, R.W., et al., *Partial conversion of Hansenula polymorpha amine oxidase into a "plant" amine oxidase: implications for copper chemistry and mechanism.* Biochemistry, 2007. **46**(38): p. 10817-27.

38. Ucar, G., et al., *Elevated semicarbazide-sensitive amine oxidase (SSAO) activity in lung with ischemia-reperfusion injury: protective effect of ischemic preconditioning plus SSAO inhibition.* Life Sci, 2005. **78**(4): p. 421-7.

39. Lee, J.M., et al., *Expression and immunogenicity of recombinant polypeptide VPI of human hepatitis A virus in stably transformed fruitfly (Drosophila melanogaster) Schneider 2 cells.* Biotechnology and Applied Biochemistry, 2009. **53**: p. 101-109.

40. Tota, M.R., et al., *Interaction of [Fluorescein-Trp(25)]Glucagon with the Human Glucagon Receptor Expressed in Drosophila Schneider-2 Cells.* Journal of Biological Chemistry, 1995. **270**(44): p. 26466-26472.

41. Johansen, H., et al., *Regulated Expression at High Copy Number Allows Production of a Growth-Inhibitory Oncogene Product in Drosophila Schneider Cells.* Genes & Development, 1989. **3**(6): p. 882-889.

42. Rubin, D.M., et al., *Genomic Structure and Sequence-Analysis of Drosophila-Melanogaster Hsc70 Genes.* Gene, 1993. **128**(2): p. 155-163.

43. Moore, P.A. and V. Kery, *High-throughput protein concentration and buffer exchange: comparison of ultrafiltration and ammonium sulfate precipitation.* Methods Mol Biol, 2009. **498**: p. 309-14.

44. Cai, D. and J.P. Klinman, *Copper amine oxidase: heterologous expression, purification, and characterization of an active enzyme in Saccharomyces cerevisiae.* Biochemistry, 1994. **33**(24): p. 7647-53.

45. Brazeau, B.J., B.J. Johnson, and C.M. Wilmot, *Copper-containing amine oxidases. Biogenesis and catalysis; a structural perspective.* Arch Biochem Biophys, 2004. **428**(1): p. 22-31.

46. Nobeli, I., A.D. Favia, and J.M. Thornton, *Protein promiscuity and its implications for biotechnology.* Nature Biotechnology, 2009. **27**(2): p. 157-167.

47. Hou, L., et al., *Functional promiscuity correlates with conformational heterogeneity in A-class glutathione S-transferases.* Journal of Biological Chemistry, 2007. **282**(32): p. 23264-23274.

48. Skopalik, J., P. Anzenbacher, and M. Otyepka, *Flexibility of human cytochromes P450: Molecular dynamics reveals differences between CYPs 3A4, 2C9, and 2A6, which correlate with their substrate preferences.* Journal of Physical Chemistry B, 2008. **112**(27): p. 8165-8173.

49. Blokzijl, W. and J.B.F.N. Engberts, *Hydrophobic Effects - Opinions and Facts.* Angewandte Chemie-International Edition, 1993. **32**(11): p. 1545-1579.

50. Afriat, L., et al., *The latent promiscuity of newly identified microbial lactonases is linked to a recently diverged phosphotriesterase.* Biochemistry, 2006. **45**(46): p. 13677-13686.

51. Chuman, H., *Toward basic understanding of the partition coefficient log P and its application in QSAR.* Sar and Qsar in Environmental Research, 2008. **19**(1-2): p. 71-79.

52. Kaitaniemi, S., et al., *The unique substrate specificity of human AOC2, a semicarbazide-sensitive amine oxidase.* Cell Mol Life Sci, 2009. **66**(16): p. 2743-57.

53. Marti, L., et al., *Exploring the binding mode of semicarbazide-sensitive amine oxidase/VAP-1: identification of novel substrates with insulin-like activity.* J Med Chem, 2004. **47**(20): p. 4865-74.

54. Diana Wertz, *unpublished data*.

55. Smith, D.J., et al., *Cloning of vascular adhesion protein 1 reveals a novel multifunctional adhesion molecule.* J Exp Med, 1998. **188**(1): p. 17-27.
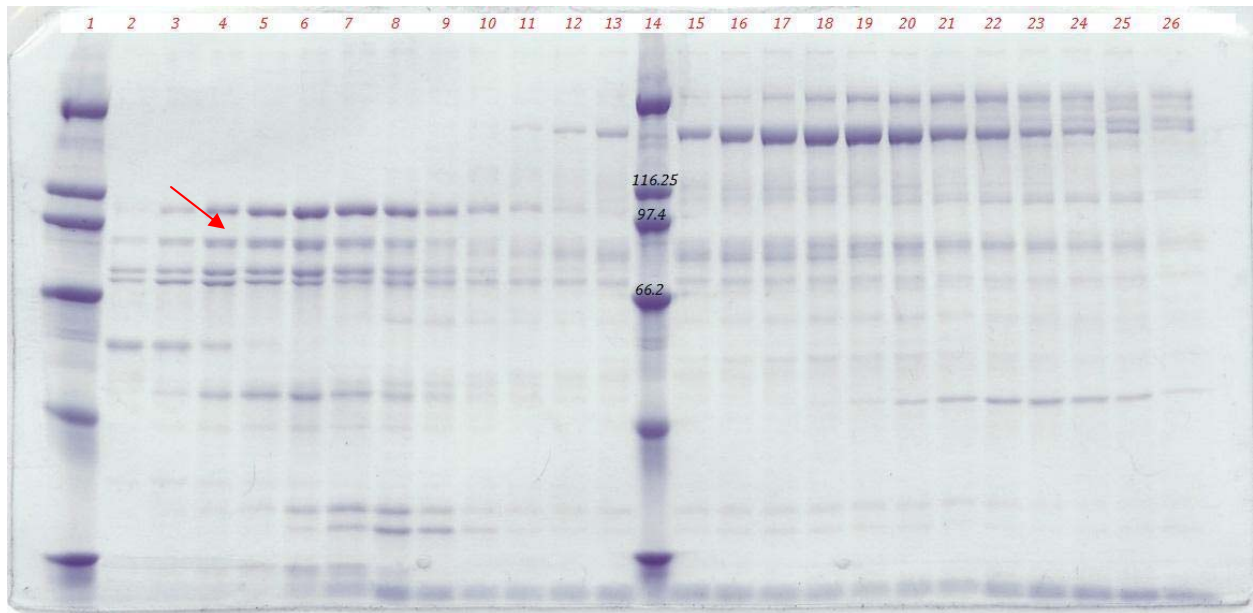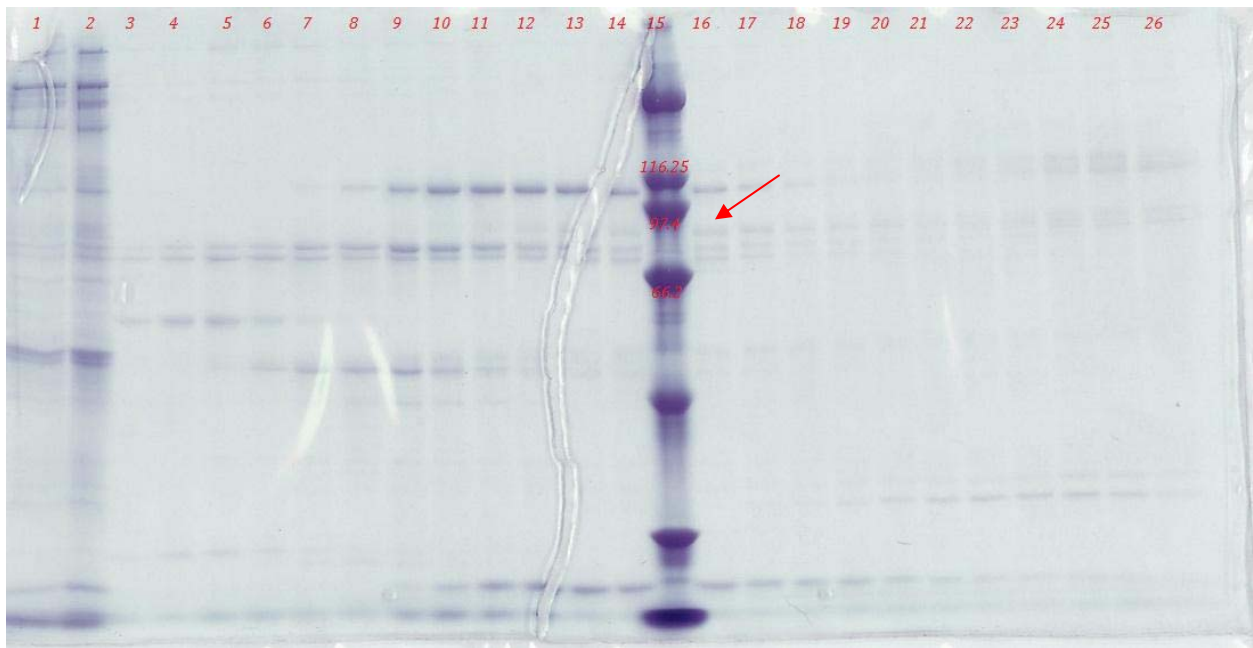
Figure 3.1- SDS-PAGE gel of fractions after DEAE anion exchange column. Column equilibrated at pH 7.2 Lanes 4 – 8 show human AOC3 monomer at approximately 90 kDa. Protein ladder standards are in lanes 1 and 14. Red arrow shows band corresponding to AOC3.
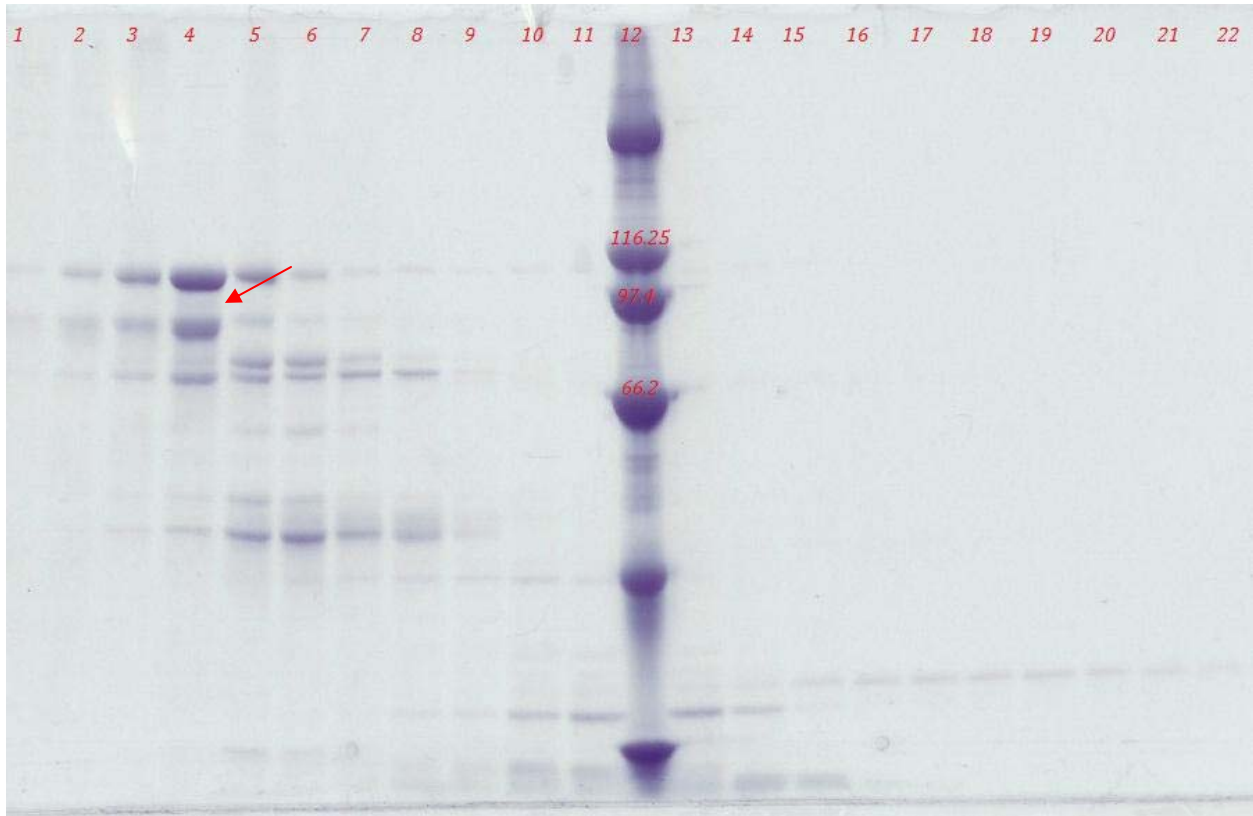
Figure 3.2- SDS-PAGE gel after gel filtration column. Lanes 2 – 4 show human AOC3 monomer at approximately 90 kDa. Protein ladder standard is shown in Lane 12. Red arrow shows band corresponding to AOC3.
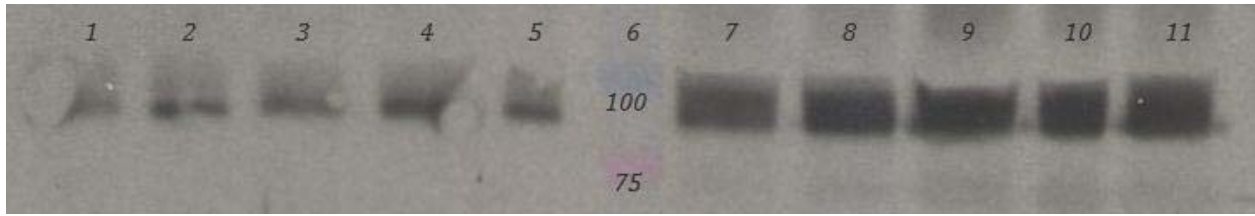
Figure 3.3- Immunoblot of fractions from DEAE and gel filtration columns. Lanes 1 – 5 correspond to gel filtration fractions much like Lanes 2 – 6 in Figure 2 transferred to nitrocellulose membrane. Lanes 7 – 11 correspond to DEAE anion exchange fractions much like Lanes 4 – 8 in Figure 1 transferred to nitrocellulose membrane. All bands correspond to AOC3 as control lanes did not produce a signal.
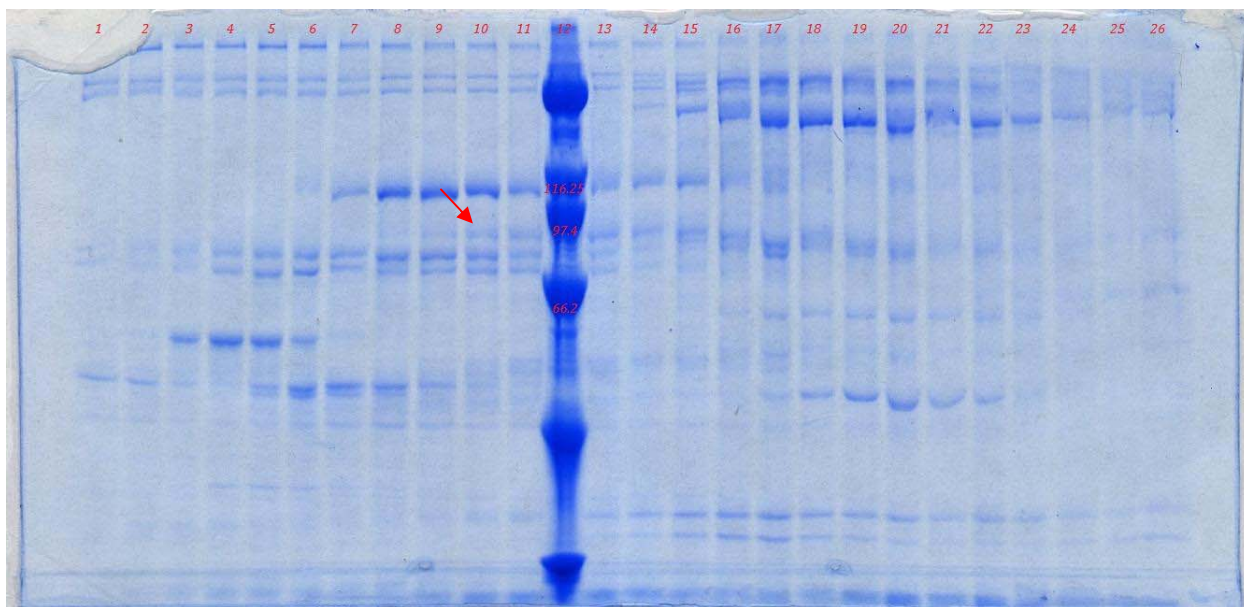
Figure 3.4- SDS-PAGE gel of fractions after Q-Sepharose anion exchange column. Lanes 9 – 11 and 13 – 15 show human AOC3 monomer at approximately 90 kDa. Protein ladder standard is in lane 12. Red arrow shows band corresponding to AOC3.

Figure 3.5- SDS-PAGE gel of fractions after DEAE anion exchange column. Column equilibrated at pH 8.0 Lanes 13 - 14 and 16 – 18 show human AOC3 monomer at approximately 90 kDa. Protein ladder standard is in lane 15. Red arrow shows band corresponding to AOC3.
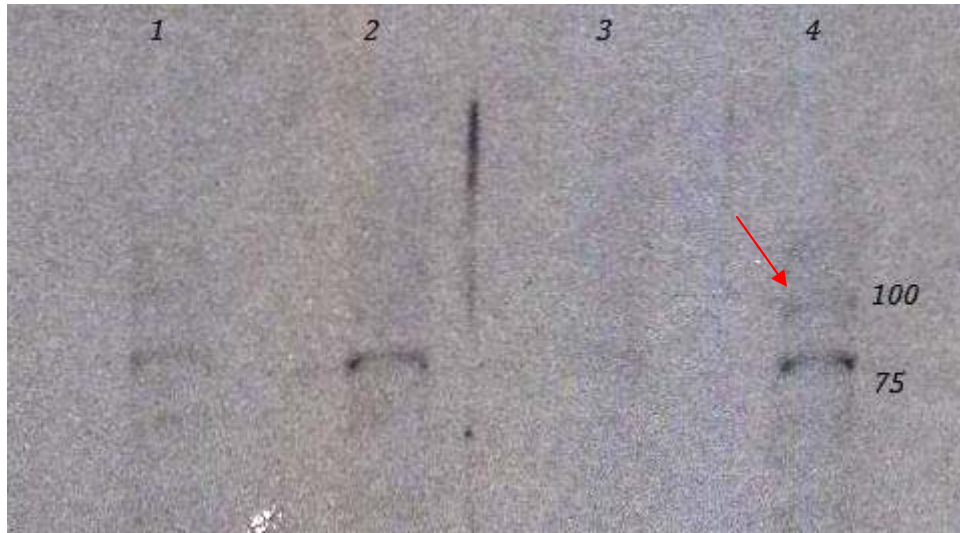
Figure 3.6- Immunoblot of test expressions from 4 successful His-tagged shAOC3 transfections. Lane 1 corresponds to empty expression plasmid transfection, while Lanes 2 – 4 correspond to three successfully selected s2 cell lines after transfection. Lane 2 and 4 shows a band at approximately 80 kDa that could correspond to shAOC3, though control Lane 1 also show a faint band at that location.
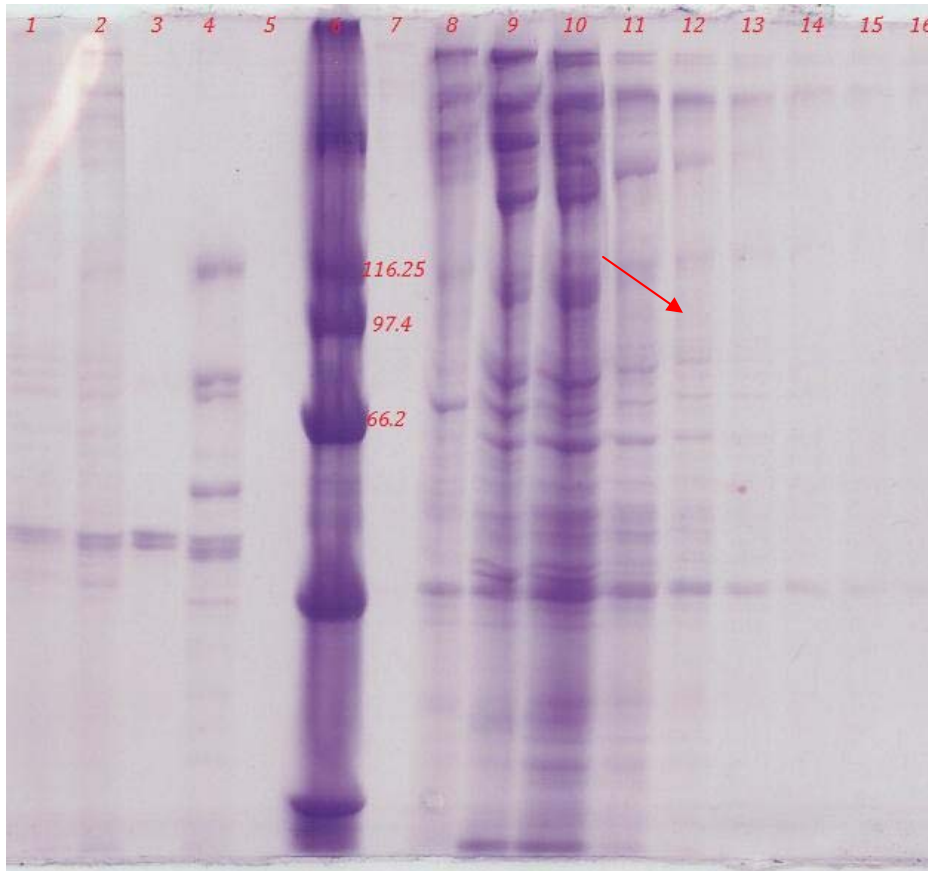
Figure 3.7- SDS-PAGE gel of fractions after DEAE anion exchange column flushed with 0.5M EDTA, pH 7.2 Lane 12 and 13 has a very faint band corresponding where shAOC3 should appear. Lanes 8 – 14 were combined to be loaded onto Talon column. Raw media was loaded in Lane 1, dialyzed media loaded in Lane 2, load flow-through loaded in Lane 3, EDTA wash flow-through loaded in Lane 4. Fractions loaded from Lanes 7 – 16. Red arrow shows band corresponding to possible AOC3.
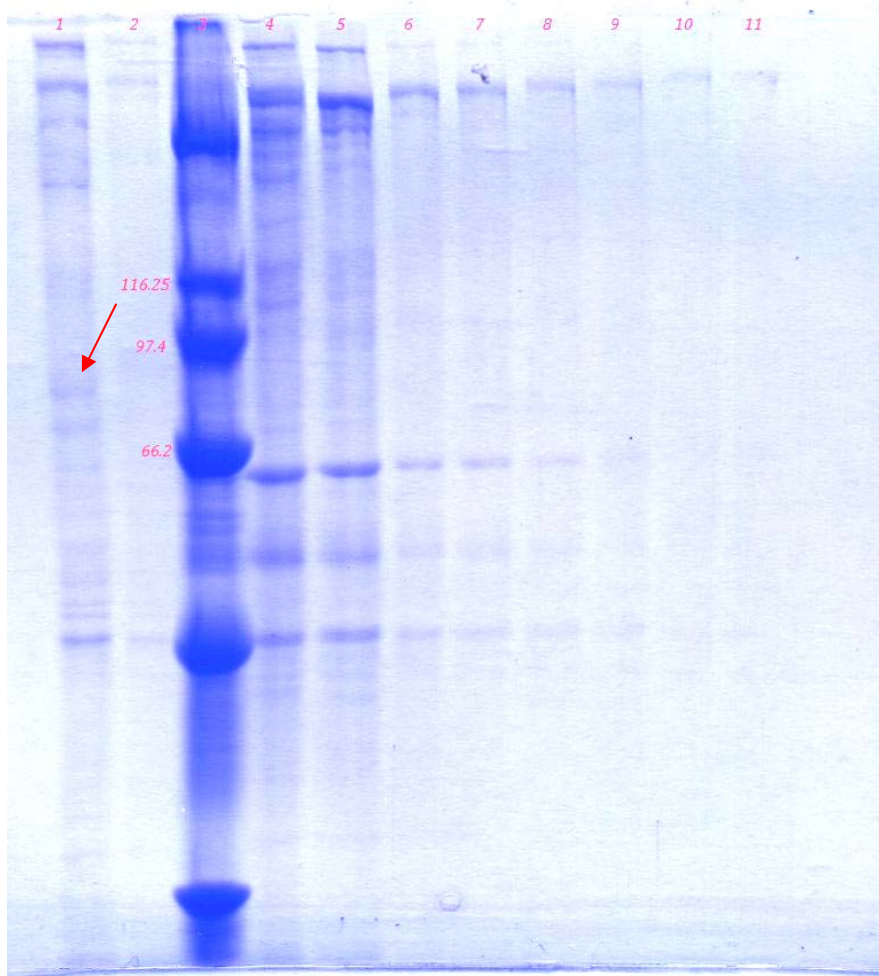
Figure 3.8- SDS-PAGE gel of fractions after TALON column eluted with 150 mM imidazole. Lane 1 corresponds to loading eluant after EDTA wash. Lane 2 is the eluant from the wash step.   Lanes 4 – 11 were fractions eluted using imidazole buffer. Red arrow shows where AOC3 should be found.
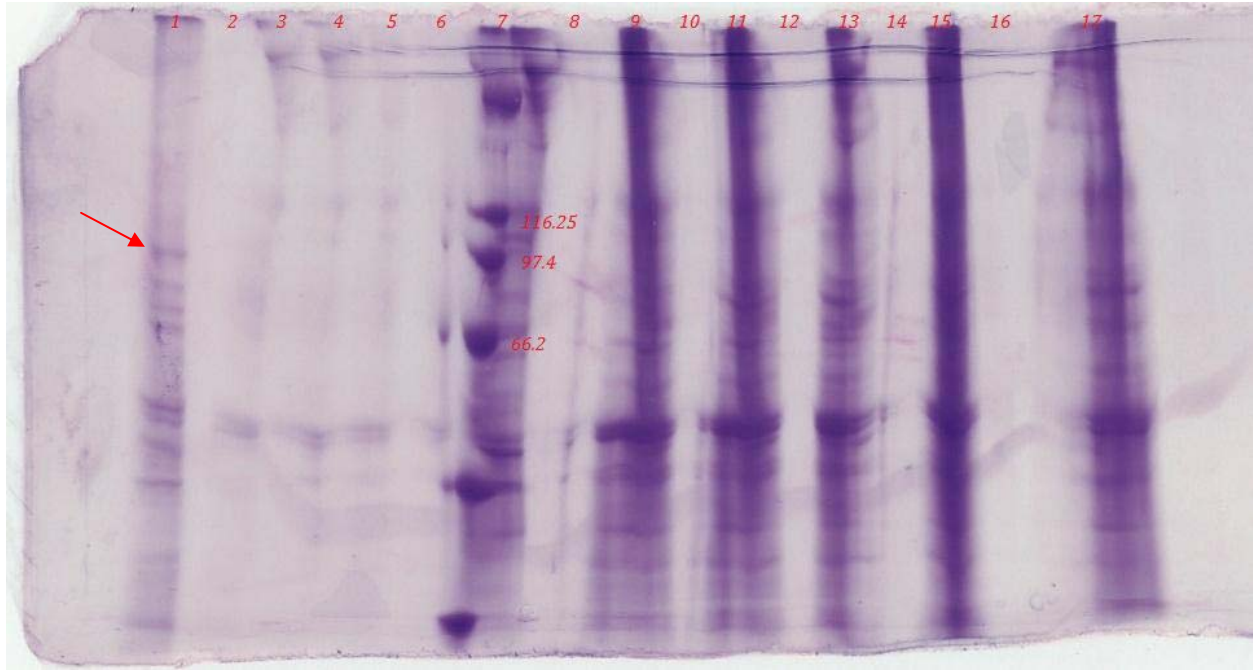
Figure 3.9- Ammonium sulfate precipitation of raw media containing shAOC3. Ammonium sulfate solubility at 0°C is 70.6 g/ 100 mL of water. Raw media precipitated 10% - 80% saturated solution of ammonium sulfate. Red arrow shows band corresponding to AOC3. All samples were precipitates redissolved in sample buffer. Supernatants were also loaded onto gel, but after concentration, did not exhibit a band corresponding to AOC3.

Lane 1 – AOC3 from lysed s2
Lane 4 – 10% saturated $(NH4)_2SO_4$
        (7.06 g/ 100 mL)
Lane 5 – 20% saturated
        (14.12 g/ 100 mL)
Lane 6 – 30% saturated

Lane 7 – Protein standard ladder
Lane 9 – 40% saturated
Lane 11 – 50% saturated
Lane 13 – 60% saturated
Lane 15 – 70% saturated
Lane 17 – 80% saturated
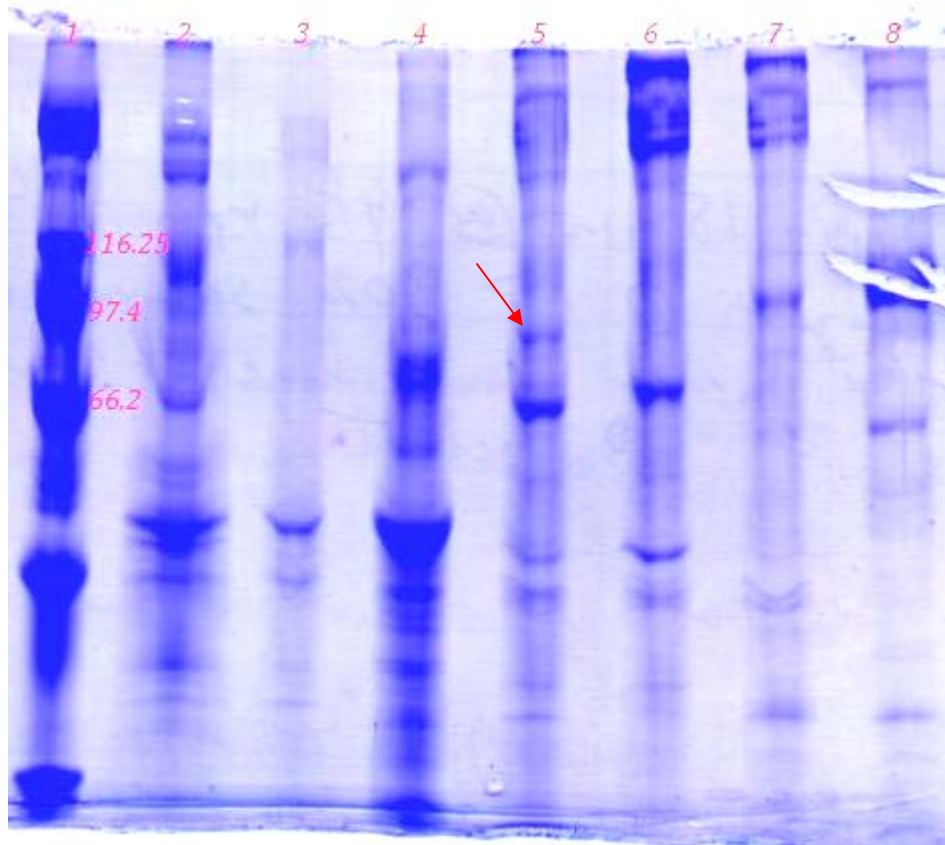
Figure 3.10- Step gradients of cation exchange at pH 6.5 Lane 1 is the ladder; Lane 2 and 3 were the load and wash (0 uM NaCl) flow-through respectively; Lane 4 is elution with 100 mM NaCl; Lane 5 is elution with 200 mM NaCl; Lane 6 is elution with 300mM NaCl; Lane 7 is elution with 400 mM NaCl; Lane 8 is elution with 500mM NaCl. Red arrow points to shAOC3 eluted with 200 mM NaCl.
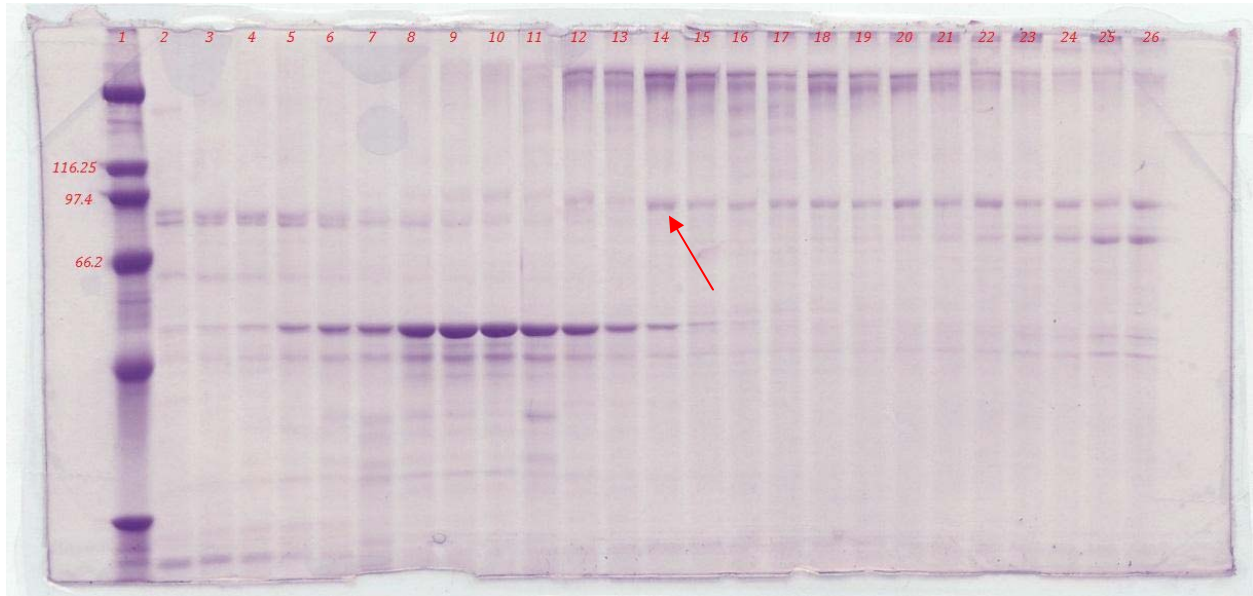
Figure 3.11- SDS-PAGE gel of fractions after SP Sepharose cation exchange. Column equilibrated at pH 6.5. Lanes 14 – 22 all containing AOC3 were combined, concentrated, and loaded onto gel filtration column. Red arrow shows band corresponding to AOC3.
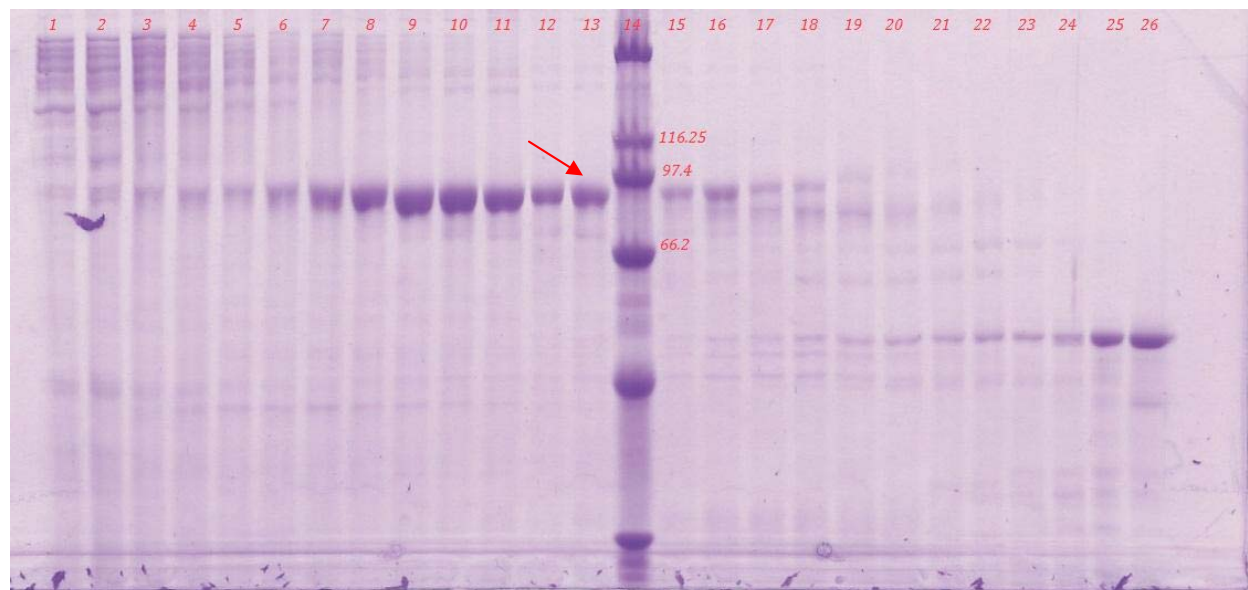
Figure 3.12- SDS-PAGE gel after gel filtration. Lanes 2 – 18 all show AOC3, however only fractions corresponding to lanes 9 – 15 (excluding ladder) were selected, concentrated, and used as purified AOC3. Red arrow points to band corresponding to AOC3.
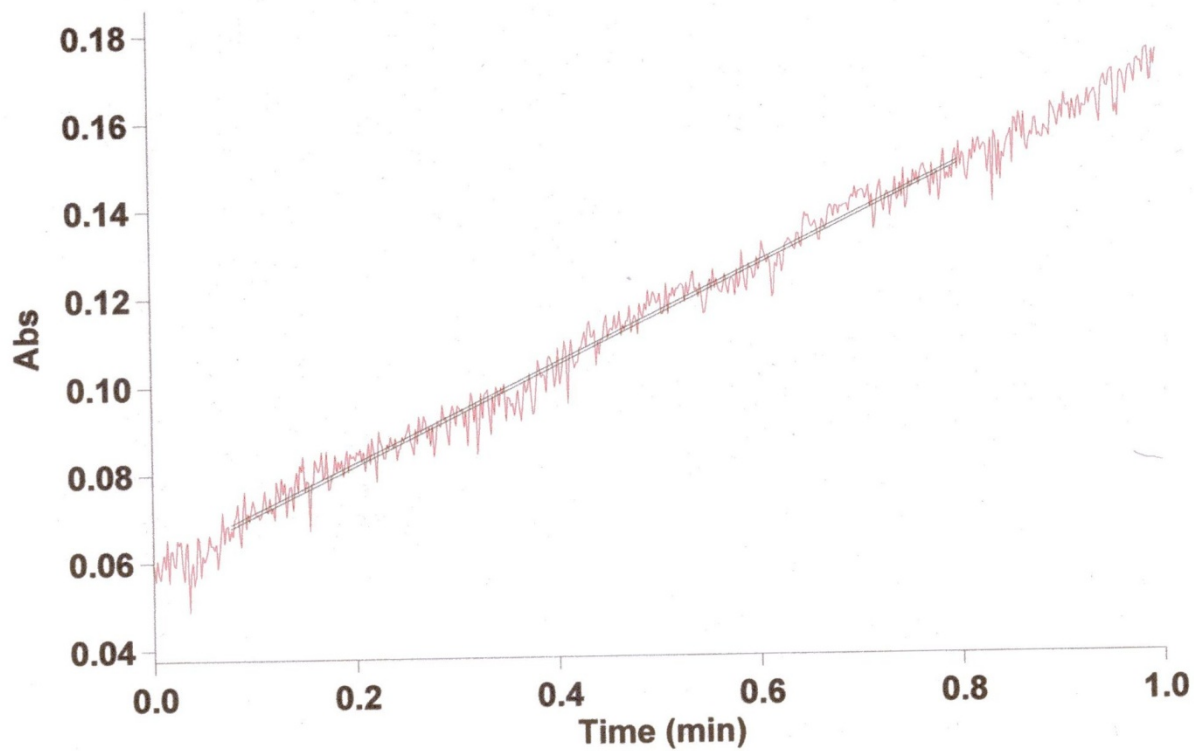
Figure 3.13- Benzylamine activity with purified soluble human AOC3. 2 mM benzylamine substrate is blanked prior to addition of purified hAOC3 to initiate reaction and benzaldehyde product is monitored at absorbance of λ = 250 nm for 1 minute.
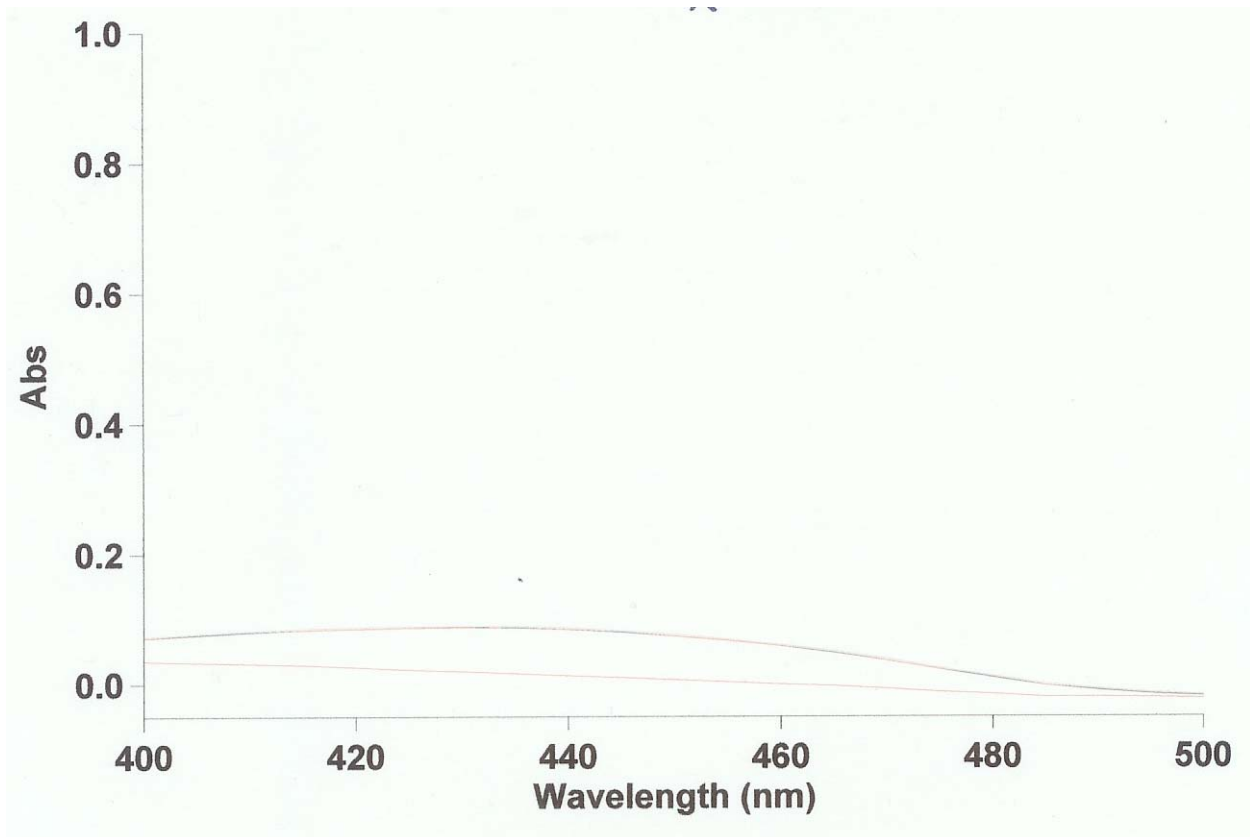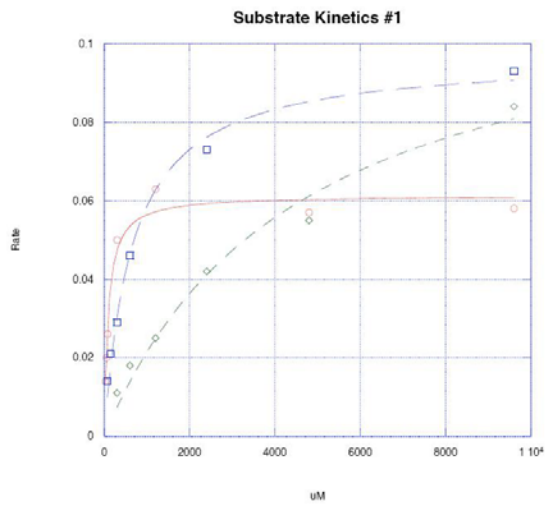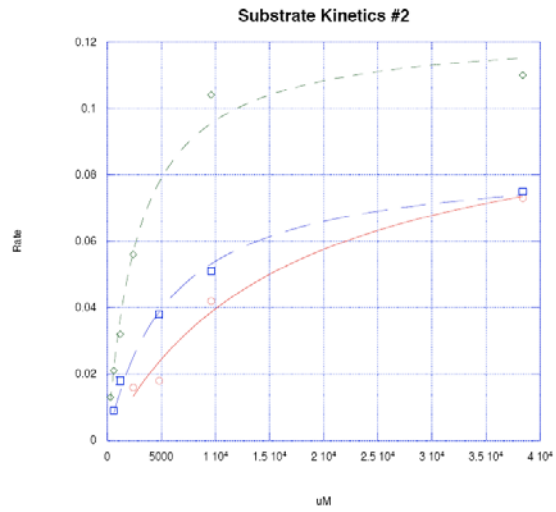
Figure 3.14- Purified hAOC3 with phenylhydrazine. Phenylhydrazine was added to a final concentration of 2 mM in 50 mM KPi, pH 6.5 and incubated for 10 minutes at room temperature. Derivatized TPQ can be monitored at λ = 448 nm with the absorbance due to enzyme blank also shown. A total enzyme concentration of 56.7 uM was used, of which 3.46 uM was found to contain TPQ.
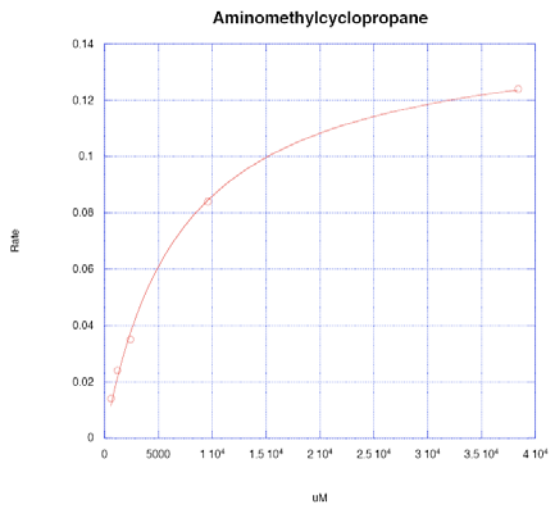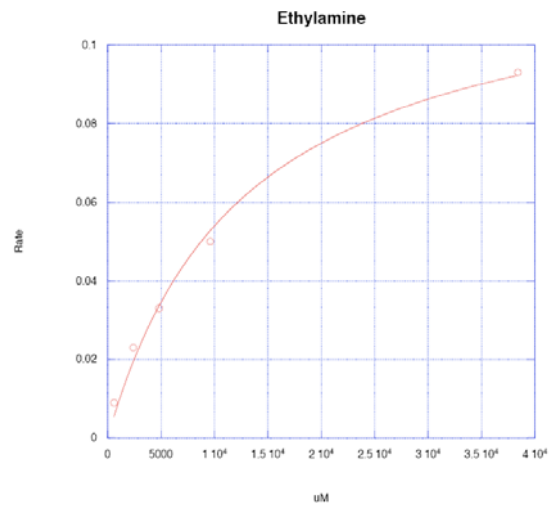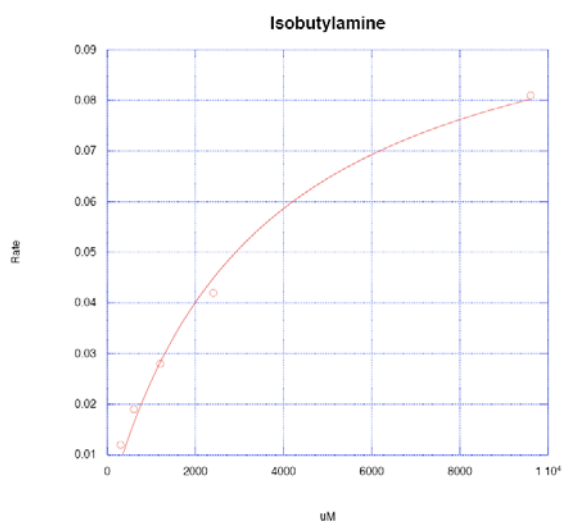
Figure 3.15- hAOC3 steady state kinetic profile of various amines fitted to Michaelis-Menton equation. Measurements of oxygen consumption were taken using oxygen electrode. A – Methylamine (blue squares), benzylamine (red circles), isoamylamine (green diamonds). B – Cyclohexanemethylamine (red circles), amylamine (blue squares), butylamine (green diamonds). C – Aminomethylcyclopropane. D – Ethylamine. All substrate concentrations are in uM unless noted.

E.

F.
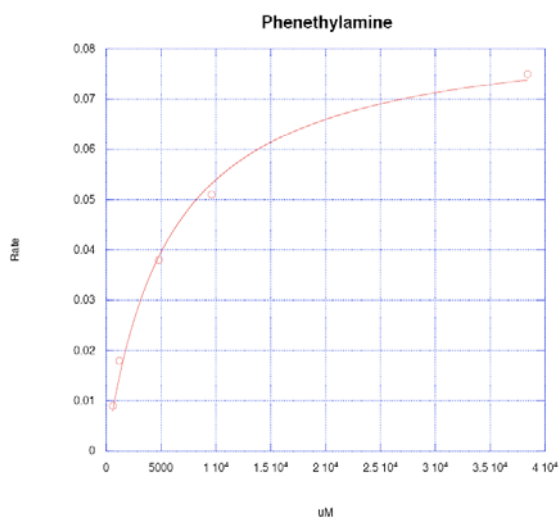
G.
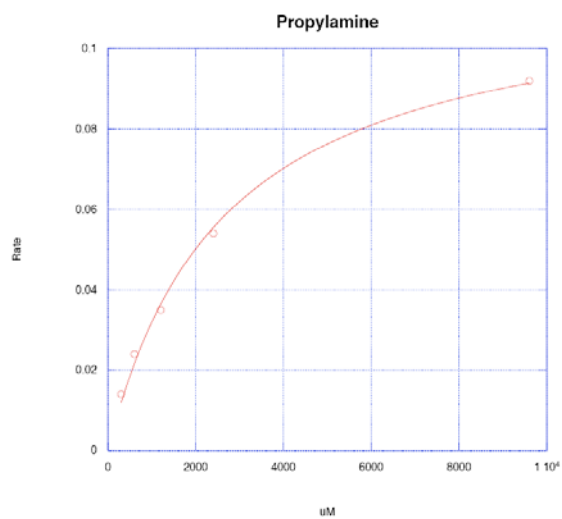
H.
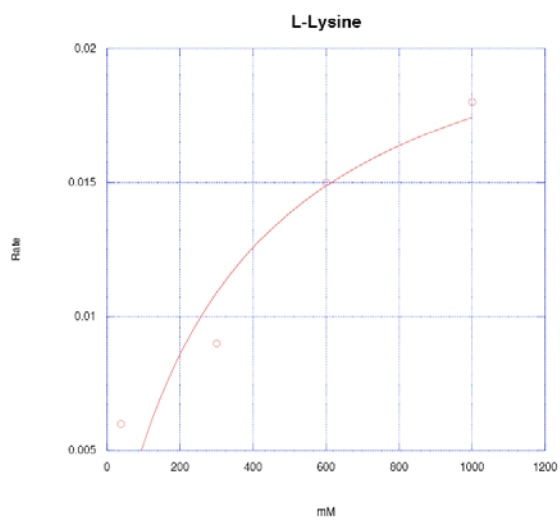
Figure 3.15 (cont.)- hAOC3 steady state kinetic profile of various amines fitted to Michaelis-Menton equation. E – Isobutylamine. F – Phenethylamine. G – Propylamine. H – L-Lysine (substrate concentrations in mM).

Figure 3.16- Correlation between catalytic efficiency (log k_{cat}/K_m) and substrate hydrophobicity (log P). log P values were determined computationally using cLog P software from Actelion Pharmaceuticals (Switzerland). Red point corresponds to L-lysine, which was found to be a weak substrate.

Catalytic efficiency vs. volume of substrate

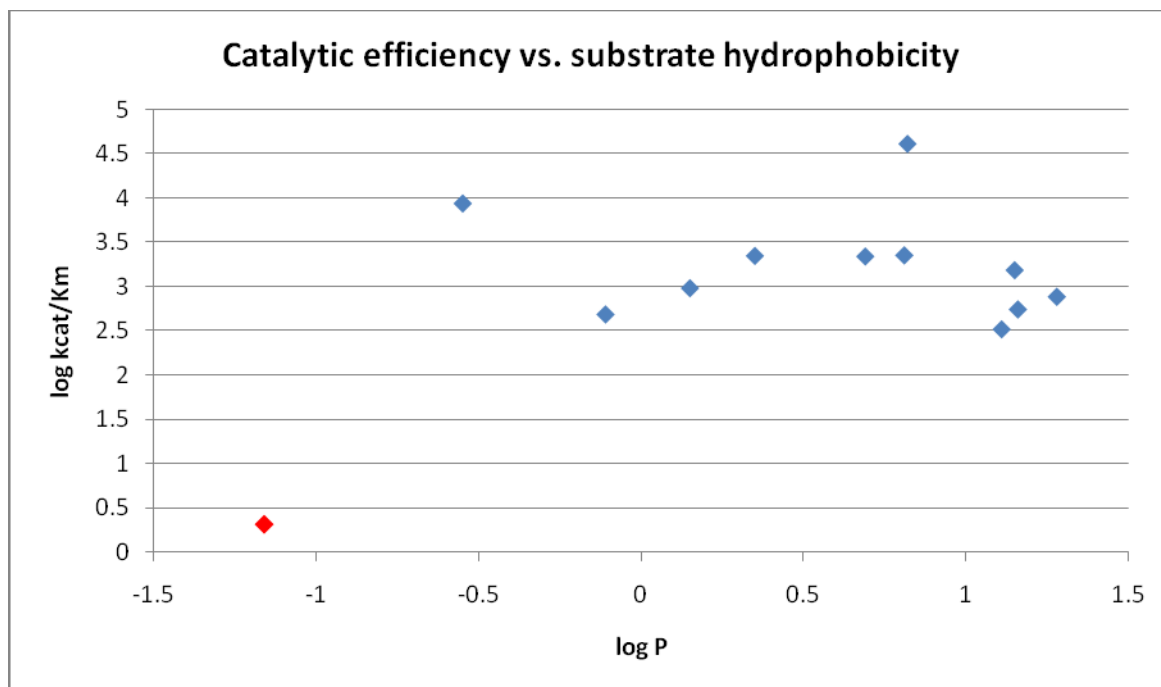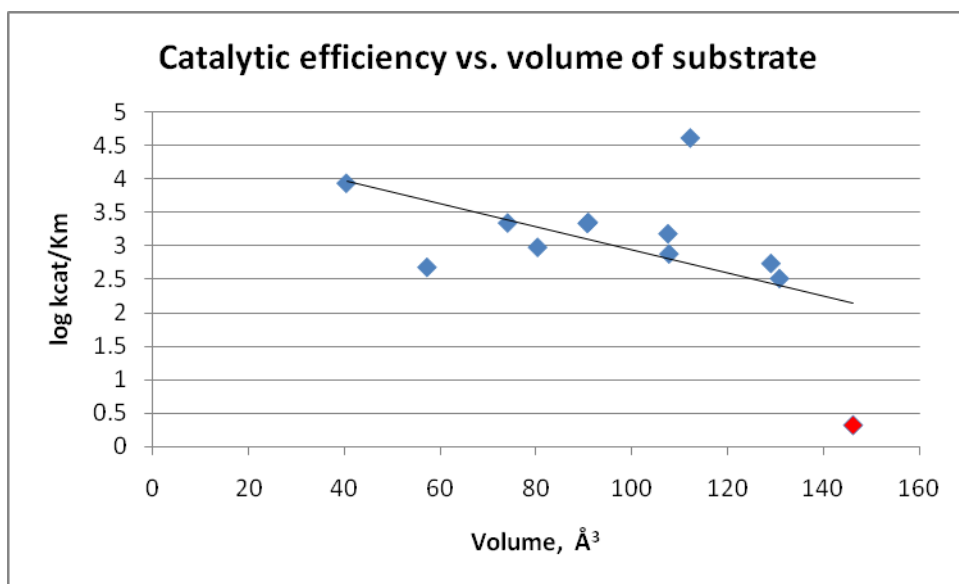| Substrate	Volume, Å^3
Methylamine	40
Ethylamine	57
Propylamine	74
Aminomethylcyclopropane	80
Isobutylamine	91
Butylamine	91
Isoamylamine	107
Amylamine	108
Benzylamine	112
Phenethylamine	129
Cyclohexanemethylamine	131
L-Lysine	146

Figure 3.17- Correlation between catalytic efficiency (log k_{cat}/K_m) and substrate molecular volumes. Molecular volumes arrived at computationally based on group contributions from Molinspiration software. Software computations were optimized by fitting fragment contributions calculated theoretically to real 3D volume for a set of 12000 drug-like molecules. A table of substrate volumes is also shown, with the red point corresponding to L-lysine.
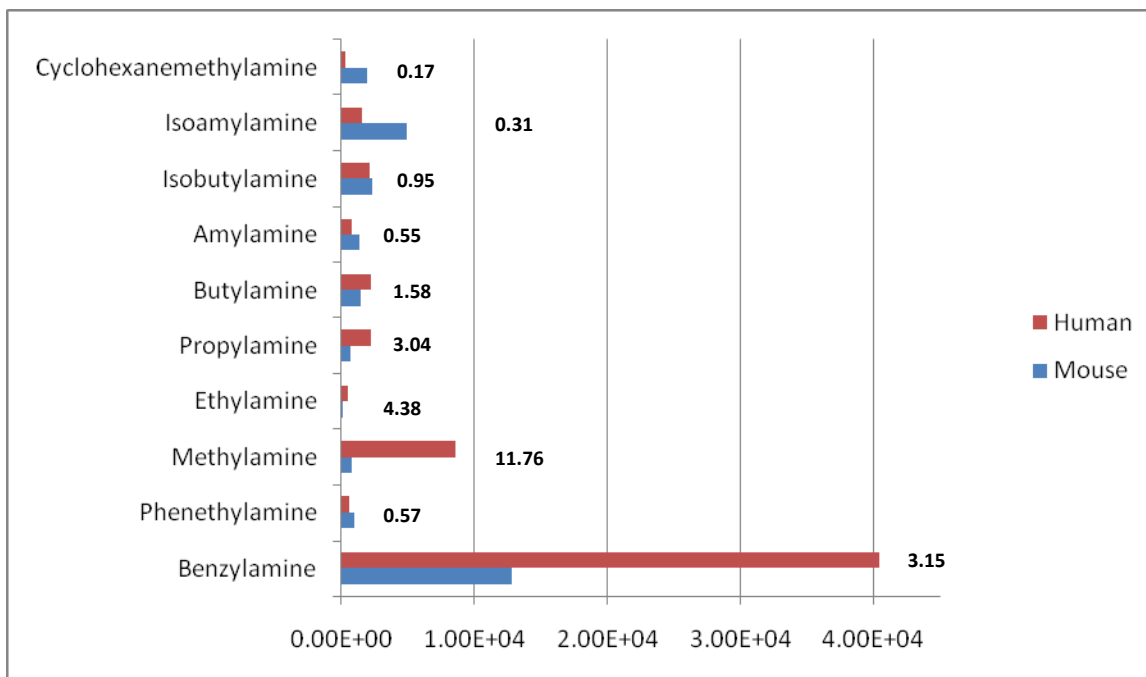
Figure 3.18- Comparison of k_{cat}/K_m between mouse and human AOC3. The ratio of human to mouse k_{cat}/K_m is shown to the right of the bars. Substrate kinetics of mouse AOC3 was performed by Diana Wertz.
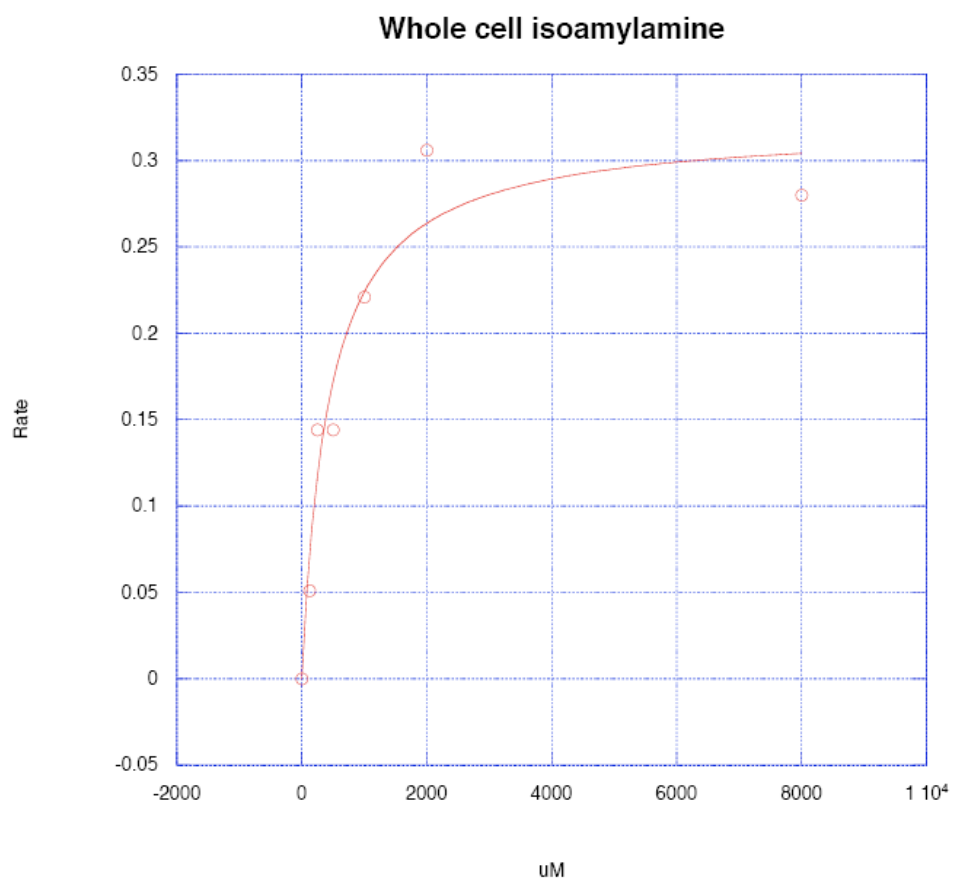
Figure 3.19- Adipocyte whole cell analysis of AOC3 enzyme activity with isoamylamine. Rates are measured in uM/min/million adipocytes.

Substrate	k_{cat} (s^{-1})	K_m (uM)	K_{cat}/K_m (s^{-1}M^{-1})
Methylamine $H_3C—NH_2$	5.5977	652.44	8.58E+03
Ethylamine	6.1154	12787	4.78E+02
Propylamine	5.8015	2645.9	2.19E+03
Butylamine	6.3101	2833.8	2.23E+03
Amylamine	4.3269	5713.8	7.57E+02
Isobutylamine	7.4037	3423.1	2.16E+03

Table 2.1- Kinetic parameters for human AOC3 were measured by oxygen consumption at 37°C, pH 7.4, and atmospheric oxygen. All values were corrected for active AOC3 with TPQ.
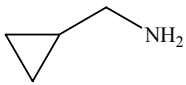
Substrate	k_{cat} (s^{-1})	K_m (uM)	K_{cat}/K_m (s^{-1}M^{-1})
Isoamylamine	6.8936	4558.7	1.51E+03
Benzylamine	3.4211	84.521	4.05E+04
Phenethylamine	1.1181	2050.4	5.45E+02
Cyclohexanemethylamine	5.3554	16489	3.25E+02
Aminomethylcyclopropane	6.6481	7017	9.47E+02
L-Lysine	0.7109	346500	2.05E+00

Table 2.1 (cont.) - Kinetic parameters for human AOC3 were measured by oxygen consumption at 37°C, pH 7.4, and atmospheric oxygen. All values were corrected for active AOC3 with TPQ.

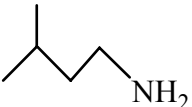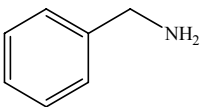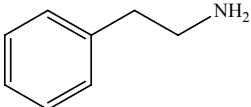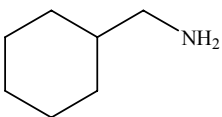Chapter 4:

Isolation of mesenchymal stem cells from AOC3 knockout mice

Introduction

Cell-based assays to determine the physiological role of AOC3 always require an inhibitor control in order to determine whether any cellular effect can be attributable to AOC3. Semicarbazide (SC) is the most frequently used inhibitor, though its cellular effect is unknown, requiring another control involving incubation of cells with just SC. It would be expedient for screening methodologies if the complications due to inhibitor usage can be circumvented.

Mesenchymal stem cells (MSC) are multi-potent with the ability to differentiate into several distinct cell types, including osteoblasts, adipocytes, muscle cells, and neurons [1, 2]. MSCs have also been shown to be self-renewing, with the ability to differentiate even after 20 – 30 cell doublings in culture [3]. If MSCs can be isolated from mouse bone marrow, they pose an elegant solution to the inhibitor issue if these stem cells can be isolated and purified from AOC3 knockout (KO) mice and shown to be differentiable into adipocytes. These adipocytes would not express AOC3 and would serve as a better control for cell-based assays, though the possibility of gene compensation is unknown and would require characterization [4]. The AOC3 knockout mouse was generated in 2005 and the mice were found to develop normally, were healthy by visual inspection, maintained normal body weight, and had a full life span, with some mice living over 2 years [5]. Neither overt macroscopic nor microscopic phenotype was exhibited upon inspection of tissues and organs in the knockout mice. Visceral fat pads seemed to develop normally in KO mice compared to wild-type (WT) upon visual inspection during dissection, showing that there is no impairment of adipose tissue development in the KO mice. In addition, the mice were maintained in a pathogen-free environment, so changes in both the immune response and the immune system were not examined.

The isolation of MSC has been based upon adherence of marrow-derived cells to the plastic substrate of tissue culture plates, and a concomitant lack of adherence by hematopoietic cells [6], though it has been shown that the nonadherent cell population also contains MSC [7]. Prior to enrichment, the adherent cells contain a heterogeneous mixture of osteoblasts, adipocytes, fibroblasts, macrophages, and endothelial cells. The presence of MSCs in culture can be ascertained if a subpopulation of these marrow-derived cells differentiates into multiple cell lineages [8]. Human MSCs were labeled with antibodies to cell surface markers of marrow stromal tissue and colony forming unit-fibroblasts (CFU-F), including STRO-1, a monoclonal antibody reactive to nonhematopoietic progenitor bone marrow stromal cells [9], nerve growth factor (NGF) [10], and SH-2, -3, -4, which are all monoclonal antibodies raised against epitopes expressed by human MSC [11, 12], and enriched using magnetic-activated cell sorting (MACS) and fluorescence-activated cell sorting (FACS) in order to get a 5000-fold enrichment [13]. However, enrichment of mouse MSCs has been more difficult. In fact, the relative abundance of MSCs can vary 10-fold depending on the mouse strain [14]. In addition, MSCs from different mouse strains differed in their media requirement for optimal growth, growth rate, and exhibited a different repertoire of cell surface markers [15]. These cell surface markers are present prior to differentiation of the stem cells into adipocytes.

The enrichment and characterization of mouse MSC has not been very well documented. On the other hand, enrichment of MSCs has been reported for rat [16], cat [17], dog [18], baboon [19], rabbit [20] , pig [21], goat [22], and sheep [23]. Reports of C57BL/6 strain mouse MSC enrichment include the negative selection of granulo-monocytic cells using cluster of differentiation (CD)11b marker, resulting in approximately 50% of the population differentiating

into adipocytes [24]. CD is used in the identification of cell surface molecules found on leukocytes. Again using C57BL/6 strain mice, a more complicated enrichment process involved the positive selection of cells expressing surface markers stem cell antigen -1 (Sca-1), CD29, CD44, c-kit (CD117), and CD105 while negatively selecting for CD45, CD31, and CD34 by flow cytometry [25]. Basic fibroblast growth factor was added to the culture media in order to increase the life span, growth rate, and differentiation potential of MSC, resulting in 90% of the cells exhibiting stem cell characteristics [26]. Unfortunately the population of stem cells capable of differentiating into adipocytes was not reported. Another report of mouse MSC enrichment involved the use of a discontinuous Percoll gradient in which cells between densities of 1.070-1.076 g/mL were found to contain cells positive for Sca-1 and c-kit markers, though the capacity to differentiate into adipocytes was limited [27]. With these considerations in mind, an enrichment of mouse bone marrow MSC was undertaken to facilitate the use of cell-based assays in determining the physiological function of AOC3.

Methods

These MSC experiments were complicated by limited access to AOC3 knockout mice. KO mice were maintained locally by Berlex, Inc., a pharmaceutical company. However, they were purchased by Bayer, which decided to discontinue research on AOC3. The KO mice were originally made by Prof. Sirpa Jalkanen at the University of Turku, Finland, where I was able to conduct research for 2 months. However, due to the slow growth of bone marrow cells in culture, more enrichment by adherence selection could not be carried out. In addition, differentiation of adipocytes is usually a 3 – 4 week process, which also limited enrichment.

Isolation of mouse bone marrow. 12 week old male mice (C57BL/6J background), both AOC3 knockout and wild-type, were sacrificed by asphyxiation with CO_2. Femur bones from each mouse were dissected and each end of the bone cut off using surgical scissors. Using a 27G needle (Terumo, Somerset, NJ) and 2 mL syringe (BD Bioscience, San Jose, CA), bone marrow was flushed out with Dulbecco's modified Eagle medium (DMEM) or Hank's Buffered Salt Solution (HBBS) (both from Invitrogen) with 200 U/mL heparin (Sigma Aldrich) and marrow filtered with 70 um cell strainer (BD Biosciences). Marrow was collected in 5 mL polystyrene round bottom tube (BD Falcon). The single cell suspension was then centrifuged at 4°C, 3000 rpm, for 1.5 minutes and suspended in fresh DMEM plus 10% fetal bovine serum (FBS) (Hyclone), supplemented with MEM non-essential amino acid (NEAA) (Invitrogen), penicillin-streptomycin (P/S) and plated 7 mL onto gelatin-coated 10 cm tissue culture (TC) dish (Corning). All mice were handled in accordance with the institutional animal care policy of Berlex (now Bayer Healthcare, Richmond, CA) and University of Turku (Turku, Finland).

MSC cell culture during adherence selection. 10 cm TC dish were pretreated with 1% gelatin phosphate buffered saline (PBS) buffer for at least 15 minutes at room temperature in order to coat the bottom of the dish to facilitate and increase stem cell adherence. After 15 minutes, the dish was washed twice with PBS and ready for use. Cells were grown in αMEM, supplemented with 10% FBS, MEM NEAA, and P/S. Cells were counted using hemacytometer with nonviable cells determined by Trypan blue dye. Cells were plated at approximately $6 - 8 \times 10^6$ cells/mL. Fresh media was supplied every 3 days and cells grown for approximately 16 days until cells were approximately 90% confluent. During media replacement, only adherent cells were retained while non-adherent cells were discarded. Cells were then split after treatment with 0.5 g/L trypsin (Invitrogen) for 10 minutes at 37°C. Trypsin was inactivated by FBS in cell media. After the split, cells were grown to confluence as described.

Differentiation to wildtype and knockout adipocytes after adherence selection. Cells were grown to confluence in gelatin-coated 6-well plates or T-25 flask. For cells to be differentiated into adipocytes, media contained 10% newborn calf serum (NCS) (Invitrogen) rather than FBS. Once confluent, cellular differentiation was induced using 1 ug/mL insulin, 0.25 uM dexamethasone, and 0.1 mM methylisobutylxanthine as previously described [28]. Briefly, cells were cultured in DMEM supplemented with 10% FBS and P/S. Differentiation takes approximately 8 – 10 days. After differentiation conditions, cells were examined for adipocyte phenotype.

Differentiation to knockout adipocytes with AdipoDiff. Alternative differentiation protocol in which 1.5 mL of bone marrow cells are plated on gelatin-coated 35mm TC dish at 5×10^4 cells/mL and differentiated with NH AdipoDiff medium (Miltenyi Biotec, Auburn, CA) warmed to 37°C. AdipoDiff medium was changed every 3rd day for 3 weeks.

Oil Red O cell staining. A saturated solution of approximately 1% Oil Red O (Sigma Aldrich, St. Louis, MO) stock solution was prepared in 99% isopropanol (EMD Chemicals, Gibbstown, NJ). 60 mL of stock solution was diluted with 40 mL of 1% dextrin (Fluka BioChemika, Switzerland) solution made with Millipore water. The diluted solution was allowed to stand overnight and then filtered. The filtrate is the working solution. Cells were stained for 10 minutes and rinsed in 60% isopropanol, and then Millipore water. Nuclei were counterstained for 5 minutes in 0.1% hematoxylin solution according to Mayer (Fluka BioChemika, Switzerland) and placed in Millipore water until blue. Fat globules were stained orange-red while nuclei were blue.

Fluorescence activated cell sorting (FACS) of murine bone marrow cells. Bone marrow cells from knockout mouse were labeled with 1 ug/mL wheat germ agglutinin, which selectively binds to primitive multipotent cells, conjugated to fluorescein [29] and incubated for approximately 15 minutes. Cells positive for fluorescein were sorted and collected by FACS using a DAKO-Cytomation MoFlo High Speed Sorter with 2 Coherent Innova I-90 laser tuned for 488 nm excitation at the Berkeley Flow Cytometry Facility. Positive cells were cultured as previously described until confluent and differentiated into adipocytes with AdipoDiff.

Light Microscopy. Images of cells were taken either with a Zeiss upright Axioplan microscope with a 40x or 100x oil objective or an Olympus CX31-P Polarizing Light Microscope with 20x or 40x air objective.

Separation of mononuclear cells by Ficoll gradient. Bone marrow cells carefully layered onto HISTOPAQUE-1083 (Sigma-Aldrich) density gradient and centrifuged at 750g for 20 minutes at room temperature. Centrifugation was stopped with no brakes. Erythrocytes aggregate and sediment while mononuclear cells, including mesenchymal stem cells can be found at the plasma-HISTOPAQUE interface. Interface cells were carefully removed by pipette and cultured at 0.5×10^6 cells/mL on gelatin-coated T-75 in 20 mL DMEM, supplemented with 20% Knockout™ serum replacement (SR) (Invitrogen) to grow and maintain undifferentiated stem cells, 1 mM L-glutamine, 0.1 mM β-mercaptoethanol, 1% NEAA, and 5 ng/mL human basic fibroblast growth factor [25]. Media was replaced every 3 – 4 days and until cells were 80 – 90% confluent after 14 days. Cells were split to 0.5×10^6 cells/mL and grown to confluence. After two more splits, confluent adherent cells were detached from TC flask with nonenzymatic cell dissociation solution (Sigma) and washed with DMEM media and sorted by FACS.

Results

Mouse MSC were enriched by separation of mononuclear cells using a Ficoll gradient [30] and plated at a cell density of 1.3×10^5 cells/cm^2. The cell density and culture media has been found to influence the differentiation potential of MSC [31, 32]. Cells were grown to confluence on gelatin-coated tissue culture plastic using DMEM, supplemented with serum replacement media which is used instead of FBS to support the growth of undifferentiated embryonic stem cells; this is because FBS may contain unwanted growth factors. In addition, 5 ng/mL basic fibroblast growth factor (bFGF) was added in order to increase growth rate. MSC cultured in gelatin-coated flasks with embryonic stem cell media was shown to exhibit a four to five fold higher rate of proliferation [29]. The marrow derived cells from AOC3 KO mice exhibited characteristics typical of fibroblasts after two passages and did not contain any adipocytes, as shown in Figure 1. Rather than use both negative and positive selection of cell surface markers, a more facile one step positive selection based on cells reactive to wheat germ agglutinin (WGA) was tried. WGA was found to bind mesenchymal stem cells with low reactivity toward cells without stem cell characteristics [33]. After three passages in which only the adherent cells were retained, the remaining cells were treated with WGA conjugated to fluorescein and enriched using FACS. The one-parameter histogram of the cell sorting results is shown in Figure 2. A total of 450,000 cells were sorted with 27,000 negative WGA cells and 180,000 positive WGA cells. Cells found at higher channel numbers (x-axis of histogram) reacted more strongly with WGA (Figure 2B) and resulted in higher fluorescence. The positive cells were plated at a cell density of 9.3×10^4 cells/cm^2 and cultured to confluence prior to differentiation into adipocytes with a commercially available differentiation media, AdipoDiff, over 3 weeks. Upon differentiation, cells were stained with Oil Red O, a fat soluble dye used for staining lipid vacuoles, and counterstained with hematoxylin as shown in Figure 3 (100x magnification) and Figure 4 (40x magnification). The fat vacuoles have been stained red while the nuclei are blue. The cells did not exhibit the normal cultured adipocyte morphology, typically mono-vacuolar or containing several large lipid laden vacuoles with the nucleus located on the periphery. In these cells, the nucleus is clearly visible with small lipid vacuoles located on the periphery of the cell. This cellular phenotype fits the description of macrophages that have accumulated lipids and cholesterol to form foam cells [34-36].

Rather than use cell surface markers to enrich the marrow cells for MSC, a simpler selection process involving just adherence to tissue culture plastic at a higher cell density of 4.3×10^6 cells/cm^2 using αMEM cell media, supplemented with fetal bovine serum rather than embryonic stem cell media. During each cell passage, only the adherent cells were retained and cell density was maintained at a cell density of 33 times the previous protocol, at approximately 4.3×10^6 cells/cm^2. After two passages, the cells were grown to confluence and differentiated with insulin, dexamethasone, and methylisobutylxanthine. Differentiated marrow derived cells from AOC3 KO mice are shown in Figure 5. From this method, cells exhibiting phenotype typical of adipocytes were seen, though at approximately 1 – 2 % of total cell population. The cells are usually differentiated over a period of 10 – 12 days, though the cells shown were after Day 7, not allowing enough time for full differentiation to occur. Therefore, the actual total cell population differentiable into adipocytes may be higher. In Figure 5, suspected adipocytes in the early stages of differentiation can be observed. This preliminary result demonstrates that it is possible to enrich marrow mesenchymal stem cells from AOC3 knockout mice. Marrow derived

cells from wild type mice under the same enrichment protocol also can be differentiated into adipocytes as shown in Figure 6. However, the resulting adipocyte population after differentiation was found to be similar to the knockout study at approximately 1 – 2% of total cultured cells.

Discussion

MSC from humans and various mammals have been enriched successfully. However, mouse MSC derived from bone marrow has not been shown to be enriched to at least 90% of total cultured cell population. With enrichment of MSCs, it would be more expedient to perform cell based assays to determine the physiological function of AOC3 without the use of enzyme inhibitors. Reports of mouse MSC enrichment have found that even cell density and culture media is important. After isolating cells from mouse bone marrow, combining three rounds of adherent cell selection at low cell density with positive selection of cells reactive to wheat germ agglutinin, the differentiated cells exhibited foam cell phenotype. This was not the anticipated result, though a procedure to isolate macrophages from mouse bone marrow and effectively modify them into foam cells with greater than 90% efficiency was found.

In another attempt to isolate mouse MSC, rather than use cell surface markers, a simpler methodology based on increased cell density and adherence to tissue culture plastic was used. Unfortunately, due to time constraints, only two passages of adherent cells could be finished rather than the planned six passages which would allow more rounds of selection. In addition, only 7 days were allowed for differentiation rather than the typical $10 - 12$ days. In fact, cultured adipocytes will become hypertrophied with larger lipid vacuoles exhibiting a more typical adipocytic phenotype if allowed to differentiate to Day 21 [37]. Given the constraints, the results of this selection process outweighed the more sophisticated method involving cell surface markers with 1 -2 % of total cell population exhibiting adipocyte phenotype, with a maximal yield of 5%, if suspected cells exhibiting early stage fat vacuole formation is also counted. These preliminary results demonstrate a proof of principle that MSCs from AOC3 KO mice can be enriched, grown in culture, and differentiated into adipocytes. Future methods of enrichment could involve adherence selection for six passages using typical cell culture media at high cell density of 4.3×10^6 cells/cm^2 with the addition of positive and/or negative selection of cells expressing a set of cell surface markers, including the CD11b marker which resulted in a 50% adipocyte cell population [24].

References

1. Caplan, A.I., *Mesenchymal stem cells.* J Orthop Res, 1991. **9**(5): p. 641-50.
2. Kohyama, J., et al., *Brain from bone: efficient "meta-differentiation" of marrow stroma-derived mature osteoblasts to neurons with Noggin or a demethylating agent.* Differentiation, 2001. **68**(4-5): p. 235-44.
3. Friedenstein, A.J., R.K. Chailakhyan, and U.V. Gerasimov, *Bone marrow osteogenic stem cells: in vitro cultivation and transplantation in diffusion chambers.* Cell Tissue Kinet, 1987. **20**(3): p. 263-72.
4. Majzoub, J.A. and L.J. Muglia, *Molecular medicine - Knockout mice.* New England Journal of Medicine, 1996. **334**(14): p. 904-907.
5. Stolen, C.M., et al., *Absence of the endothelial oxidase AOC3 leads to abnormal leukocyte traffic in vivo.* Immunity, 2005. **22**(1): p. 105-15.
6. Alhadlaq, A. and J.J. Mao, *Mesenchymal stem cells: isolation and therapeutics.* Stem Cells Dev, 2004. **13**(4): p. 436-48.
7. Wan, C., et al., *Nonadherent cell population of human marrow culture is a complementary source of mesenchymal stem cells (MSCs).* J Orthop Res, 2006. **24**(1): p. 21-8.
8. Pittenger, M.F., et al., *Multilineage potential of adult human mesenchymal stem cells.* Science, 1999. **284**(5411): p. 143-147.
9. Gronthos, S., et al., *The Stro-1(+) Fraction of Adult Human Bone-Marrow Contains the Osteogenic Precursors.* Blood, 1994. **84**(12): p. 4164-4173.
10. Quirici, N., et al., *Isolation of bone marrow mesenchymal stem cells by anti-nerve growth factor receptor antibodies.* Experimental Hematology, 2002. **30**(7): p. 783-791.
11. Barry, F., et al., *The SH-3 and SH-4 antibodies recognize distinct epitopes on CD73 from human mesenchymal stem cells.* Biochemical and Biophysical Research Communications, 2001. **289**(2): p. 519-524.
12. Barry, F.P., et al., *The monoclonal antibody SH-2, raised against human mesenchymal stem cells, recognizes an epitope on endoglin (CD105).* Biochemical and Biophysical Research Communications, 1999. **265**(1): p. 134-139.
13. Gronthos, S., et al., *Molecular and cellular characterisation of highly purified stromal stem cells derived from human bone marrow.* J Cell Sci, 2003. **116**(Pt 9): p. 1827-35.
14. Phinney, D.G., et al., *Plastic adherent stromal cells from the bone marrow of commonly used strains of inbred mice: variations in yield, growth, and differentiation.* J Cell Biochem, 1999. **72**(4): p. 570-85.
15. Peister, A., et al., *Adult stem cells from bone marrow (MSCs) isolated from different strains of inbred mice vary in surface epitopes, rates of proliferation, and differentiation potential.* Blood, 2004. **103**(5): p. 1662-8.
16. Schwarz, E.J., et al., *Multipotential marrow stromal cells transduced to produce L-DOPA: Engraftment in a rat model of Parkinson disease.* Human Gene Therapy, 1999. **10**(15): p. 2539-2549.
17. Martin, D.R., et al., *Isolation and characterization of multipotential mesenchymal stem cells from feline bone marrow.* Experimental Hematology, 2002. **30**(8): p. 879-886.
18. Kadiyala, S., et al., *Culture expanded canine mesenchymal stem cells possess osteochondrogenic potential in vivo and in vitro.* Cell Transplantation, 1997. **6**(2): p. 125-134.
19. Devine, S.M., et al., *Mesenchymal stem cells are capable of homing to the bone marrow of non-human primates following systemic infusion.* Experimental Hematology, 2001. **29**(2): p. 244-255.
20. Awad, H.A., et al., *Autologous mesenchymal stem cell-mediated repair of tendon.* Tissue Engineering, 1999. **5**(3): p. 267-277.
21. Ringe, J., et al., *Porcine mesenchymal stem cells - Induction of distinct mesenchymal cell lineages.* Cell and Tissue Research, 2002. **307**(3): p. 321-327.
22. Mosca, J.D., et al., *Mesenchymal stem cells as vehicles for gene delivery.* Clinical Orthopaedics and Related Research, 2000(379): p. S71-S90.
23. Jessop, H.L., B.S. Noble, and A. Cryer, *The Differentiation of a Potential Mesenchymal Stem-Cell Population within Ovine Bone-Marrow.* Biochemical Society Transactions, 1994. **22**(3): p. S248-S248.
24. Tropel, P., et al., *Isolation and characterisation of mesenchymal stem cells from adult mouse bone marrow.* Experimental Cell Research, 2004. **295**(2): p. 395-406.
25. Sun, S., et al., *Isolation of mouse marrow mesenchymal progenitors by a novel and reliable method.* Stem Cells, 2003. **21**(5): p. 527-35.

26. Tsutsumi, S., et al., *Retention of multilineage differentiation potential of mesenchymal cells during proliferation in response to FGF.* Biochemical and Biophysical Research Communications, 2001. **288**(2): p. 413-419.

27. Rosca, A.M. and A. Burlacu, *Isolation of a mouse bone marrow population enriched in stem and progenitor cells by centrifugation on Percoll gradient.* Biotechnol Appl Biochem.

28. Stephens, J.M., J. Lee, and P.F. Pilch, *Tumor necrosis factor-alpha-induced insulin resistance in 3T3-L1 adipocytes is accompanied by a loss of insulin receptor substrate-1 and GLUT4 expression without a loss of insulin receptor-mediated signal transduction.* Journal of Biological Chemistry, 1997. **272**(2): p. 971-976.

29. Testa, N.G. and G. Molineux, *Haemopoiesis : a practical approach.* The Practical approach series. 1993, Oxford ; New York: IRL Press at Oxford University Press. xxiv, 293 p.

30. Battula, V.L., et al., *Human placenta and bone marrow derived MSC cultured in serum-free, b-FGF-containing medium express cell surface frizzled-9 and SSEA-4 and give rise to multilineage differentiation.* Differentiation, 2007. **75**(4): p. 279-91.

31. Sun, Z.L., et al., *[Effect of monoclonal or different cell seeding densities on the differentiation potential of immortalized human mesenchymal stem cells in vitro and in vivo].* Zhonghua Yi Xue Za Zhi, 2009. **89**(31): p. 2202-5.

32. Chen, H.H., et al., *In vitro initial expansion of mesenchymal stem cells is influenced by the culture parameters used in the isolation process.* Biomed Mater Eng, 2009. **19**(4-5): p. 301-9.

33. Ghilzon, R., C.A. McCulloch, and R. Zohar, *Stromal mesenchymal progenitor cells.* Leuk Lymphoma, 1999. **32**(3-4): p. 211-21.

34. Choudhury, R.P., J.M. Lee, and D.R. Greaves, *Mechanisms of disease: macrophage-derived foam cells emerging as therapeutic targets in atherosclerosis.* Nat Clin Pract Cardiovasc Med, 2005. **2**(6): p. 309-15.

35. Botham, K.M., et al., *The induction of macrophage foam cell formation by chylomicron remnants.* Biochem Soc Trans, 2007. **35**(Pt 3): p. 454-8.

36. Li, A.C. and C.K. Glass, *The macrophage foam cell as a target for therapeutic intervention.* Nat Med, 2002. **8**(11): p. 1235-42.

37. Suganami, T., J. Nishida, and Y. Ogawa, *A paracrine loop between adipocytes and macrophages aggravates inflammatory changes - Role of free fatty acids and tumor necrosis factor alpha.* Arteriosclerosis Thrombosis and Vascular Biology, 2005. **25**(10): p. 2062-2068.

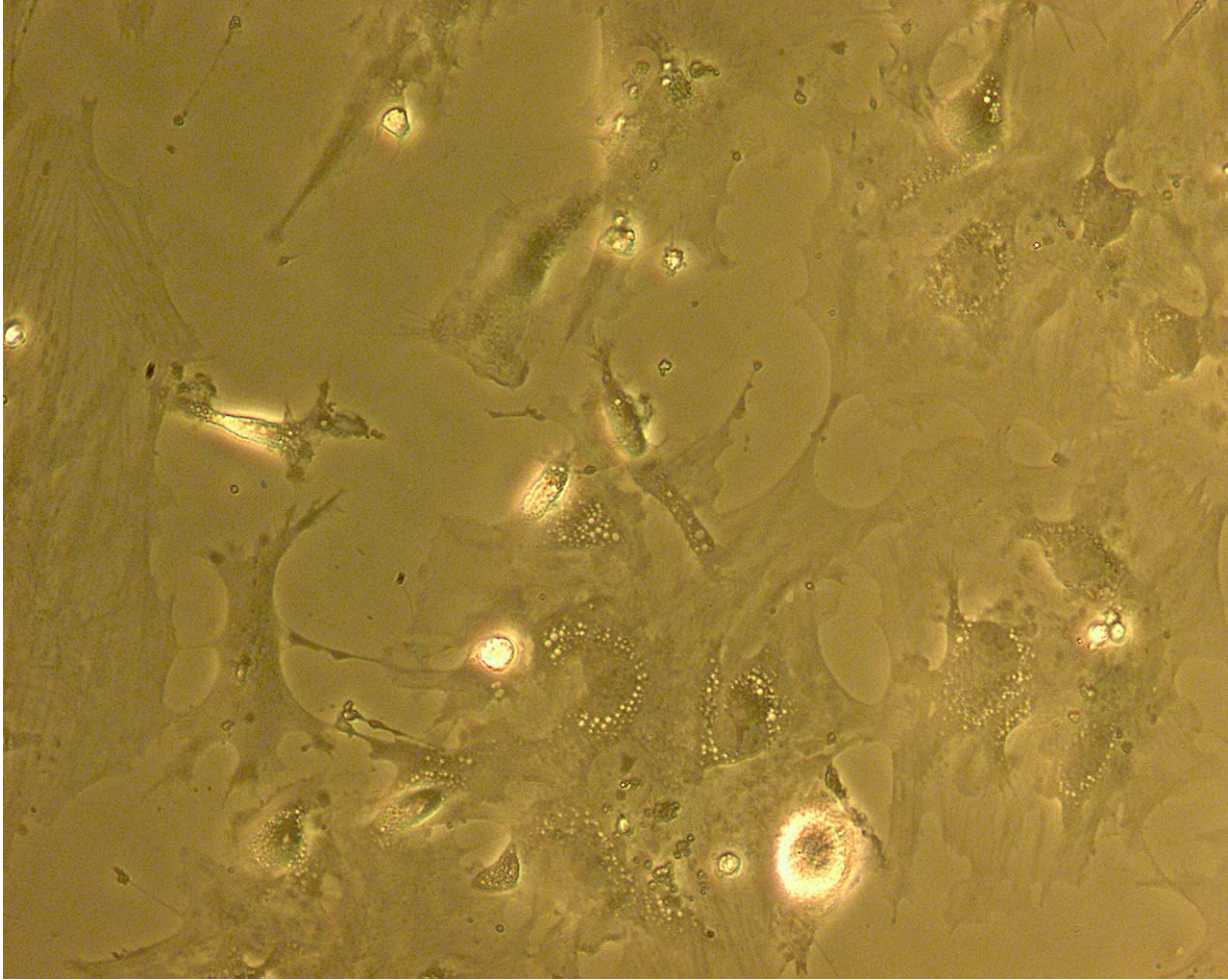Figure 4.1- AOC3 KO Mice marrow derived cells show fibroblastic phenotype. Areas that light up do not correspond to fat vacuoles.
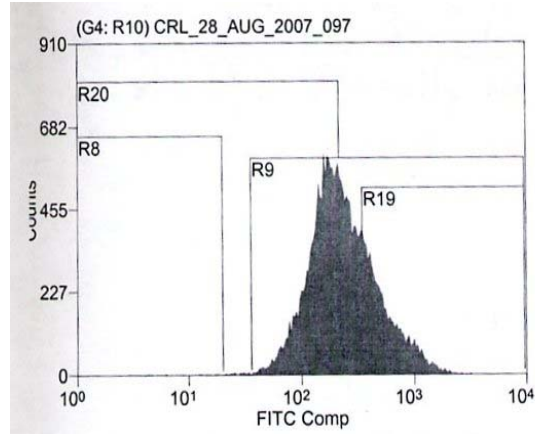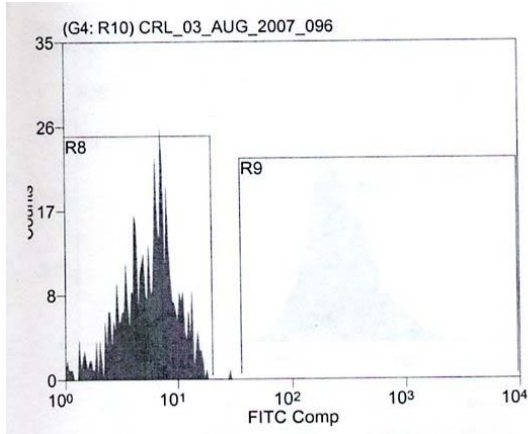
Figure 4.2- One parameter histogram of wheat germ agglutinin fluorescein conjugated (WGA-F) treated bone marrow cells sorted by FACS. The cell count is graphed on the y-axis while the channels are on the x-axis. A – Count of negative WGA-F cells. B – Count of positive WGA-F cells.
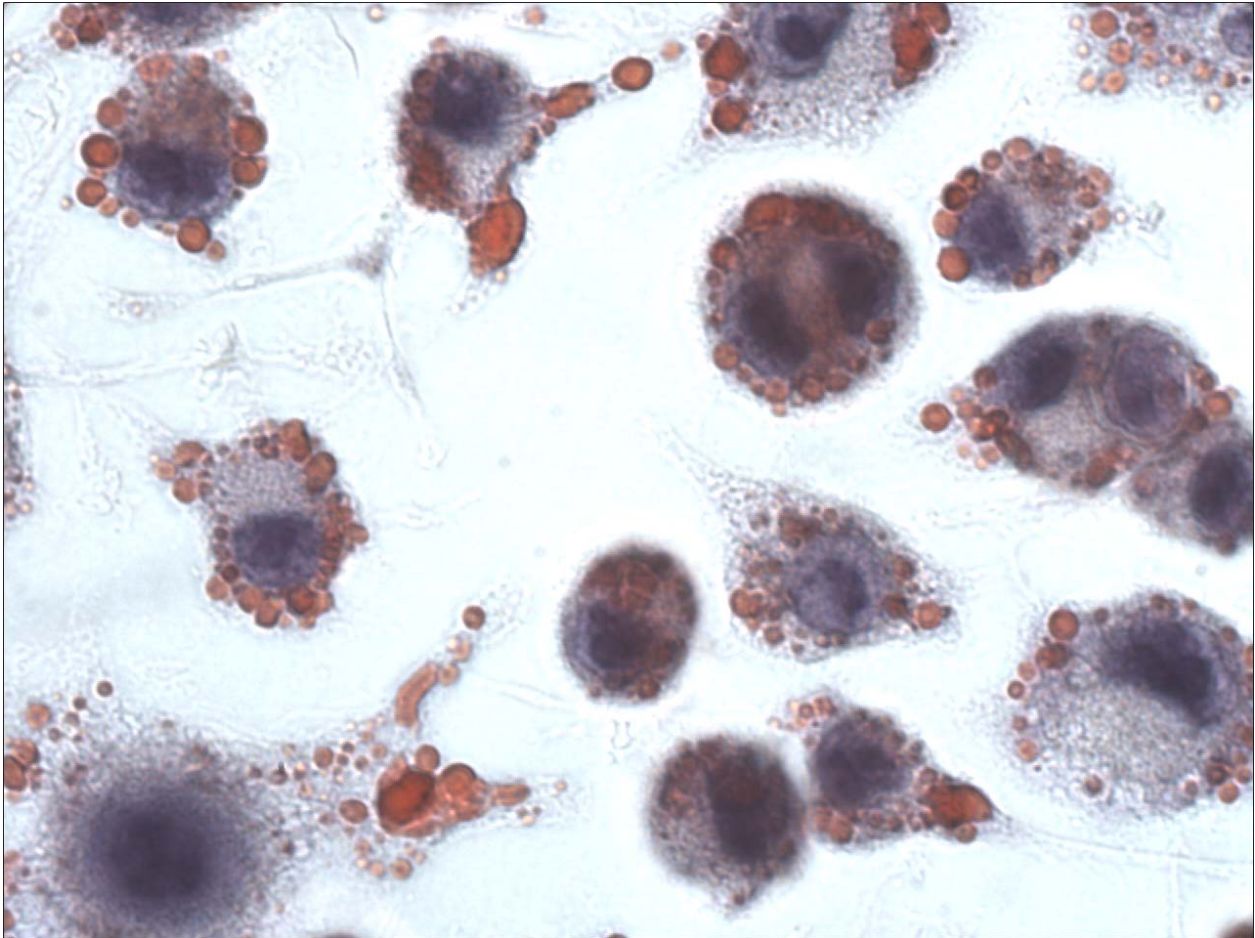
Figure 4.3- AOC3 knockout mouse bone marrow derived cells enriched with Ficoll gradient. Cells labeled with wheat germ agglutinin and purified with FACS were cultured and stained with Oil Red O and hematoxylin. The observed concentration of fat vacuoles at the cellular periphery is consistent with macrophage foam cell phenotype. 100x magnification.
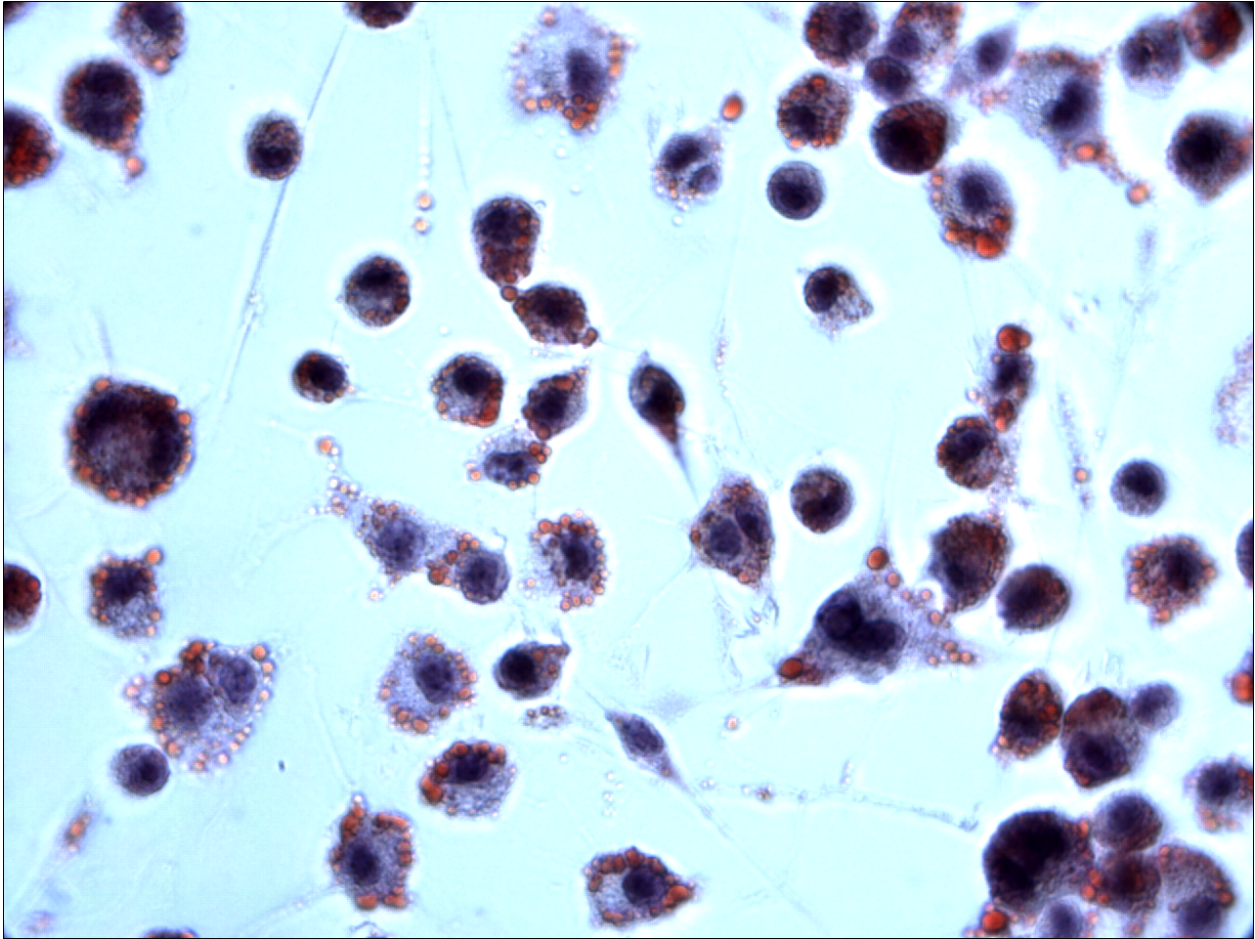
Figure 4.4- AOC3 knockout mouse bone marrow derived cells enriched with Ficoll gradient. Cells labeled with wheat germ agglutinin and purified with FACS were cultured and stained with Oil Red O and hematoxylin. The observed concentration of fat vacuoles at the cellular periphery is consistent with macrophage foam cell phenotype. 40x magnification.

Figure 4.5- AOC3 knockout mouse bone marrow derived cells enriched based on adherence to tissue culture plastic. After two passages, cells were differentiated using insulin, dexamethasone, and methylisobutylxanthine. Red arrow points out differentiated adipocytes while black arrows are suspected adipocytes at early stages of differentiation (there are more suspected adipocytes than are pointed out by black arrows). 20x magnification.
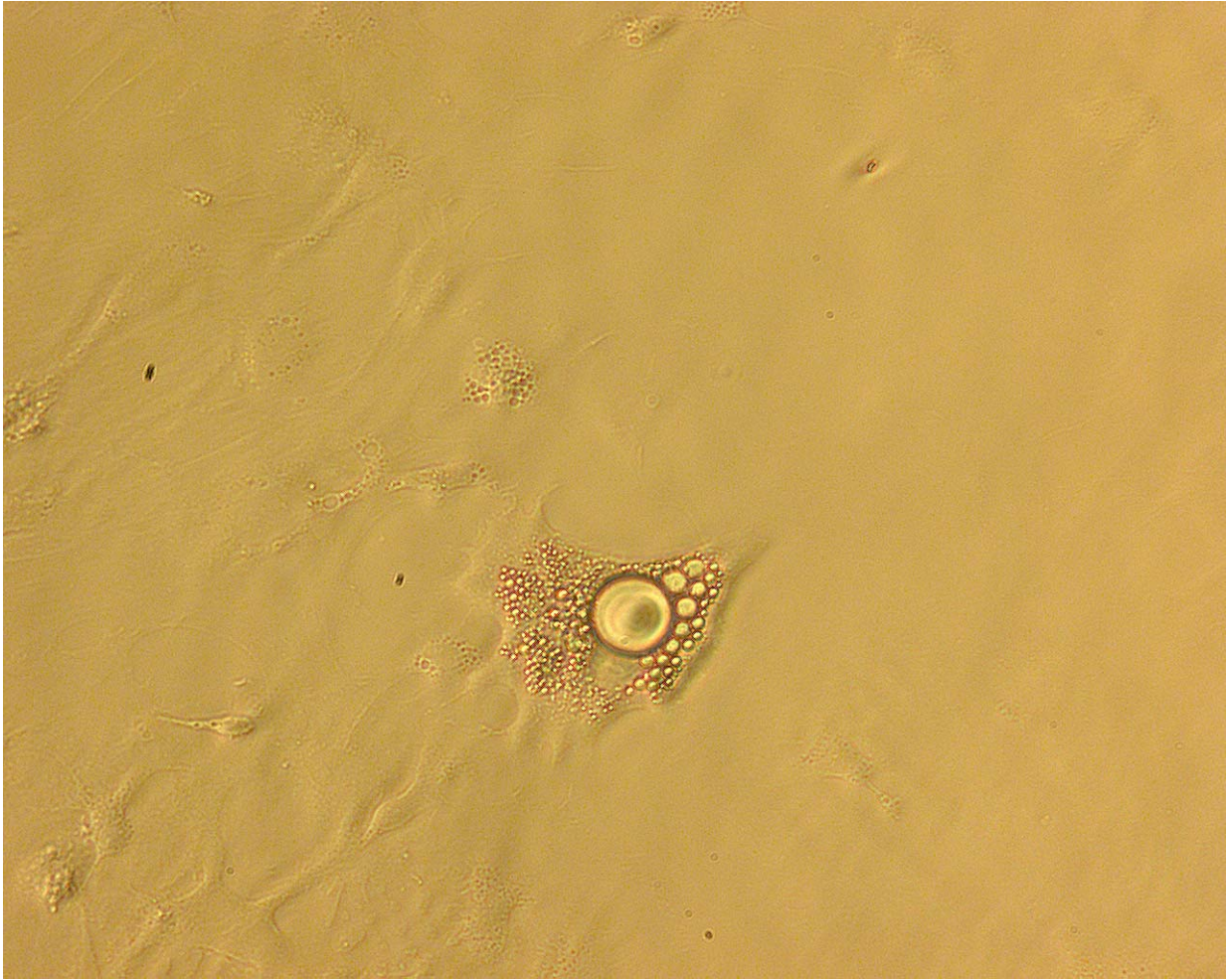
Figure 4.6- Wild type mouse bone marrow derived cells enriched based on adherence to tissue culture plastic. After two passages, cells were differentiated using insulin, dexamethasone, and methylisobutylxanthine. 40x magnification.

Chapter 5:

Monocyte chemoattractant protein-1 (MCP-1) production by adipocytes

Introduction

Obesity is characterized by low-grade inflammation, with increased plasma levels of inflammatory markers, such as interleukin-6 (IL-6), tumor necrosis factor- α (TNF-α), and monocyte chemoattractant protein-1 (MCP-1), to name a few [1]. Adipose tissue has been found to be involved in the production of these pro-inflammatory cytokines and chemokines, leading to insulin resistance and associated cardiovascular diseases.

TNF-α was one of the earliest observed pro-inflammatory cytokines produced by adipocytes [2]. TNF-α secretion by adipose tissue was found to be approximately 7.5 fold greater in obese vs. lean human subjects without diabetes [3]. It has been found to be involved in autocrine signaling, facilitating the release of lipids from adipocytes [4], as well as affecting insulin signaling [5]. In fact, TNF-α is thought to be the primary mediator of obesity-related insulin resistance [6]. Other roles of TNF-α in adipocyte function include the promotion of apoptosis and cell differentiation, the regulation of plasminogen activator inhibitor, an important component of the clotting cascade [7], and mediation of leptin production [8]. With the discovery of cytokine production and the rapidly evolving role of adipocytes in maintaining homeostasis and energy balance, the focus of the search for the physiological role of AOC3 in adipocytes shifted to a possible role in cytokine or chemokine production.

From previous work in the lab, increased production of monocyte chemoattractant protein-1 (MCP-1) was observed when cultured 3T3-L1 adipocytes were incubated with the AOC3 substrates, aminoacetone and isoamylamine, and was found to be correlated with H_2O_2. Monocytes circulate in the blood stream and migrate into various tissues to replenish the resident macrophage population. Macrophages are innate immune cells involved in antigen presentation, pathogen clearance, wound healing, and recovery from inflammatory response [9]. This migration into tissues is regulated by a set of cytokines and chemokines, including MCP-1. Obesity has been correlated with increased macrophage infiltration of adipose tissue, with approximately 30% of encoded proteins in adipose tissue characteristic of macrophages [10-12]. Plasma levels of MCP-1 were increased in genetically obese mice, with increased MCP-1 mRNA observed in adipose tissue, suggesting that MCP-1 is a contributing factor in the increase of macrophage infiltration into adipose tissue [13, 14]. In fact, MCP-1 knockout mice on a high-fat diet and morbidly obese human subjects after surgery-induced weight loss both did not exhibit the increased macrophage infiltration that wild-type mice or subjects prior to surgery showed [15]. On the other hand, overexpression of MCP-1 in adipose tissue in mice resulted in increased plasma levels of MCP-1 and increased macrophage accumulation in adipose tissue [16]. Recently, the presence of two different subsets of macrophages was reported, with the alternatively activated (M2) macrophages found in the lean population of mice and the classically activated (M1) macrophages found in obese mice [17]. Classical activation involve recognition of molecules such as lipopolysaccharide, lipoproteins, dsRNA, and heat shock proteins, by macrophages with pathogen-associated recognition receptors [18]. In response to infection, M1 macrophages have the ability to kill pathogens by the production of cytokines and generation of microbicidal products. This type of macrophage activation was the first to be recognized and became known as classical activation. On the other hand, alternatively activated macrophages remain ill-defined, mainly characterized *in vitro*, but was found to express a different set of cell surface markers, cytokines, and chemokines [19]. Specifically, the alternatively activated phenotype include high macrophage mannose receptor activity, restricted

major histocompatibility complex II antigen expression, and reduced proinflammatory cytokine release [20]. M2 macrophages participate in wound healing and elimination of extracellular pathogens too large to be phagocytosed [21]. Interestingly, it has been found that adipocytes release the cytokine, IL-13, which induces the alternative activation of resident macrophages in adipose tissue [22]. Obesity leads to a change in the activation state of macrophages from the M2 phenotype to the pro-inflammatory M1 state. In addition to the recruitment of macrophages, MCP-1 has also been shown to be an insulin responsive gene in adipocytes, with elevated MCP-1 decreasing glucose-uptake and altering the expression of adipogenic genes [23].

One of the products of AOC3-catalyzed amine oxidation is H_2O_2, which has increasingly gained recognition as a possible cellular signaling molecule [24, 25]. NADPH oxidases catalyze the reduction of dioxygen to form superoxide, which can spontaneously dismutate to H_2O_2. Cellular expression was initially discovered in neutrophils, which produced ROS in a respiratory burst as a defensive mechanism against invading pathogens. However, the presence of NADPH oxidase on non-immune cell types have spurred speculation of a signaling role for the H_2O_2 produced [26]. It has been shown that human adipocytes and cultured 3T3-L1 adipocytes express an isoform of NADPH oxidase, which produces H_2O_2, upon stimulation with insulin [27, 28]. This H_2O_2-generating oxidase is also under regulation by a variety of hormones, growth factors, and cytokines, providing evidence of a possible signaling role [29]. Though H_2O_2 has been demonstrated to be necessary in insulin signaling, other possible signaling roles, particularly in an immuno-modulatory capacity, will be explored. An investigation of whether H_2O_2 generated by AOC3 turnover could be involved in the production and secretion of cytokines and chemokines, was conducted.

Methods

Cell culture. The differentiation protocol starts with a 100 mm tissue culture dish of murine 3T3-L1 fibroblasts obtained from American Type Cell Culture (ATCC). Cells were grown to confluence 7 days after initial plating. Once confluent, cellular differentiation was induced using insulin, dexamethasone, and methylisobutylxanthine as previously described [30]. Cells were cultured in Dulbecco's Modified Eagle Medium (DMEM) (Invitrogen, Carlsbad, CA) supplemented with 10% Fetal Bovine Serum (FBS) (Hyclone, Waltham, MA). Differentiation takes 8 days. Only passage 1 or 2 differentiated adipocytes were used at Day 8 - 10. C2C12 mouse myoblast cells [31] (ATCC) were cultured in DMEM and 10% FBS at passages 70 – 72. U20S human osteosarcoma cells (ATCC) were cultured in DMEM and 10% FBS at passages 10 – 12. Prior to use, adipocytes were checked for confluency within each experimental well. Partially confluent wells were not used in experiments so that effects due to variable cell numbers could be minimized.

MCP-1 ELISA. Differentiated adipocytes in 6-well plates were washed with warmed (37°C) phosphate buffered saline, pH 7.4 twice and then with warmed Dulbecco's Modified Eagle Medium with 1% HEPES (1M HEPES, Invitrogen) once. Hydrogen peroxide (EM Science), made at 1000x, were then introduced into each well from 25 uM – 1 mM. Semicarbazide treatment involved incubation of adipocytes at 1 mM for 5 minutes. Isoamylamine was introduced at 750 uM, ammonium sulfate at 200 uM, isovaleraldehyde at 200 uM for 24 hours. For adipocytes treated with only hydrogen peroxide, supernatant was harvested at 0, 0.5, 1, 4, 8, 12, 14.5, 20, and 24 hour time points. Each time point was performed on a separate set of adipocytes. After treatment of adipocytes, an aliquot of cell media supernatant was taken and snap frozen. Samples were maintained at -80°C prior to analysis. Samples were completely thawed and subjected to mouse MCP-1 immunoassay kit (Invitrogen). The recommended procedure for kit use was followed except handwork with reagents was minimized using a Fluidics Automation Integration – Velocity 11 Bravo with a 96 well head (Agilent Technologies, Santa Clara, CA). With the exception of washing wells 7 times rather than 6 due to volume constraints of Velocity 11, all other procedures were followed as prescribed. The results were visualized using a Perkin Elmer EnVision Multilabel plate reader with a 450 nm optical filter. Both Fluidics Automation and Envision plate reader were used at the Berkeley Screening Center. All chemicals were purchased from Sigma Aldrich unless otherwise stated.

Millipore 22-plex cytokine ELISA. Differentiated adipocytes were treated as described above in the ELISA section for 24 hours. After treatment of adipocytes for 24 hours, an aliquot of cell media supernatant was taken and snap frozen. Samples were maintained at -80°C. After all samples were collected, they were shipped to Millipore on dry ice for analysis using their proprietary multiplex ELISA. Cell media from adipocytes were screened for twenty two cytokines, including G-CSF, GM-CSF, IFN-γ, IL-10, IL-12 (p70), IL-13, IL-15, IL-17, IL-1α, IL-1β, IL-2, IL-4, IL-5, IL-6, IL-7, IL-9, IP-10, KC, MCP-1, MIP-1α, RANTES, TNF-α using the MILLIPLEX MAP mouse cytokine/chemokine assay.

Immunoblot of cytochrome c. Cytochrome c released into cell media upon adipocyte death was assayed after treatments of adipocytes with either 200 uM or 1 mM hydrogen peroxide for 0, 4,

8, 12, 17.5, 20, and 24 hours. Samples were taken and immediately snap frozen and stored at -80 °C until analysis. Upon complete thaw, 10 uL of samples was mixed with equal volume Laemmli Sample Buffer (Bio-rad Laboratories, Hercules, CA) + 5% β-mercaptoethanol for electrophoresis. Before loading on a 10% acrylamide gel, samples were boiled for 7 minutes at 100°C. The resolved proteins were transferred to nitrocellulose membrane (Bio-rad Laboratories, Hercules, CA) using a Mini-PROTEAN II (Bio-rad Laboratories, Hercules, CA) system kept on ice. Effectiveness of protein transfer was determined using Precision Plus Protein Standards Kaleidoscope (Bio-rad). Blocking was performed with TBS (2.42 g Tris base, 8 g NaCl, adjusted to pH 7.6 with HCl), 5% nonfat dry milk (Carnation, Nestle), and 0.1% Tween-20 for 1 hour at room temperature. After washing 3 times with TBS/T (TBS buffer, 0.1% Tween-20), membrane was incubated with a 1:1000 dilution of primary anti-mouse cytochrome c antibody (Cell Signaling Technology, Danvers, MA) in blocking buffer with gentle agitation overnight (approximately 14 - 16 hours) at 4°C. Membrane was then washed 3 times with TBS/T buffer and the membrane incubated in 1:1000 dilution of secondary antibody, horseradish peroxidase conjugated anti-rabbit IGG (Cell Signaling Technology, Danvers, MA) with gentle agitation for 1 hour at room temperature. After washing the membrane 3 times, mouse cytochrome c was detected using ECL Plus Western Blotting Detection System (GE Healthcare, Buckinghamshire, UK).

Quantitation of intracellular MCP-1. Adipocytes were treated with 200 uM H_2O_2 for 0, 4, 8, 16, 20, and 24 hours. Upon harvest of adipocytes, media was aspirated and cells washed twice with cold phosphate buffered saline, pH 7.4. Adipocytes were then incubated with Lysis buffer (0.1% Triton X-100 (Sigma), protease inhibitor cocktail (Sigma), PBS, pH 7.4) at equal volume as adipocyte incubation for ELISA. Adipocytes were then scraped from the bottom of the well and placed into 15 mL Falcon (BD Biosciences). Cells were sonicated at 4°C using a micro-tip with a Misonix Sonicator 3000 ultrasonic liquid processor (Qsonica, Newtown, CT) with a power setting of 1 for 10 seconds, 30 second rest on ice, and another 10 seconds at power setting 1. After sonication, cells were pelleted by centrifuge at 4000 rpm for 20 minutes at 4°C. The cell supernatants were collected, disregarding the upper layer of lipids, snap frozen, and stored at -80 °C until analysis by ELISA.

Results

With a large number of cytokines and chemokines that could be associated with AOC3 turnover, it was expedient to screen for a large number of these molecules using a sensitive multiplex technology. Multiplex detection also allows for the quantitation of these proteins from a single biological sample. The Luminex xMAP technology is a multiplex ELISA with simultaneous detection of up to 32 cytokines and chemokines with sensitivities ranging from 3.2 – 10,000 pg/mL. As a service offered by Millipore, samples were collected, snap frozen with liquid nitrogen, and sent to their screening labs.

3T3-L1 adipocytes, at day 8 – 10 post-differentiation and passage 1 or 2, were incubated with isoamylamine substrate, with or without semicarbazide inhibitor pre-incubation for 24 hours. In addition to AOC3 substrate, the products of isoamylamine oxidation were also screened for activity. Isovaleraldehyde is the aldehyde product of isoamylamine oxidation, as shown below:

isoamylamine   isovaleraldehyde
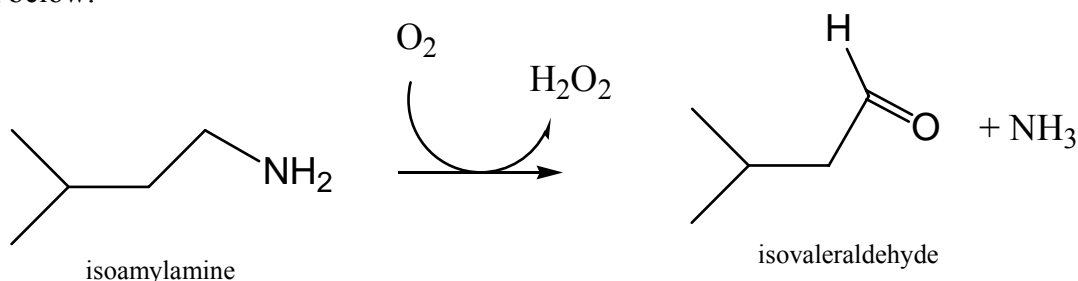
A panel of 22 cytokines/chemokines was selected for screening, consisting of G-CSF, GM-CSF, IFN-γ, IL-10, IL-12 (p70), IL-13, IL-15, IL-17, IL-1α, IL-1β, IL-2, IL-4, IL-5, IL-6, IL-7, IL-9, IP-10, KC, MCP-1, MIP-1α, RANTES, and TNF-α. Interleukins (IL) are secreted signaling molecules involved in the function of the immune system. Granulocyte colony-stimulating factor (G-CSF) , granulocyte-macrophage colony-stimulating factor (GM-CSF), IL-2, IL-7, IL-9, IL-12, IL-15, IP-10, and RANTES (Regulated upon activation, normal T-cell expressed, and secretes) are factors that promote the differentiation, proliferation, and/or regulation of granulocytes (basophils, eosinophils, and neutrophils), monocytes, natural killer cells, B cells, and/or T cells [32-39]. IL-1α, IL-1β, IL-17, and TNF-α are pro-inflammatory cytokines [40, 41]. IL-4, IL-5, and IL-10 are involved in B lymphocyte regulation [42-44]. IL-6 can be both pro- or anti-inflammatory [45]. Interferon-gamma (IFN-γ) is involved in the immune response to viral and intracellular infections[46]. Keratinocyte chemoattractant (KC) and macrophage inflammatory proteins (MIP-1α) are both neutrophil chemoattractants and pro-inflammatory [47, 48]. IL-13 is critical in the promotion of allergic responses [49] and also possesses anti-inflammatory properties by inhibiting inflammatory cytokine production [50]. Though each cytokine and chemokine has been assigned a classification, their functions are frequently complex and usually exhibit pleiotropic effects.

The results of the cytokine/chemokine screening are shown in Figure 1. Only seven (IL-1α, IL-6, IL-13, IP-10, KC, MCP-1, and RANTES) produced a detectable signal out of the 22 molecules screened. Adipocytes are currently known to produce IL-1β [51], IL-6 [52], IL-8 (KC) [53], MIP-1α, TNF-α [54], IL-10 [55], IL-15 [56], IL-18 [57], RANTES [58], IL-13 [22], and MCP-1. A search in the literature for adipocyte production of IL-1α and IP-10 was not

successful, though with the exception of IP-10, cytokine production was relatively low. Hydrogen peroxide incubation produced increased secretion of IL-6, IP-10, KC, and MCP-1 by adipocytes compared to isoamylamine incubation and no treatment. However, any increase or decrease in cytokine production, including MCP-1, did not seem to be AOC3 dependent as adipocytes pre-treated with semicarbazide inhibitor secreted similar levels of cytokine compared to cells without inhibitor treatment. Semicarbazide itself did not seem to affect cytokine release when compared to cells undergoing no treatment. The other products of isoamylamine oxidation, ammonia and isovaleraldehyde, also did not affect cytokine secretion when compared to adipocytes with no treatment. Interestingly, when the level of IL-13 were examined more closely as shown in Figure 2, the increase in IL-13 production was correlated with AOC3 turnover, as inhibitor treated cells exhibited less IL-13 production. However, the levels are relatively low at 25 – 50 pg/mL, which may not be enough to have a physiological effect and did not correlate with H_2O_2 production.   IL-13 production was also greater when compared to cells with no treatment.

An effort to replicate these results using a separate ELISA method, looking strictly at MCP-1 production by adipocytes, was undertaken. The ELISA was performed in a 96-well plate with the antibody to MCP-1 adsorbed to the bottom of each well. Significant errors in the results can arise due to variability of introducing samples and reagents to the plate using hand pipetting. Therefore, a liquid handling robot was programmed to perform the ELISA protocol so that all samples and reagents were introduced to the 96 wells at the same time and in a consistent fashion. Experiments performed on different days will also be more comparable. The results are shown in Figure 3. Again, change in MCP-1 production was not correlated with AOC3 turnover of isoamylamine. A slight increase in MCP-1 secretion due to H_2O_2 incubation was observed, but not as drastic as the change seen in the previous screen with most levels of MCP-1 production approximately 50% higher than before. Though AOC3 turnover did not result in a significant change in MCP-1 production by adipocytes, both ELISA results showed increased MCP-1 production due to addition of H_2O_2, which may potentially act as a pro-inflammatory signaling molecule.

To look at the effects of H_2O_2 on adipocyte secretion of MCP-1, adipocytes were treated with 0 – 200 uM H_2O_2 for 0 -24 hours, with conditioned cell media taken after 0, 0.5, 1, 4, 8, 14.5, and 24 hours for analysis of MCP-1 release. The results are shown in Figure 4 with the accompanying table showing standard errors associated with each incubation condition. Upon inspection after 24 hour peroxide incubation, the morphological phenotype of the adipocytes did not appear to change and the difference in levels of floating and dead cells between cells incubated with and without peroxide was minimal. There does not seem to be any H_2O_2– dependent effect on MCP-1 release with incubations from 0 – 50 uM for all time points. However, at 100 uM H_2O_2, after 4 hours, MCP-1 release by adipocytes increased relative to no treatment. The increase in MCP-1 release occurred between 4 – 14.5 hours. The same is true for the 200 uM H_2O_2 incubation, with the increase mostly occurring between 4 – 8 hours. Figure 5 shows MCP-1 release by adipocytes between 4 – 24 hours incubation with 100 uM and 200 uM H_2O_2 , with accompanying table of rates of MCP-1 release. Comparing results of cells with no treatment, the greatest increase in rate of MCP-1 release was observed during the 200 uM H_2O_2 incubation, with an approximate two-fold increase between 4 – 8 hours. Increase in MCP-1 release during the 100 uM H_2O_2 incubation occurred mostly during 8 – 14.5 hours incubation, with an approximate 1.5 fold increase. It is interesting to note that MCP-1 release from 14.5 –

24 hours were both decreased for 100 uM and 200 uM H_2O_2 incubation compared to cells under no treatment, at approximately 70% of values observed.

Since the endpoint values (24 hours) of MCP-1 release were all different, absolute values of MCP-1 release for the time points at various H_2O_2 concentrations will also be different, making strict comparisons difficult. Each experimental condition was performed on a different set of adipocytes to minimize disturbances to the cells during the harvesting of supernatant and the changes in MCP-1 concentrations that occur as well volumes decreased if aliquots were taken over a 24 hour period from the same well. Therefore, a great deal of variability is expected as adipocyte cell numbers may vary from well to well, effects due to passaging may occur, and variations during the differentiation process may all affect results. These variations could account for the null effects at 25 uM and 50 uM H_2O_2 on adipocyte release of MCP-1, with both absolute values of MCP-1 release below those of cells under no treatment after 24 hours. Normalizing the data and presenting MCP-1 release as a percentage of final MCP-1 (at 24 hours) concentration is shown in Figure 6, with accompanying table of actual percentages. MCP-1 release at 100 uM and 200 uM H_2O_2 both show increases compared to no treatment between 4 – 14.5 hours, as previously observed. However, increase in MCP-1 release was also seen for 25 uM and 50 uM H_2O_2 between 8 – 14.5 hours of incubation. Effects at lower concentrations of H_2O_2 are more important as cellular signaling is thought to proceed with low concentrations of H_2O_2, typically below 50 uM, while greater concentrations occur due to oxidative stress. Generally, MCP-1 release increased as adipocytes were incubated for longer times, including cells under no treatment. There seems to be a constitutive release of MCP-1 by 3T3-L1 adipocytes under culture conditions. In addition, there is also an increase in MCP-1 release due to addition of exogenous H_2O_2 in a concentration dependent manner. Adipocytes were also incubated with 1 mM H_2O_2, however it was found that a greater amount of cell death occurred during the incubation. Occurrence of adipocyte cell death was determined by immunoblot of cytochrome c in the supernatant media. Cytochrome c is released from the mitochondria during the controlled process of cellular death known as apoptosis [59]. In addition, it has been reported that cytochrome c is also released from necrotic cells [60]. Necrosis is events associated with uncontrolled cell death, and effects are always detrimental. 3T3-L1 adipocytes were incubated with 200 uM exogenous H_2O_2 for 0, 4, 8, 12, 17.5, 20, and 24 hours and an immunoblot for cytochrome c was performed as shown in Figure 7A. As incubation time increased, released cytochrome c also increased. Incubations with 1 mM H_2O_2 also resulted in increased cytochrome c at a much faster rate as seen in Figure 7B. Upon incubation with 1 mM exogenous H_2O_2, released cytochrome c after 4 hours was comparable to the level measured after 24 hours in the 200 uM incubations. From these results, higher concentrations of H_2O_2 may cause oxidative stress and cell duress, which may promote death. As a consequence, the intracellular MCP-1 would be released and contaminate our measurements of controlled cytokine release. It is unknown what intracellular MCP-1 levels would be found in adipocytes upon treatment with H_2O_2 and whether changes occur over time. Therefore, adipocytes were treated with 0 uM and 200 uM H_2O_2 and harvested after 0, 4, 8, 16, 20, and 24 hours. The adipocytes were lysed and MCP-1 levels determined by ELISA as shown in Figure 8. The amount of intracellular MCP-1 seemed to be independent of incubation time and peroxide concentration, ranging from approximately 350 pg/mL – 450 pg/mL for both adipocytes incubated with and without 200 uM H_2O_2. If all the adipocytes within each well were lysed, the MCP-1 concentration would be, on average, approximately 400 pg/mL. Interestingly, intracellular MCP-1 levels seemed to decrease over time for both adipocytes treated with and without H_2O_2, though this change may be within

the errors of detection. Relatively constant levels of intracellular MCP-1 imply a steady state level of intracellular MCP-1 with induction of release of additional MCP-1 by H_2O_2. In addition, the rate of MCP-1 release by adipocytes is most likely higher when incubated with higher peroxide concentrations. Lysed adipocytes will also contribute to the overall measurements of released MCP-1, with a greater contribution at the higher peroxide concentrations. However, the number of cell deaths as a percentage of the total population during the experiment is not expected to be high, as visually inspected cells after peroxide incubation for 24 hours did not differ markedly from cells under no treatment.

Another concern is the differentiation efficiency of 3T3-L1 fibroblast. It is not possible to differentiate every 3T3-L1 fibroblast into lipid-laden adipocytes for the purpose of these experiments. Usually, under experimental conditions, the percentage of adipocyte differentiation approaches 90 – 95% efficiency. Therefore, it was possible that MCP-1 release could be attributed to 3T3-L1 fibroblasts. Figure 9 shows an image of 3T3-L1 fibroblast cellular morphology. It is relatively easy to differentiate between the undifferentiated fibroblast and adipocytes upon visual inspection. Therefore, it is also necessary to determine whether the fibroblasts release MCP-1, with and without peroxide treatment. Undifferentiated 3T3-L1 fibroblasts were incubated with 0 uM and 200 uM H_2O_2, and released MCP-1 concentrations were examined after 8 hours, 16 hours, and 20 hours as shown in Figure 10. With no exogenous peroxide added, the fibroblasts do release a basal level of MCP-1, ranging from 128 – 211 pg/mL, as shown in Figure 10, bottom table. Since only 5 – 10% of the cell population of differentiated adipocytes was fibroblasts, this would contribute 21.1 pg/mL MCP-1 at most. However, paracrine signaling and cellular contact between adipocytes and fibroblasts may alter MCP-1 release. When fibroblasts were incubated in 200 uM H_2O_2, levels of release increased dramatically, from 318 – 704 pg/mL, which can maximally contribute 70.4 pg/mL MCP-1. In fact, MCP-1 released by adipocytes incubated with 200 uM H_2O_2 for 24 hours was approximately 69.7 pg/mL greater than that of adipocytes under no treatment. Therefore, the increased MCP-1 release could be entirely attributable to the fibroblasts. The top table shows the rate of MCP-1 release between 8 – 16 hours and 16 – 20 hours. When compared to adipocytes, the rate of MCP-1 release by fibroblasts was relatively small, at approximately 21% and 54% of adipocytes at 8 – 16 hours and 16 – 20 hours, respectively. From these results, undifferentiated fibroblasts will also contribute to MCP-1 release.

Since it was unexpected that 3T3-L1 fibroblasts would produce and release MCP-1 upon introduction of exogenous peroxide, cell lines without known immune functions were also subjected to H_2O_2 and assayed for MCP-1 release. From previous results in our lab, 3T3-L1 fibroblasts were shown to express AOC3 during the process of differentiation and were found to be devoid of AOC3 prior to differentiation. U20S is a human osteosarcoma cell line cultivated from bone tissue. Upon addition of 50 uM and 200 uM exogenous H_2O_2, U20S cells did not respond with increased release of MCP-1 in a time-dependent manner as shown in Figure 11A. Due to relatively flat MCP-1 standard curve at lower concentrations, measurements of MCP-1 concentration were presented using raw absorbances at $\lambda = 450$ nm. This result suggests that osteocytes do not release MCP-1 upon incubation by H_2O_2. On the other hand, when C2C12 myoblasts, a mouse cell line that can be differentiated into muscle cells, were incubated with 50 uM and 200 uM exogenous H_2O_2, MCP-1 release increased over a 24 hour time period, as shown in Figure 11B. However, the rate of increase did not depend on H_2O_2 concentration, which suggests that MCP-1 release could be constitutive or promoted by some other factor in the cell

media. These results suggest that MCP-1 release may be more prevalent than previously thought and may be involved in a non-immune function.

Adipocytes incubated with AOC3 substrate did not result in differential MCP-1 release when compared with inhibited enzyme after a 24 hour incubation period. However, it is unknown whether an effect may occur at shorter incubation times. Therefore, adipocytes were incubated with 750 uM isoamylamine, either with or without semicarbazide pretreatment. Aliquots from both treatments were taken at 0 hr, 8 hr, 17.5hr, and 24 hrs and assayed for MCP-1 release by ELISA as shown in Figure 12. No difference in MCP-1 release was found between 0 - 8 hours. However, rate of MCP-1 release with isoamylamine incubation was found to be 35 pg/mL/hr between 8 – 17.5 hours while inhibited adipocytes released MCP-1 at a slightly lower rate of 32 pg/mL/hr. After 17.5 hours, MCP-1 release decreased for both isoamylamine incubations, with MCP-1 concentration decreasing in the case of isoamylamine incubation. This decrease was unexpected, most likely due to variability of MCP-1 release in each experimental well. Decreases were not observed in the H_2O_2 incubations, supporting previously observed results.

Discussion

3T3-L1 adipocytes were incubated with isoamylamine substrate, with or without semicarbazide inhibitor pre-incubation for various time points to determine whether increased cytokine release occurred. In addition to AOC3 substrate, the products of isoamylamine oxidation were also screened for activity. A panel of 22 cytokines/chemokines was selected for screening, with seven cytokines (IL-1α, IL-6, IL-13, IP-10, KC, MCP-1, and RANTES) found to have detectable levels of release by adipocytes. MCP-1, IL-6, KC, and IP-10 release were found to be H_2O_2 dependent, though with little correlation to AOC3 turnover. This finding may occur if AOC3-catalyzed production of H_2O_2 was slow, resulting in a concentration of H_2O_2 too low to be involved in signaling. From whole cell kinetic studies in Chapter 3, the maximal rate of isoamylamine oxidation was found to be approximately 0.078 uM/min/well, resulting in the total production of 112 uM H_2O_2 over a 24 hour period. Adipocyte incubations with isoamylamine was carried out at a concentration of 750 uM (approximately five time K_m = 148 uM), which would decrease to 638 uM after 24 hours. The final isoamylamine concentration should still saturate AOC3, at approximately 4.3 times K_m. Of course, the continuous production of 0.078 uM H_2O_2 per minute may have a different signaling effect on adipocytes than a bolus addition of 220 uM H_2O_2. Therefore, the increase in cytokine release by adipocytes observed require a higher H_2O_2 concentration, which AOC3-catalyzed isoamylamine turnover was unable to produce over a 24 hour period.

Though this result may preclude AOC3 involvement, H_2O_2 signaling could be involved in cytokine release in adipocytes. With reports of obesity as a disorder characterized by mild inflammation and increased macrophage infiltration, release of MCP-1, a monocyte chemoattractant, by H_2O_2 signaling was investigated further. MCP-1 release by adipocytes was found to increase as cells were treated with greater concentration of H_2O_2, with maximal controlled release at 200 uM H_2O_2. Minimal differences in MCP-1 release were observed at 25 uM and 50 uM H_2O_2 when compared to control conditions of no treatment. In addition, MCP-1 release generally increased from 0 hours to 24 hours, even when adipocytes were not treated with H_2O_2. This result suggests that adipocytes may be capable of constitutive release of MCP-1. Control experiments show that 3T3-L1 fibroblasts also release MCP-1 in direct proportion to level of exogenous H_2O_2 concentration, though fibroblasts typically make up 5 − 10 % of total cells in each experiment. In addition, due to the exogenous H_2O_2, adipocytes do experience increased level of cellular stress, resulting in cell lysis, which also contributed to levels of MCP-1 release.

Though MCP-1 release was found to be dependent on both concentration of H_2O_2 and time period during incubations, the actual contribution of controlled MCP-1 release by adipocytes is most likely lower than the numbers reported. However, this does not preclude involvement of H_2O_2 signaling in MCP-1 release and suggests there may be a link in cytokine release. Three other cytokines were also found in increased concentrations upon H_2O_2 incubation. IP-10, IL-6, KC, and MCP-1 are typically considered to be pro-inflammatory cytokines. Increased release of these cytokines was observed after high concentrations of exogenous H_2O_2 (100 uM - 220 uM) were added. Rather than have a signaling role, this level of H_2O_2 could induce cellular stress, inducing release of pro-inflammatory cytokines. Interestingly, IL-13 release was shown to be dependent on AOC3 turnover, though the increase was very low, at approximately 50 pg/mL.

Differences in absolute levels of MCP-1 release were also observed from experiment to experiment. For example, a final concentration of MCP-1 release was found to be approximately 450 pg/mL after 24 hour incubation with isoamylamine in one experiment, approximately 1600 pg/mL in another experiment, and 1000 pg/mL in another. This kind of absolute MCP-1 concentration differences was observed in most experiments, making relative and percent change comparisons between each experiment far more important than absolute comparisons between experiments. These differences could arise due to variable passage number of the adipocytes (either passage 1 or 2), variability in cell number in each experimental well, differences in differentiation efficiency, and handling during differentiation.

References

1. Fantuzzi, G., *Adipose tissue, adipokines, and inflammation.* Journal of Allergy and Clinical Immunology, 2005. **115**(5): p. 911-919.
2. Hotamisligil, G.S., N.S. Shargill, and B.M. Spiegelman, *Adipose Expression of Tumor-Necrosis-Factor-Alpha - Direct Role in Obesity-Linked Insulin Resistance.* Science, 1993. **259**(5091): p. 87-91.
3. Kern, P.A., et al., *Adipose tissue tumor necrosis factor and interleukin-6 expression in human obesity and insulin resistance.* American Journal of Physiology-Endocrinology and Metabolism, 2001. **280**(5): p. E745-E751.
4. Feingold, K.R., et al., *Effect of Tumor Necrosis Factor (Tnf) on Lipid-Metabolism in the Diabetic Rat - Evidence That Inhibition of Adipose-Tissue Lipoprotein-Lipase Activity Is Not Required for Tnf-Induced Hyperlipidemia.* Journal of Clinical Investigation, 1989. **83**(4): p. 1116-1121.
5. Kanety, H., et al., *Tumor-Necrosis-Factor-Alpha Induced Phosphorylation of Insulin-Receptor Substrate-1 (Irs-1) - Possible Mechanism for Suppression of Insulin-Stimulated Tyrosine Phosphorylation of Irs-1.* Journal of Biological Chemistry, 1995. **270**(40): p. 23780-23784.
6. Hofmann, C., et al., *Altered Gene-Expression for Tumor-Necrosis-Factor-Alpha and Its Receptors during Drug and Dietary Modulation of Insulin-Resistance.* Endocrinology, 1994. **134**(1): p. 264-270.
7. Skurk, T. and H. Hauner, *Obesity and impaired fibrinolysis: role of adipose production of plasminogen activator inhibitor-1.* International Journal of Obesity, 2004. **28**(11): p. 1357-1364.
8. Sethi, J.K. and G.S. Hotamisligil, *The role of TNF alpha in adipocyte metabolism.* Seminars in Cell & Developmental Biology, 1999. **10**(1): p. 19-29.
9. Gordon, S., *The macrophage: past, present and future.* Eur J Immunol, 2007. **37 Suppl 1**: p. S9-17.
10. Weisberg, S.P., et al., *Obesity is associated with macrophage accumulation in adipose tissue.* Journal of Clinical Investigation, 2003. **112**(12): p. 1796-1808.
11. Cancello, R., et al., *Increased infiltration of macrophages in omental adipose tissue is associated with marked hepatic lesions in morbid human obesity.* Diabetes, 2006. **55**(6): p. 1554-1561.
12. Yu, R.N., et al., *Mesenteric adipose tissue-derived monocyte chemoattractant protein-1 plays a crucial role in adipose tissue macrophage migration and activation in obese mice.* Obesity, 2006. **14**(8): p. 1353-1362.
13. Kanda, H., et al., *MCP-1 contributes to macrophage infiltration into adipose tissue, insulin resistance, and hepatic steatosis in obesity.* Journal of Clinical Investigation, 2006. **116**(6): p. 1494-1505.
14. Takahashi, K., et al., *Adiposity elevates plasma MCP-1 levels leading to the increased CD11b-positive monocytes in mice.* Journal of Biological Chemistry, 2003. **278**(47): p. 46654-46660.
15. Cancello, R., et al., *Reduction of macrophage infiltration and chemoattractant gene expression changes in white adipose tissue of morbidly obese subjects after surgery induced weight loss.* Diabetes, 2005. **54**(8): p. 2277-2286.
16. Kamei, N., et al., *Overexpression of monocyte chemoattractant protein-1 in adipose tissues causes macrophage recruitment and insulin resistance.* Journal of Biological Chemistry, 2006. **281**(36): p. 26602-26614.
17. Lumeng, C.N., J.L. Bodzin, and A.R. Saltiel, *Obesity induces a phenotypic switch in adipose tissue macrophage polarization.* Journal of Clinical Investigation, 2007. **117**(1): p. 175-184.
18. Van Ginderachter, J.A., et al., *Classical and alternative activation of mononuclear phagocytes: picking the best of both worlds for tumor promotion.* Immunobiology, 2006. **211**(6-8): p. 487-501.
19. Martinez, F.O., L. Helming, and S. Gordon, *Alternative activation of macrophages: an immunologic functional perspective.* Annu Rev Immunol, 2009. **27**: p. 451-83.
20. Stein, M., et al., *Interleukin 4 potently enhances murine macrophage mannose receptor activity: a marker of alternative immunologic macrophage activation.* J Exp Med, 1992. **176**(1): p. 287-92.
21. Qian, B.Z. and J.W. Pollard, *Macrophage Diversity Enhances Tumor Progression and Metastasis.* Cell, 2010. **141**(1): p. 39-51.
22. Kang, K., et al., *Adipocyte-derived Th2 cytokines and myeloid PPARdelta regulate macrophage polarization and insulin sensitivity.* Cell Metab, 2008. **7**(6): p. 485-95.
23. Sartipy, P. and D.J. Loskutoff, *Monocyte chemoattractant protein 1 in obesity and insulin resistance.* Proceedings of the National Academy of Sciences of the United States of America, 2003. **100**(12): p. 7265-7270.

24. Forman, H.J., M. Maiorino, and F. Ursini, *Signaling Functions of Reactive Oxygen Species.* Biochemistry, 2010. **49**(5): p. 835-842.

25. Veal, E.A., A.M. Day, and B.A. Morgan, *Hydrogen peroxide sensing and signaling.* Molecular Cell, 2007. **26**(1): p. 1-14.

26. Geiszt, M., *NADPH oxidases: New kids on the block.* Cardiovascular Research, 2006. **71**(2): p. 289-299.

27. Kriegerbrauer, H.I. and H. Kather, *Human Fat-Cells Possess a Plasma-Membrane Bound H2o2-Generating System That Is Activated by Insulin Via a Mechanism Bypassing the Receptor Kinase.* Journal of Clinical Investigation, 1992. **89**(3): p. 1006-1013.

28. Kriegerbrauer, H.I. and H. Kather, *Antagonistic Effects of Different Members of the Fibroblast and Platelet-Derived Growth-Factor Families on Adipose Conversion and Nadph-Dependent H2o2 Generation in 3t3 L1-Cells.* Biochemical Journal, 1995. **307**: p. 549-556.

29. Kriegerbrauer, H.I. and H. Kather, *The Stimulus-Sensitive H2o2-Generating System Present in Human Fat-Cell Plasma-Membranes Is Multireceptor-Linked and under Antagonistic Control by Hormones and Cytokines.* Biochemical Journal, 1995. **307**: p. 543-548.

30. Stephens, J.M., J. Lee, and P.F. Pilch, *Tumor necrosis factor-alpha-induced insulin resistance in 3T3-L1 adipocytes is accompanied by a loss of insulin receptor substrate-1 and GLUT4 expression without a loss of insulin receptor-mediated signal transduction.* Journal of Biological Chemistry, 1997. **272**(2): p. 971-976.

31. Yaffe, D. and O. Saxel, *Serial Passing and Differentiation of Myogenic Cells Isolated from Dystrophic Mouse Muscle.* Nature, 1977. **270**(5639): p. 725-727.

32. Root, R.K. and D.C. Dale, *Granulocyte colony-stimulating factor and granulocyte-macrophage colony-stimulating factor: Comparisons and potential for use in the treatment of infections in nonneutropenic patients.* Journal of Infectious Diseases, 1999. **179**: p. S342-S352.

33. Goodwin, R.G., et al., *Human Interleukin-7 - Molecular-Cloning and Growth-Factor Activity on Human and Murine B-Lineage Cells.* Proceedings of the National Academy of Sciences of the United States of America, 1989. **86**(1): p. 302-306.

34. Knoops, L. and J.C. Renauld, *IL-9 and its receptor: From signal transduction to tumorigenesis.* Growth Factors, 2004. **22**(4): p. 207-215.

35. D'Acquisto, F., F. Maione, and M. Pederzoli-Ribeil, *From IL-15 to IL-33: the never-ending list of new players in inflammation. Is it time to forget the humble aspirin and move ahead?* Biochemical Pharmacology, 2010. **79**(4): p. 525-534.

36. Goriely, S., M.F. Neurath, and M. Goldman, *How microorganisms tip the balance between interleukin-12 family members.* Nature Reviews Immunology, 2008. **8**(1): p. 81-86.

37. Christen, U. and M.G. Von Herrath, *IP-10 and type 1 diabetes: A question of time and location.* Autoimmunity, 2004. **37**(4): p. 273-282.

38. Levy, J.A., *The Unexpected Pleiotropic Activities of RANTES.* Journal of Immunology, 2009. **182**(7): p. 3945-3946.

39. Kuziel, W.A. and W.C. Greene, *Interleukin-2 and the Il-2 Receptor - New Insights into Structure and Function.* Journal of Investigative Dermatology, 1990. **94**(6): p. S27-S32.

40. Dinarello, C.A., *The Interleukin-1 Family - 10 Years of Discovery.* Faseb Journal, 1994. **8**(15): p. 1314-1325.

41. Gaffen, S.L., *Structure and signalling in the IL-17 receptor family.* Nature Reviews Immunology, 2009. **9**(8): p. 556-567.

42. Howard, M., *Interleukins for Lymphocytes-B.* Survey of Immunologic Research, 1983. **2**(3): p. 210-212.

43. Howard, M., et al., *Biological Properties of Interleukin-10.* Journal of Clinical Immunology, 1992. **12**(4): p. 239-247.

44. Takatsu, K., T. Kouro, and Y. Nagai, *Interleukin 5 in the Link Between the Innate and Acquired Immune Response.* Advances in Immunology, Vol 101, 2009. **101**: p. 191-236.

45. Heinrich, P.C., et al., *Principles of interleukin (IL)-6-type cytokine signalling and its regulation.* Biochemical Journal, 2003. **374**: p. 1-20.

46. Schoenborn, J.R. and C.B. Wilson, *Regulation of interferon-gamma during innate and adaptive immune responses.* Advances in Immunology, Vol 96, 2007. **96**: p. 41-101.

47. Zhang, X.W., et al., *Redundant function of macrophage inflammatory protein-2 and KC in tumor necrosis factor-alpha-induced extravasation of neutrophils in vivo.* European Journal of Pharmacology, 2001. **427**(3): p. 277-283.

48. Maurer, M. and E. von Stebut, *Macrophage inflammatory protein-1.* International Journal of Biochemistry & Cell Biology, 2004. **36**(10): p. 1882-1886.

49. Grunig, G., et al., *Requirement for IL-13 independently of IL-4 in experimental asthma.* Science, 1998. **282**(5397): p. 2261-2263.

50. Wynn, T.A., *IL-13 effector functions.* Annual Review of Immunology, 2003. **21**: p. 425-456.

51. Fain, J.N., et al., *Comparison of the release of adipokines by adipose tissue, adipose tissue matrix, and Adipocytes from visceral and subcutaneous abdominal adipose tissues of obese humans.* Endocrinology, 2004. **145**(5): p. 2273-2282.

52. Rajala, M.W. and P.E. Scherer, *Minireview: The adipocyte - At the crossroads of energy homeostasis, inflammation, and atherosclerosis.* Endocrinology, 2003. **144**(9): p. 3765-3773.

53. Neels, J.G., et al., *Keratinocyte-derived Chemokine in Obesity EXPRESSION, REGULATION, AND ROLE IN ADIPOSE MACROPHAGE INFILTRATION AND GLUCOSE HOMEOSTASIS.* Journal of Biological Chemistry, 2009. **284**(31): p. 20692-20698.

54. Sell, H., et al., *Cytokine secretion by human adipocytes is differentially regulated by adiponectin, AICAR, and troglitazone.* Biochemical and Biophysical Research Communications, 2006. **343**(3): p. 700-706.

55. Bradley, R.L., F.M. Fisher, and E. Maratos-Flier, *Dietary fatty acids differentially regulate production of TNF-alpha and IL-10 by murine 3T3-L1 adipocytes.* Obesity, 2008. **16**(5): p. 938-944.

56. Spurlock, M., et al., *Adipocytes, myofibers, and cytokine biology: New horizons in the regulation of growth and body composition.* Journal of Animal Science, 2005. **83**: p. 115-115.

57. Sun, J.Z., et al., *Intermittent High Glucose Stimulate MCP-l, IL-18, and PAI-1, but Inhibit Adiponectin Expression and Secretion in Adipocytes Dependent of ROS.* Cell Biochemistry and Biophysics, 2009. **55**(3): p. 173-180.

58. Skurk, T., et al., *Expression and Secretion of RANTES (CCL5) in Human Adipocytes in Response to Immunological Stimuli and Hypoxia.* Hormone and Metabolic Research, 2009. **41**(3): p. 183-189.

59. Perkins, G., E. Bossy-Wetzel, and M.H. Ellisman, *New insights into mitochondrial structure during cell death.* Experimental Neurology, 2009. **218**(2): p. 183-192.

60. Jemmerson, R., B. LaPlante, and A. Treefull, *Release of intact, monomeric cytochrome c from apoptotic and necrotic cells.* Cell Death and Differentiation, 2002. **9**(5): p. 538-548.
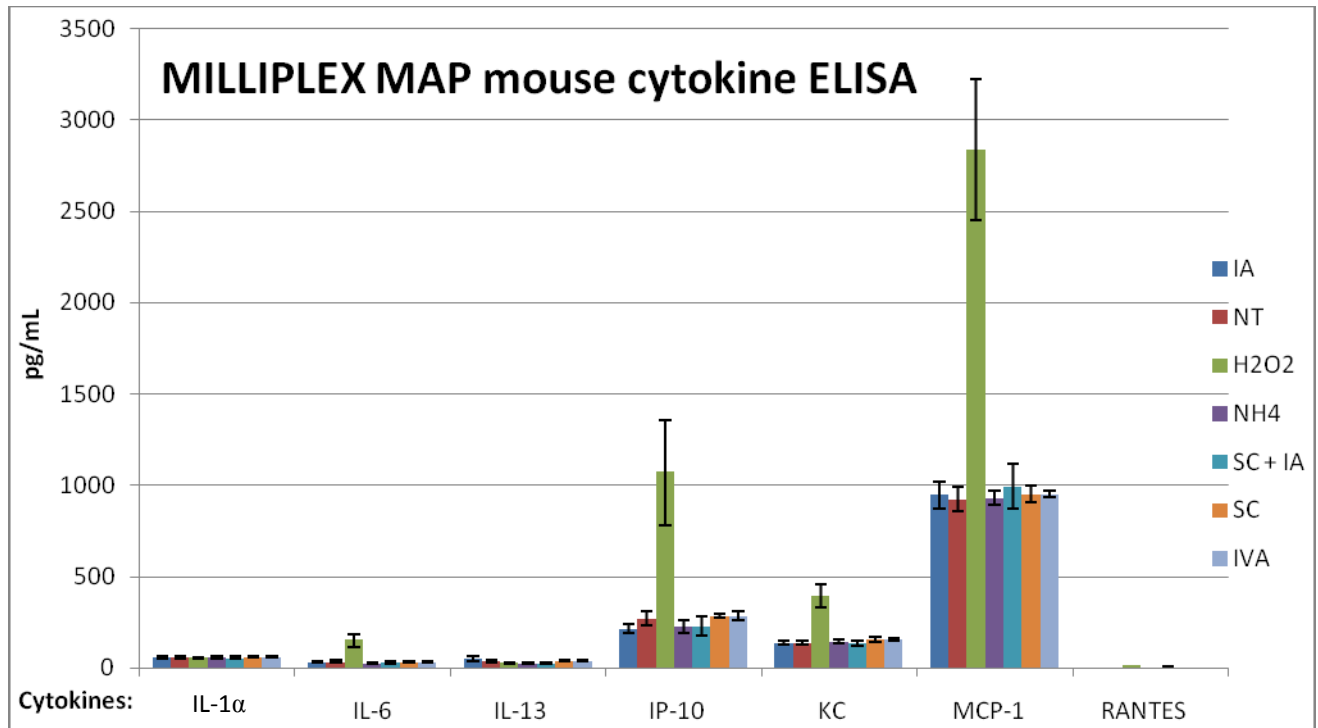
Figure 5.1- Millipore MAP mouse cytokine/chemokine assay. A 22- plex cytokine/chemokine panel was screened of which only seven (shown above) produced detectable signals. 3T3-L1 adipocytes were incubated with either 750 uM isoamylamine (IA) (with or without 1 mM semicarbazide (SC) for 5 minutes), 200 uM ammonium sulfate (NH4), 200 uM isovaleraldehyde (IVA), 220 uM H_2O_2, or 1 mM semicarbazide, or no treatment (NT) for 24 hours. (n=5)
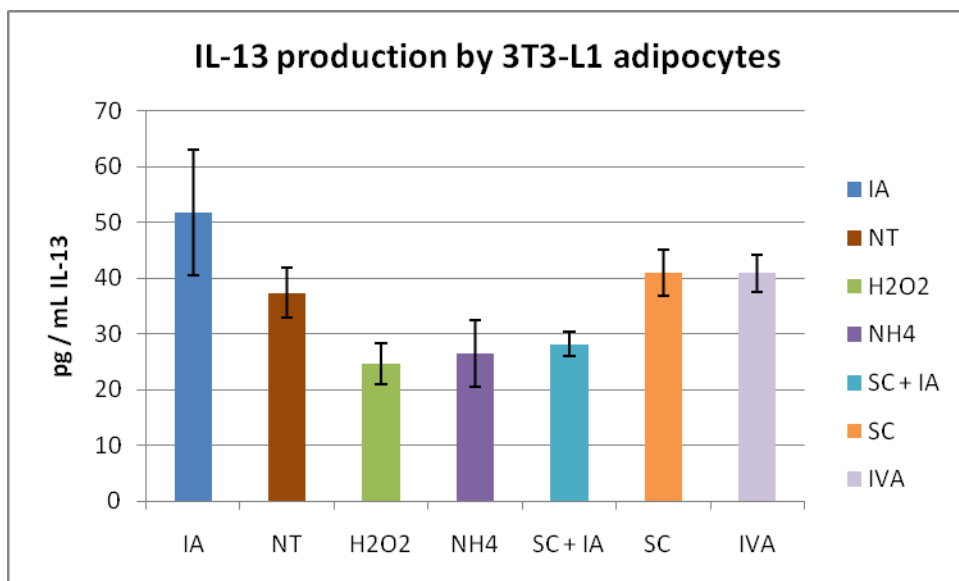
Figure 5.2- Millipore MAP mouse cytokine/chemokine assay showing only the result of IL-13. An increase in IL-13 production may be attributable to AOC3 oxidation of isoamylamine.
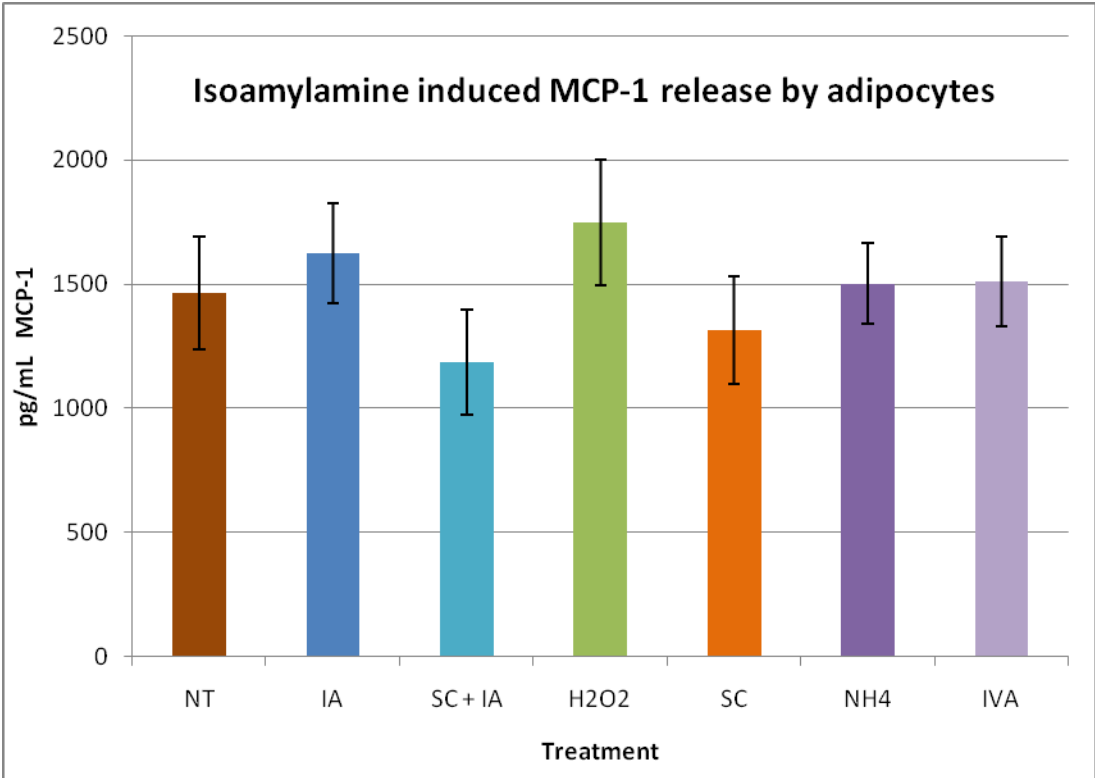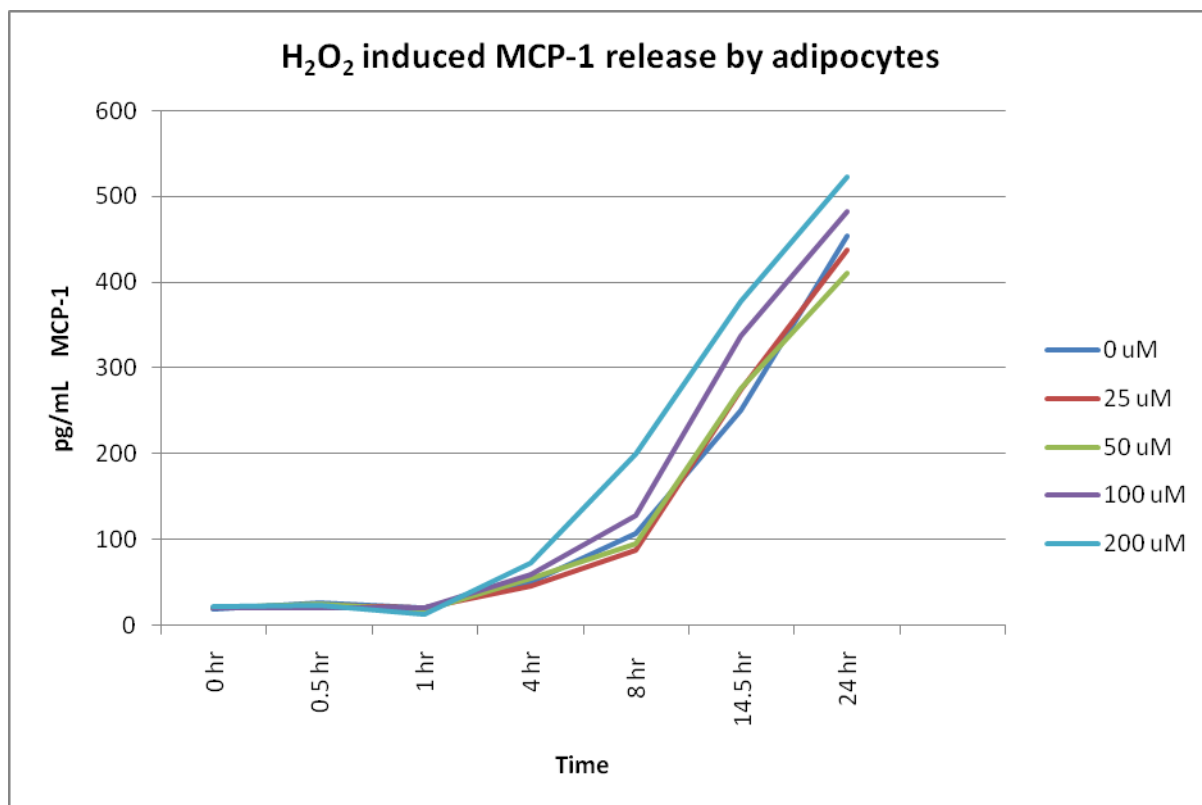
Figure 5.3- Adipocyte treated separately with isoamylamine and resultant products of oxidation for 24 hours and levels of MCP-1 secretion quantified using ELISA. (n = 5)

H₂O₂ induced MCP-1 release by adipocytes

|	0 hr	0.5 hr	1 hr	4 hr	8 hr	14.5 hr	24 hr
0 uM	18.32 ± 2.35	26.22 ± 4.06	20.08 ± 3.25	50.30 ± 8.79	107.19 ± 21.34	250.62 ± 48.77	453.73 ± 15.97
25 uM	20.17 ± 2.51	22.47 ± 2.87	20.90 ± 3.17	46.34 ± 9.00	87.68 ± 6.14	274.34 ± 49.43	437.83 ± 43.66
50 uM	20.11 ± 2.08	25.66 ± 3.53	17.79 ± 5.35	55.09 ± 8.51	95.66 ± 9.08	276.91 ± 54.95	410.91 ± 25.49
100 uM	20.32 ± 4.48	20.29 ± 4.71	20.61 ± 1.80	59.65 ± 9.02	127.75 ± 16.08	337.61 ± 63.27	483.12 ± 37.73
200 uM	22.64 ± 6.42	23.26 ± 2.49	13.38 ± 2.89	73.79 ± 14.52	200.06 ± 61.65	378.60 ± 32.52	523.38 ± 26.64

All values are pg/mL of MCP-1

Figure 5.4- MCP-1 released by adipocytes upon incubation with 0 – 200 uM H_2O_2 for different time points. Accompanying table shows actual results with standard error. (n=5)

H2O2 induced MCP-1 release by adipocytes, 4 - 24 hours
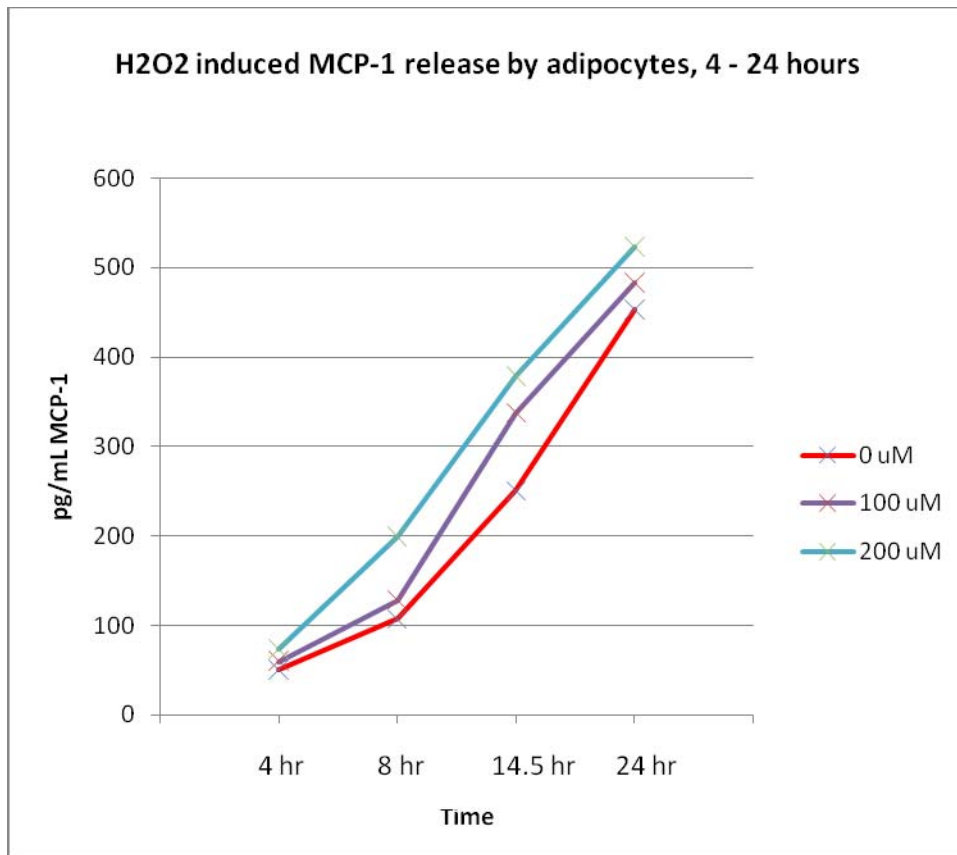
	4 - 8 hrs	8 - 14.5 hrs	14.5 - 24 hrs
0 uM	14.2	22.1	21.4
100 uM	17.0	32.3	15.3
200 uM	31.6	27.5	15.2

Figure 5.5- MCP-1 released by adipocytes upon incubation for 4 – 24 hours. Rate of MCP-1 release for 3 time intervals at 0, 100, and 200 uM H_2O_2 incubation of adipocytes. Measurements are in concentration changes per hour, pg/mL/hr MCP-1.
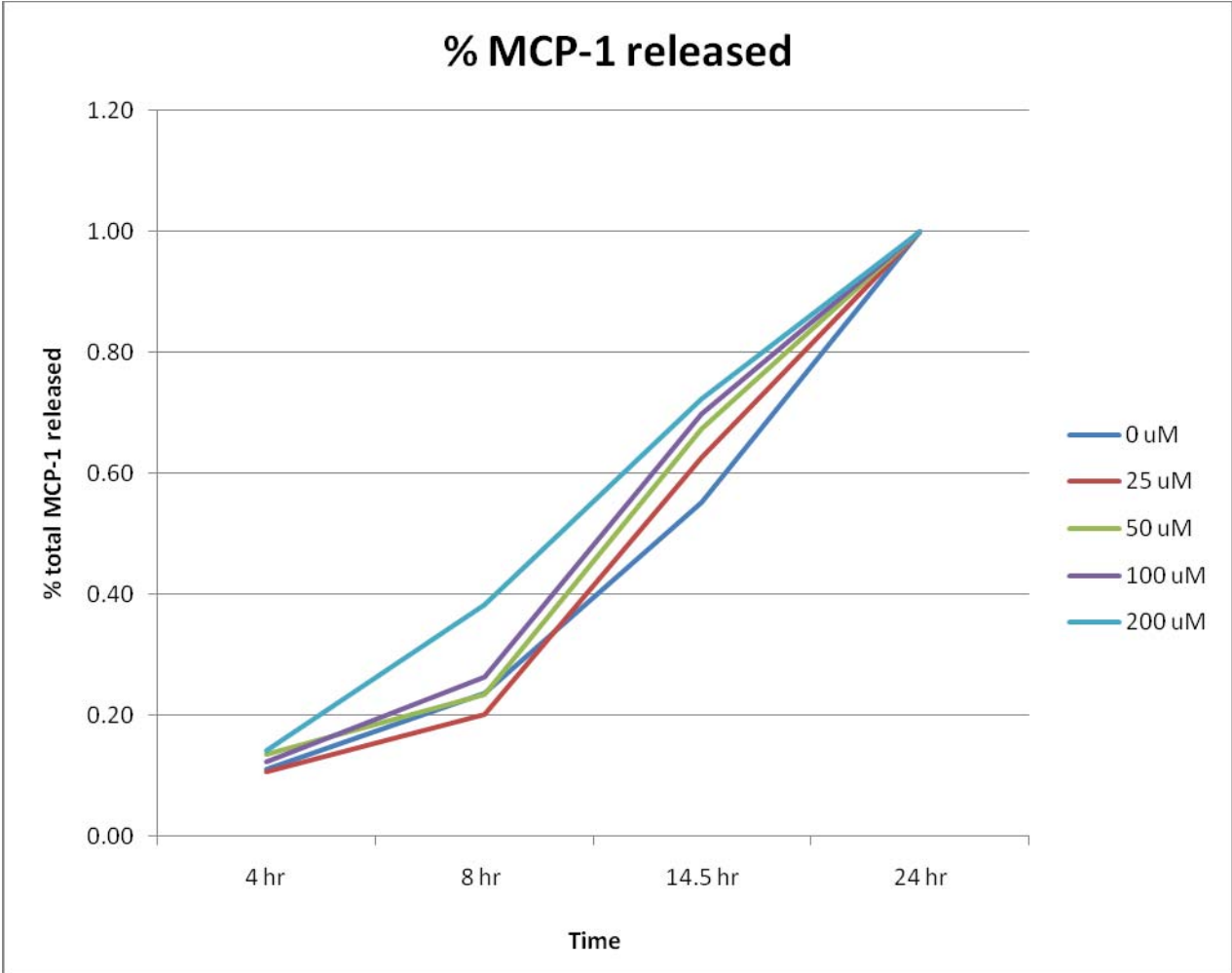
% MCP-1 released

	4 hr	8 hr	14.5 hr	24 hr
0 uM	11%	24%	55%	100%
25 uM	11%	20%	63%	100%
50 uM	13%	23%	67%	100%
100 uM	12%	26%	70%	100%
200 uM	14%	38%	72%	100%

Figure 5.6- Percentage of MCP-1 release by adipocytes compared to MCP-1 release after 24 hours, with accompanying table of actual values.

Figure 5.7- Immunoblot of murine cytochrome c from adipocyte-conditioned media after addition of H_2O_2 and harvested after various time points. All bands were found at approximately 11.6 kDa. A. Addition of 200 uM H_2O_2. Lanes 1: 0 hr, 2: 4 hr, 3: 8 hr, 4: 12 hr, 5: 17.5 hr, 6: 20 hr, 7: 24 hr, 8: media control. B. Addition of 1 mM H_2O_2. Lanes 1: 0 hr, 2: 4 hr, 3: 8 hr, 4: 12 hr, 5: 17.4 hr, 6: 20 hr, 7: 24 hr.
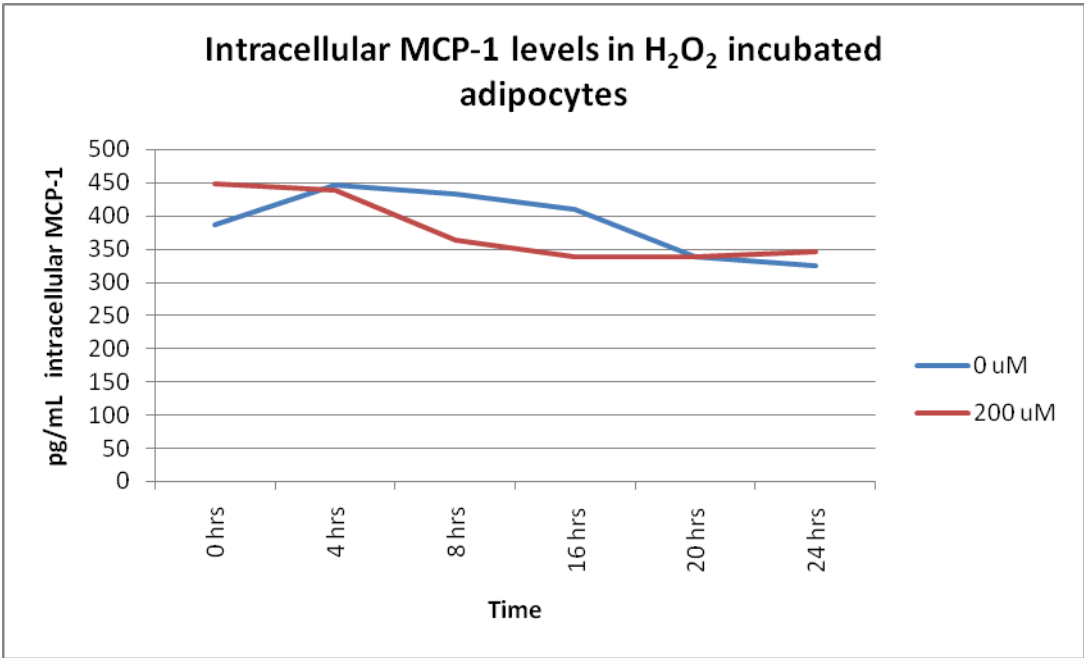
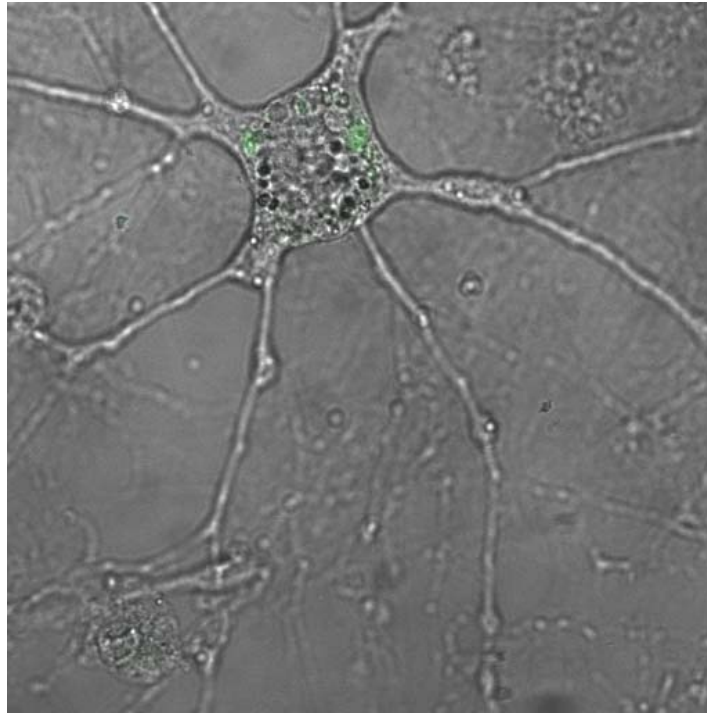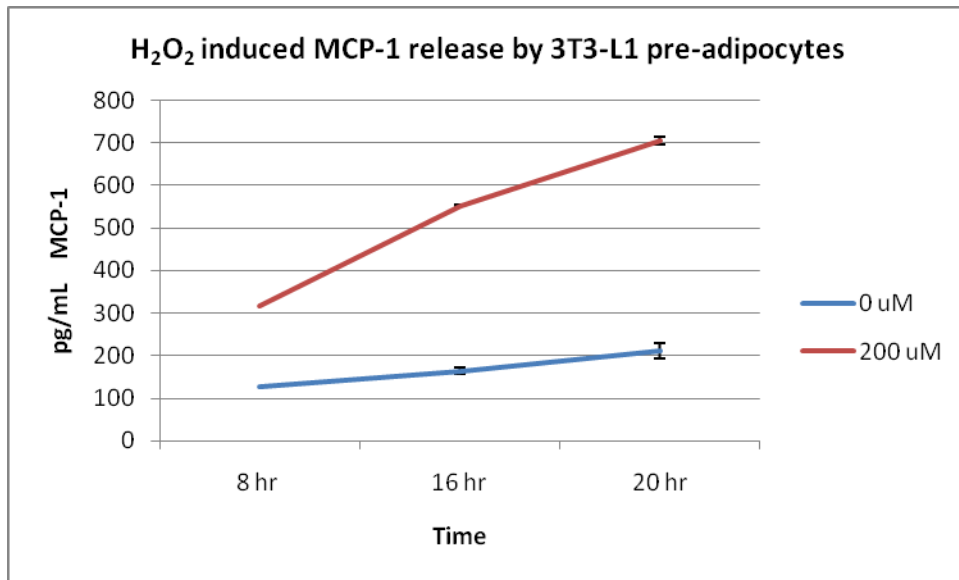Figure 5.8- Detection of intracellular MCP-1 concentration in adipocytes after no treatment and treatment with 200 uM H_2O_2. (n=2)

Figure 5.9- A differential interference contrast image of a 3T3-L1 pre-adipocyte (fibroblast). 63x magnification.

H₂O₂ induced MCP-1 release by 3T3-L1 pre-adipocytes

	8 - 16 hours	16 - 20 hours
0 uM	4.6	11.5
200 uM	29.2	38.0

	8 hr	16 hr	20 hr
0 uM	128	165	211
200 uM	318	552	704

Figure 5.10- Release of MCP-1 by 3T3-L1 pre-adipocytes at 8 – 20 hours with 0 uM and 200 uM H₂O₂, incubation. Top table shows the rate of MCP-1 release in pg/mL/hr between the indicated times. Bottom table shows the MCP-1 concentrations in pg/mL. (n=3)
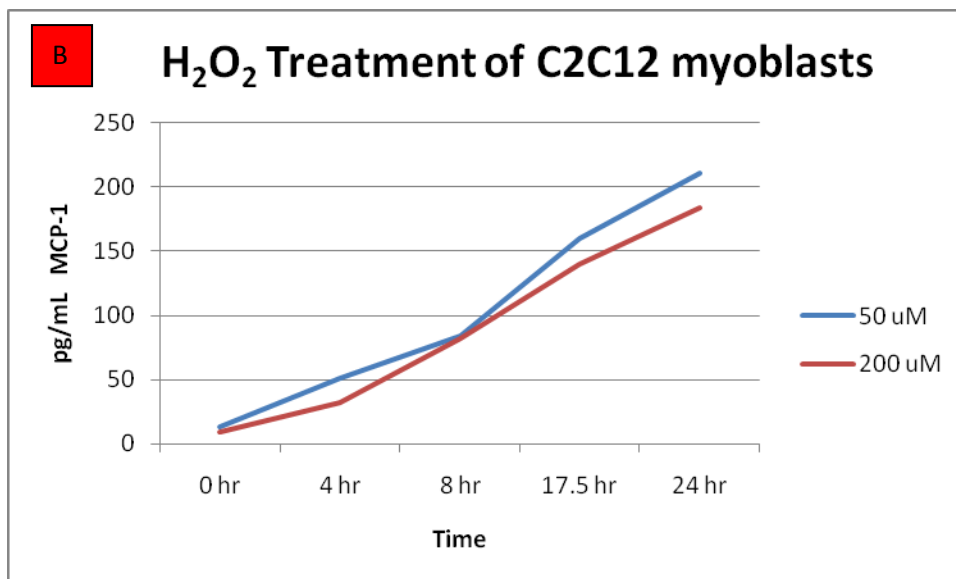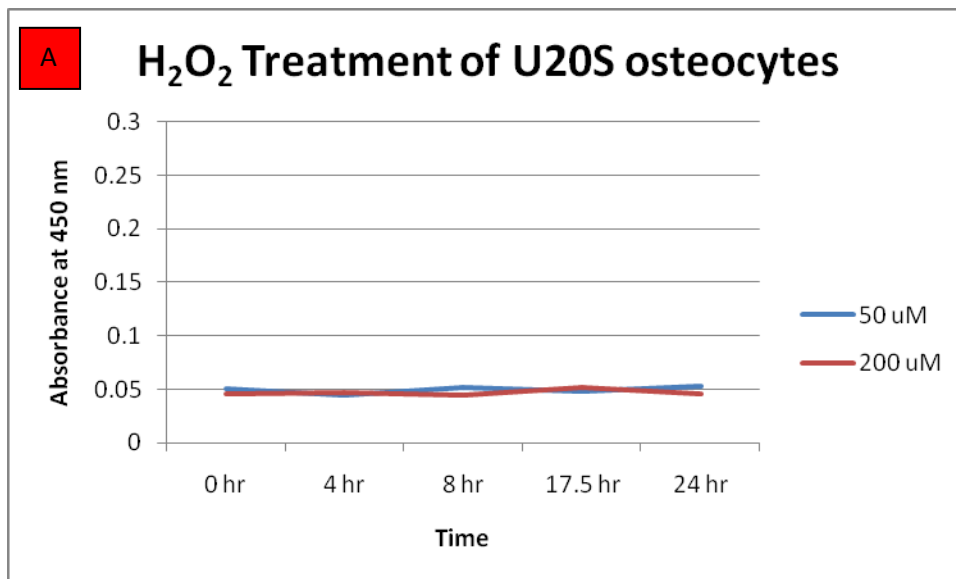
Figure 5.11- A. U20S osteocytes were incubated with either 50 uM or 200 uM H_2O_2 for 0 hr, 4 hr, 8 hr, 17.5 hr, and 24 hrs. At each time point, aliquots of cell supernatant were collected and assayed for MCP-1 by ELISA. B. C2C12 myoblasts were incubated with either 50 uM or 200 uM H_2O_2 for 0 hr, 4 hr, 8 hr, 17.5 hr, and 24 hrs. At each time point, aliquots of cell supernatant were collected and assayed for MCP-1 by ELISA.
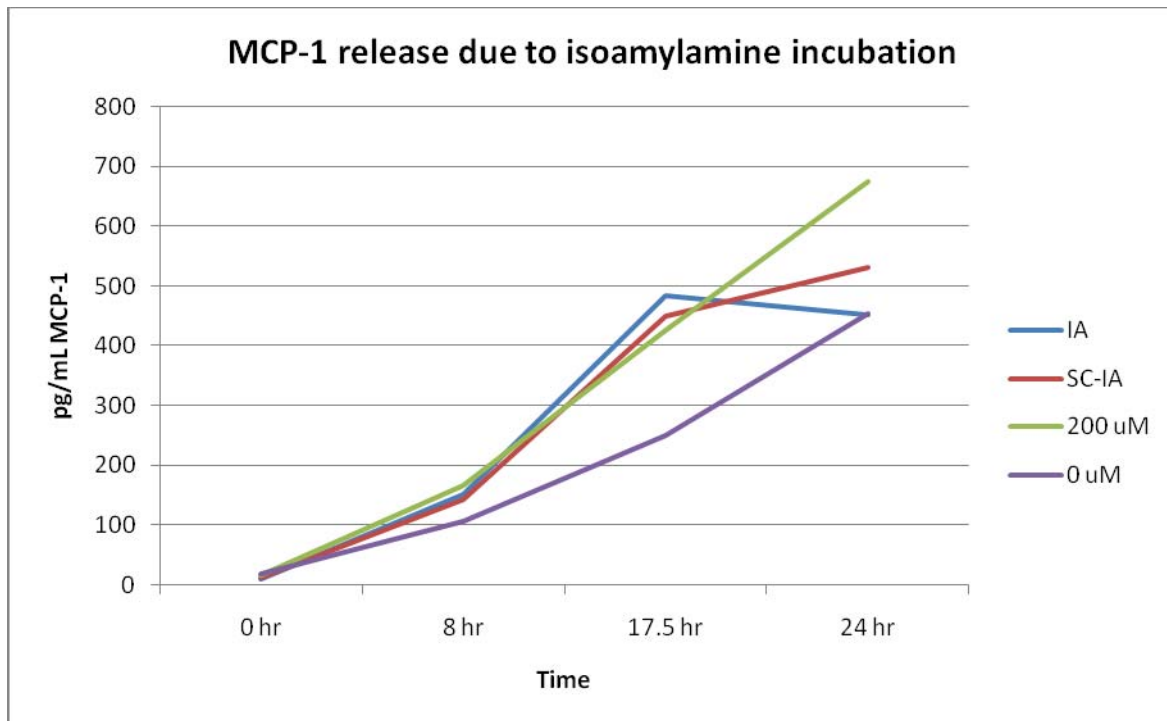
Figure 5.12- 3T3-L1 adipocytes were incubated with 750 uM isoamylamine, with or without 1mM pretreatment with semicarbazide inhibitor for 5 minutes. After specified time period, cell supernatant were assayed for MCP-1 release by ELISA. 0 uM and 200 uM H_2O_2 incubations have also been performed for comparison.

Chapter 6:

Involvement of adipocyte-derived chemokine(s) in macrophage

chemotaxis

Introduction

For AOC3 expressed by endothelial cells, there is mounting evidence of its involvement in lymphocyte migration from circulation into inflamed tissue, a process known as extravasation [1]. With a putative role in adhesion and immune response, an immune function for adipocyte-expressed AOC3 has also been explored. Treatment with AOC3 substrates may promote chemokine release by adipocytes, through potential signaling by H_2O_2, a product of amine oxidation. In Chapter 5, increased MCP-1 release correlated with addition of higher concentrations of exogenous H_2O_2 and longer incubation times. However, the increased chemokine release was not related to amine substrate addition, thus not correlated with AOC3.

Chemokines are a family of at least ten small (8 – 10 kDa) cytokines, which are thought to be involved in constitutive homing and recirculation of immune cells [2-4]. In addition, chemokines may also be involved in angiogenesis and leukocyte degranulation [5]. Inappropriate activation of chemokines may result in cardiovascular disease, allergic inflammatory disease, cancer, and neuroinflammation [6]. Released chemokines activate immune cells rolling along the endothelium, causing firm adhesion [7]. Prior to entry into tissue, the immune cell moves toward a chemotactic gradient formed by the chemokines on the endothelium and initiates the process of extravasation [8]. The physiological response to chemokine release is the recruitment of granulocytes, monocytes, dendritic cells, and T-cells to sites of inflammation or infection.

Though MCP-1 release by adipocytes was not attributable to AOC3, it is unknown whether AOC3 turnover could produce other chemokines and cytokines that could be involved in macrophage recruitment. In order to examine this possibility, cell-based chemotaxis assays were performed. These assays can be performed in a variety of ways, with the technique of choice being the use of Boyden chambers [9-11]. Using this method, chemoattractants are separated from macrophages by a membrane featuring micropores. Movement of macrophages toward chemoattractant is an active process as the micropores are too small for passive migration. Factors that may affect results include adhesion of cells to filter material, lack of a chemoattractant gradient, variable local concentrations of chemoattractants around micropores, and cell migration is not directly observed during the assay, but deduced by looking at the final distribution of cells. Chemotaxis assays involving the use of transwells work similarly to Boyden chambers [12, 13]. In the under agarose chemotaxis assay, migration of cells under an agarose gel is a measurement of chemoattractant potential. This assay is easy to perform and spontaneous migration, or cell behavior, can be observed [14]; however, the concentration gradient of chemoattractant does not approach a linear steady state. To establish a linear concentration gradient, a Dunn chamber [15] or Zigmond chamber [16] can be utilized. Both chambers would allow a more careful assessment of chemotactic potential. Other methods for measuring chemotaxis include using three-dimensional collagen fibers with computer-aided visualization of chemotaxis [17], automated measurements of chemotaxis by measuring impedance changes caused by cells on the surface of an electrode using an under-agarose system [18], microfluidic devices [19], and the use of degradable microspheres to release chemoattractant [20]. The initial goal of our chemotaxis assay is to determine whether chemokines are produced by adipocytes upon incubation with AOC3 substrate. Therefore, methods involving standard, easy to use, and off-the-shelf equipment would be preferred. Since a strict linear concentration gradient is not required to assess production of chemokine(s), an

approach using the Boyden chamber, transwell, or the under-agarose method was considered. A variant of the Boyden chamber utilizing chemotaxis chambers from Neuroprobe was selected since the chambers are reusable, relatively easy to use, with widespread citations of their use in the literature [21-24].

Macrophages for use in the chemotaxis assay would ideally be isolated from mice through a peritoneal lavage and used promptly prior to cell death and activation. However, cultured murine macrophage cell lines, including RAW264, RAW309Cr, PU5-1R, WEHI274.1, and WEHI 265.1, exist and chemotaxis using these cell lines could be demonstrated more conveniently [25,27], without the need to sacrifice mice for each experiment. In addition, it has been reported that both WEHI274.1 and RAW264.7 can be activated by MCP-1, and thus express the MCP-1 receptor [25, 26]. RAW264.7 cells have also been found to exhibit chemotactic properties most similar to macrophages, and therefore were used in the chemotaxis assays [27].

Methods

Cell culture. The differentiation protocol starts with a 100 mm tissue culture dish of murine 3T3-L1 fibroblasts obtained from American Type Cell Culture (ATCC). Cells were grown to confluence 7 days after initial plating. Once confluent, cellular differentiation was induced using insulin, dexamethasone, and methylisobutylxanthine as previously described [28]. Cells were cultured in Dulbecco's Modified Eagle Medium (DMEM) (Invitrogen, Carlsbad, CA) supplemented with 10% Fetal Bovine Serum (FBS) (Hyclone, Waltham, MA). Differentiation takes 8 days. Only passage 1 – 3 differentiated adipocytes were used. RAW264.7 (ATCC) cultured mouse macrophage cell lines were grown in RPMI-1640 media (Invitrogen) supplemented with 10% FBS (Hyclone) and grown on 100 mm Petri dishes (BD Falcon, Durham, NC). Macrophages were split at approximately 60 – 70% confluence, and cells were used up to passage 11.

Preparation of Endotoxin-activated mouse serum (EAMS). Preparation previously described in [29]. Briefly, mouse serum (Sigma) was incubated with lipopolysaccharides from *E. coli* O111:B4 (Sigma) for 90 minutes at 37°C. The endotoxin serum mixture was heated for 30 minutes at 56°C and centrifuged at 1000g for 10 minutes at 4°C. As a positive control, a dilution of the prepared serum was able to induce significant chemotaxis and was used for all chemotaxis assays.

Preparation of adipocyte supernatant. 3T3-L1 mouse adipocytes were cultured in 6-well plates as previously described. Cells were washed with warmed phosphate buffered saline (PBS), pH 7.4 three times prior to adding 1 mL DMEM, supplemented with 0.5% bovine serum albumin (BSA) (Sigma Aldrich) to each well. Cells were treated either with or without 100 uM semicarbazide for at least 30 minutes. After inhibitor incubation, isoamylamine substrate was added from $1/8\ K_m$ to $10K_m$ and adipocytes incubated with substrate for at least 4 hours and up to 24 hours. After incubation, supernatant was immediately used as chemoattractant in chemotaxis assay.

Chemotaxis Assay. Macrophage migration was assessed in a 12-well microchamber (Neuroprobe, Gaithersburg, MD). Lower wells were filled with approximately 155 uL adipocyte-derived supernatant, prepared as previously described. Cell media were used as negative control, and endotoxin-activated mouse serum as positive control. Upper well was filled with 105 uL of approximately 4×10^5 macrophage cells in RPMI-1640. To prepare macrophages for assay, macrophages in Petri dishes were incubated with nonenzymatic cell dissociation solution (Sigma) for 10 minutes to detach semi-adherent cells from dishes. An aliquot of cells were taken out to determine total viable cell count using hemacytometer and Trypan blue dye. Cells were washed in RPMI three times by centrifuging at 1000 rpm for 5 minutes at room temperature. After wash, cells were resuspended in RPMI-1640 to make a final concentration of approximately 4×10^6 cells/mL and cells were put on ice until use. 105 uL of these cells filled the top well of the chemotaxis chamber. The wells were separated by a polyvinylpyrrolidone-free polycarbonate track-etch filter (Neuroprobe, Gaithersburg, MD) with 5 um pores. Incubations were carried out for 4 hours at 37°C and 5% CO_2. After incubation, the filter was removed and the top-side of the filter scraped to get rid of macrophages stuck to the

top of the filter, and the filter was put on a microscope slide with the bottom-side facing up. Transmigrated cells were fixed to the membrane with ice cold histological grade methanol (Fisher Chemical, Fair Lawn, NJ) for 20 minutes. After fixing, the filters were kept at room temperature until visualization by fluorescence microscope.

Fluorescence Microscopy. Macrophages fixed to the filter membrane was visualized by treatment of membrane with 2.5 ug/mL 4',6-diamidino-2-phenylindole dihydrochloride (DAPI) (Sigma) fluorescent probe and imaged with a Zeiss Axiophot 381 epifluorescence microscope with a 40x air objective in Berkeley Biological Imaging Facility. Transmigrated cells were counted in at least 2 different fields of view and averaged.

Results

   3T3-L1 adipocytes were incubated with AOC3 substrate, isoamylamine, at various concentrations for four hours to assess the acute effects of amine administration. In order to maximize released chemokine concentration, cell media volume per well was kept to a minimum. After four hours, the supernatant was harvested and immediately used in the chemotaxis assay. Chemotaxis was allowed to occur for four hours, with longer incubation times resulting in more false positives and data showing that RAW264.7 macrophages exhibit chemotaxis within the first four hours of the assay [27]. Chemotaxis resulting from macrophages exposed to media from adipocytes incubated with $25K_m$ (3.7 mM) isoamylamine is shown in Figure 1. In Figure 1A, adipocytes were not pretreated with semicarbazide inhibitor whereas in Figure 1B, pretreatment with 100 uM semicarbazide for 30 minutes occurred prior to addition of isoamylamine. Results of chemotaxis assay did not differ markedly upon visually comparing the results with and without AOC3 inhibition. Positive controls using endotoxin-activated mouse serum and negative controls using cell culture media are shown in Figure 2A and Figure 2B, respectively. Over the four hour chemotaxis assay, unmotivated macrophage migration toward negative control chemoattractant of cell culture media was prevalent and comparable to the results seen with AOC3 substrate incubation. This result suggests that chemotaxis observed with isoamylamine incubation was not dependent on AOC3 turnover.

   A dose response curve of macrophages exposed to media from adipocytes incubated at 0 – 3.7 mM isoamylamine is shown in Figure 3. Upon addition of higher concentrations of isoamylamine to adipocytes, macrophages responded negatively with a decrease in chemotaxis, also known as fugetaxis [30]. Interestingly, with no addition of isoamylamine, macrophage chemotaxis was actually highest. This observation may be the result of the constitutive release of MCP-1 by adipocytes. If the 0 K_m point was disregarded, the resulting linear regression $R^2 =$ 0.101, a low correlation between isoamylamine and chemotaxis. Cellular migration has been shown to be dose responsive, with chemotaxis observed around an effective chemoattractant concentration. Above and below this concentration, observed chemotaxis can decline rapidly [27, 31]. Therefore, media from adipocytes incubated with low concentration of isoamylamine was also subjected to the chemotaxis assay, with the results shown in Figure 4. Again, correlation between isoamylamine concentration and macrophage chemotaxis was found to be low. At the lower isoamylamine concentrations, comparing results from adipocytes that did or did not undergo semicarbazide pretreatment, chemotaxis of macrophages to the resulting cell media did not differ significantly, as shown in Figure 5. Maximal response of adipocytes to amine incubation would most likely occur around the K_m of the AOC3 substrate. However, no difference in macrophage chemotaxis was observed when compared to results with inhibitor pretreatment.

Discussion

If AOC3 is involved in a signaling pathway that induces release of chemokines by adipocytes, the chemotaxis assay was not sensitive enough to demonstrate this response. From the results, chemotaxis by RAW264.7 macrophages was not shown to be dependent on media components from adipocytes incubated with isoamylamine. In addition, chemotactic response to MCP-1 by macrophages displays a dose dependent response. For example, chemotaxis by human monocytes was maximal upon introduction of approximately 10 ng/mL MCP-1, with negligible chemotaxis below 1 ng/mL and above 100 ng/mL [32]. Therefore, chemotaxis assay would be ineffective if released MCP-1 was not within a 1 – 100 ng/mL range. From data presented in Chapter 5, adipocytes were found to release approximately 1.6 ng/mL MCP-1 upon incubation with 750 uM isoamylamine for 24 hours. This level of MCP-1 release should promote chemotaxis if the dose response curve for RAW264.7 matches the curve found for human monocytes. However, adipocytes under no treatment also released MCP-1, which was found to be approximately 1.5 ng/mL, resulting in a difference in MCP-1 concentration of only 0.1 ng/mL. From the data presented on human monocytes [32], every one ng/mL increase in MCP-1 resulted in a 5.5% increase in migrated monocytes between 1 ng/mL and 10 ng/mL MCP-1. A 0.1 ng/mL increase in MCP-1 would therefore result in a 0.55% increase in macrophage accumulation. It has been reported that the maximal percentage of RAW264.7 that migrated in presence of chemoattractant was usually within a range of 23 – 27%, with a 1% migration observed in the absence of chemoattractant [27]. In our experiments, a total of 420,000 macrophages were used per chemotaxis experiment, resulting in a maximum of approximately 113,400 migrated cells if a potent chemoattractant was present. An increase of 0.55% in macrophage migration may be observable at this cell count. However, an increased isoamylamine incubation time of 24 hours will be required vs. the current 4 hours, to allow time for the increase in MCP-1 concentration to occur. From this study, acute administration of AOC3 substrate for 4 hours did not result in increased chemokine release by adipocytes. Minimal media volume of 1 mL was just enough to cover adherent cells, but may still be too much to allow an increase in MCP-1 concentrations required to promote macrophage chemotaxis.

After the work on macrophage chemotaxis was completed, it was found that activated macrophages behaved differently from unactivated macrophages. Every experiment was performed using unactivated macrophages. It has been reported that chemotaxis of RAW264.7 macrophages does not occur even in the presence of MCP-1 chemoattractant without prior activation of the macrophages [26]. Therefore, the most conservative conclusion from our findings is that no difference in macrophage chemotaxis was observed using chemoattractants derived from adipocyte-conditioned media. The chemotaxis experiments will be repeated using activated macrophages in the future.

References

1. Salmi, M., et al., *A cell surface amine oxidase directly controls lymphocyte migration.* Immunity, 2001. **14**(3): p. 265-276.
2. Oppenheim, J.J., et al., *Properties of the Novel Proinflammatory Supergene Intercrine Cytokine Family.* Annual Review of Immunology, 1991. **9**: p. 617-648.
3. Yoshie, O., T. Imai, and H. Nomiyama, *Novel lymphocyte-specific CC chemokines and their receptors.* Journal of Leukocyte Biology, 1997. **62**(5): p. 634-644.
4. Cyster, J.G., *Chemokines - Chemokines and cell migration in secondary lymphoid organs.* Science, 1999. **286**(5447): p. 2098-2102.
5. Mackay, C.R., *Chemokines: immunology's high impact factors.* Nature Immunology, 2001. **2**(2): p. 95-101.
6. Gerard, C. and B.J. Rollins, *Chemokines and disease.* Nature Immunology, 2001. **2**(2): p. 108-115.
7. Schall, T.J. and K.B. Bacon, *Chemokines, Leukocyte Trafficking, and Inflammation.* Current Opinion in Immunology, 1994. **6**(6): p. 865-873.
8. Thomson, A.W., *The cytokine handbook.* 3rd ed. 1998, San Diego: Academic Press. xxii, 1017 p.
9. Brooks, S.A. and U. Schumacher, *Metastasis research protocols.* Methods in molecular medicine. 2001, Totowa, N.J.: Humana Press. v. <1 >.
10. Boyden, S., *Chemotactic Effect of Mixtures of Antibody and Antigen on Polymorphonuclear Leucocytes.* Journal of Experimental Medicine, 1962. **115**(3): p. 453-&.
11. Guan, J.-L., *Cell migration : developmental methods and protocols.* 2005, Totowa, N.J.: Humana Press. xv, 364 p.
12. Coutts, A.S., *Adhesion protein protocols.* 2nd ed. 2007, Totowa, N.J.: Humana Press. x, 234 p.
13. Proudfoot, A.E.I., T.N.C. Wells, and C. Power, *Chemokine protocols.* 2000, Totowa, N.J.: Humana Press. xiii, 353 p.
14. Nelson, R.D., P.G. Quie, and R.L. Simmons, *Chemotaxis under Agarose - New and Simple Method for Measuring Chemotaxis and Spontaneous Migration of Human Polymorphonuclear Leukocytes and Monocytes.* Journal of Immunology, 1975. **115**(6): p. 1650-1656.
15. Zicha, D., G.A. Dunn, and A.F. Brown, *A New Direct-Viewing Chemotaxis Chamber.* Journal of Cell Science, 1991. **99**: p. 769-775.
16. Zigmond, S.H. and J.G. Hirsch, *Leukocyte Locomotion and Chemotaxis - New Methods for Evaluation and Demonstration of a Cell-Derived Chemotactic Factor.* Journal of Experimental Medicine, 1973. **137**(2): p. 387-410.
17. Haddox, J.L., R.R. Pfister, and C.I. Sommers, *A Visual Assay for Quantitating Neutrophil Chemotaxis in a Collagen Gel Matrix - a Novel Chemotactic Chamber.* Journal of Immunological Methods, 1991. **141**(1): p. 41-52.
18. Hadjout, N., et al., *Automated real-time measurements of leukoeyte chemotaxis.* Journal of Immunological Methods, 2007. **320**(1-2): p. 70-80.
19. Englert, D.L., M.D. Manson, and A. Jayaraman, *Flow-Based Microfluidic Device for Quantifying Bacterial Chemotaxis in Stable, Competing Gradients.* Applied and Environmental Microbiology, 2009. **75**(13): p. 4557-4564.
20. Zhao, X.J., et al., *Directed cell migration via chemoattractants released from degradable microspheres.* Biomaterials, 2005. **26**(24): p. 5048-5063.
21. Fox, S.E., et al., *The effects and comparative differences of neutrophil specific chemokines on neutrophil chemotaxis of the neonate.* Cytokine, 2005. **29**(3): p. 135-140.
22. Gudewicz, P.W., et al., *Interaction of Fibronectin (Fn) Cell-Binding Fragments and Interleukin-8 (Il-8) in Regulating Neutrophil Chemotaxis.* Biochemical and Biophysical Research Communications, 1994. **205**(1): p. 706-713.
23. Strandberg, K., et al., *Effect of formoterol and budesonide on chemokine release, chemokine receptor expression and chemotaxis in human neutrophils.* Pulm Pharmacol Ther.
24. Esemuede, N., et al., *Lovastatin Inhibits Thrombospondin-1-Induced Smooth Muscle Cell Chemotaxis.* J Surg Res, 2009.
25. Boring, L., et al., *Molecular cloning and functional expression of murine JE (monocyte chemoattractant protein 1) and murine macrophage inflammatory protein 1alpha receptors: evidence for two closely linked C-C chemokine receptors on chromosome 9.* J Biol Chem, 1996. **271**(13): p. 7551-8.

26. *Chun, K.R., et al., Suppression of the lipopolysaccharide-induced expression of MARCKS-related protein (MRP) affects transmigration in activated RAW264.7 cells. Cell Immunol, 2009. **256**(1-2): p. 92-8.*

27. *Aksamit, R.R., W. Falk, and E.J. Leonard, Chemotaxis by mouse macrophage cell lines. J Immunol, 1981. **126**(6): p. 2194-9.*

28. *Stephens, J.M., J. Lee, and P.F. Pilch, Tumor necrosis factor-alpha-induced insulin resistance in 3T3-L1 adipocytes is accompanied by a loss of insulin receptor substrate-1 and GLUT4 expression without a loss of insulin receptor-mediated signal transduction. Journal of Biological Chemistry, 1997. **272**(2): p. 971-976.*

29. *Laskin, D.L., et al., Induction of Chemotaxis in Mouse Peritoneal-Macrophages by Phorbol Ester Tumor Promoters. Cancer Research, 1981. **41**(5): p. 1923-1928.*

30. *Vianello, F., I.T. Olszak, and M.C. Poznansky, Fugetaxis: active movement of leukocytes away from a chemokinetic agent. J Mol Med, 2005. **83**(10): p. 752-63.*

31. *Lazarus, H.M., et al., Induction of human monocyte motility by lysyl oxidase. Matrix Biol, 1995. **14**(9): p. 727-31.*

32. *Lind, M., et al., Chemotaxis and activation of particle-challenged human monocytes in response to monocyte migration inhibitory factor and C-C chemokines. J Biomed Mater Res, 1999. **48**(3): p. 246-50.*
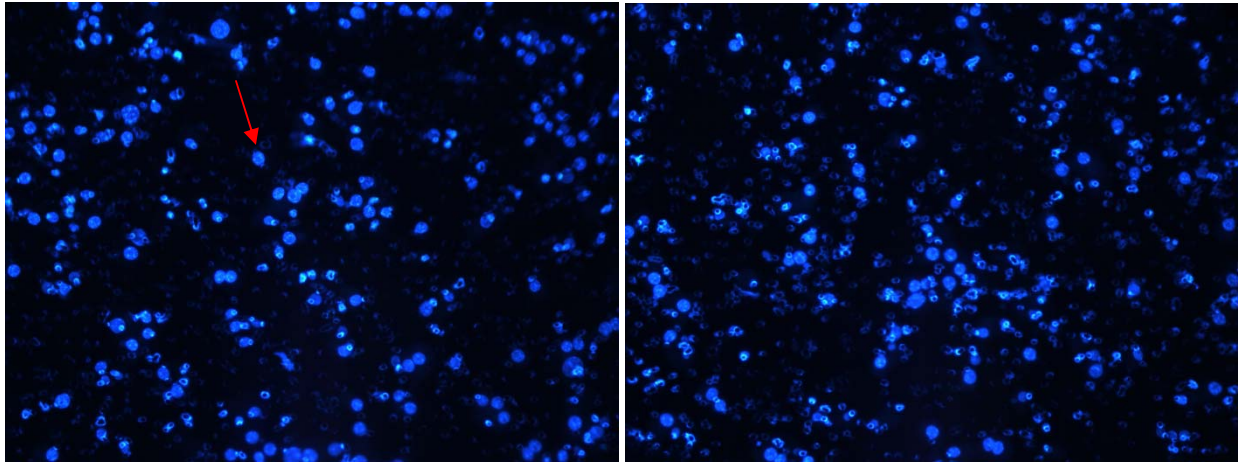
Figure 6.1- DAPI-stained RAW264.7 macrophages on chemotaxis filter membrane with 5 um pores. Treatment of adipocytes with 3.7 mM isoamylamine for 2 hours at total volume of 1 mL. The supernatant served as chemoattractant for RAW 264.7 macrophages. Chemotaxis allowed to occur for 4 hours at 37°C and 5% CO_2. Fluorescence images of macrophages taken. Relatively larger blue circles correspond to macrophages, as shown by red arrow. In A. adipocytes without initial semicarbazide treatment while in B. adipocytes were treated with 100 uM semicarbazide for 30 minutes.
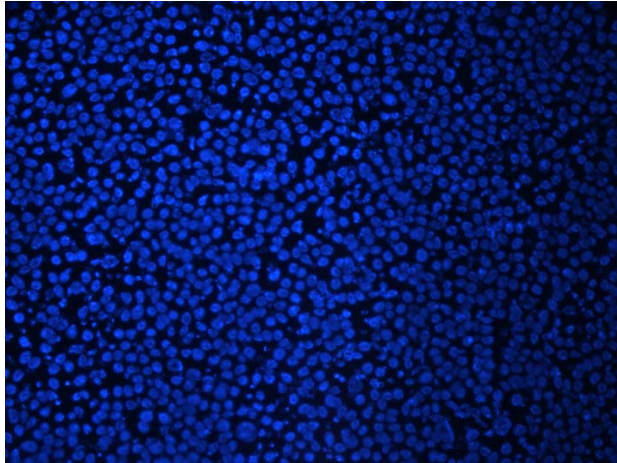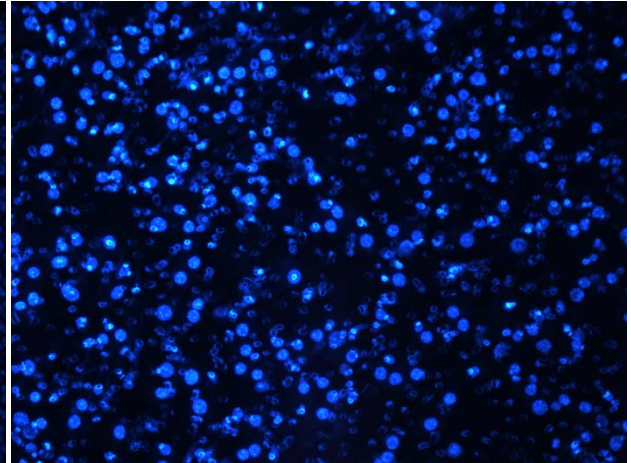
Figure 6.2- A. Positive control with endotoxin-activated mouse serum as chemoattractant and B. negative control with cell culture media.
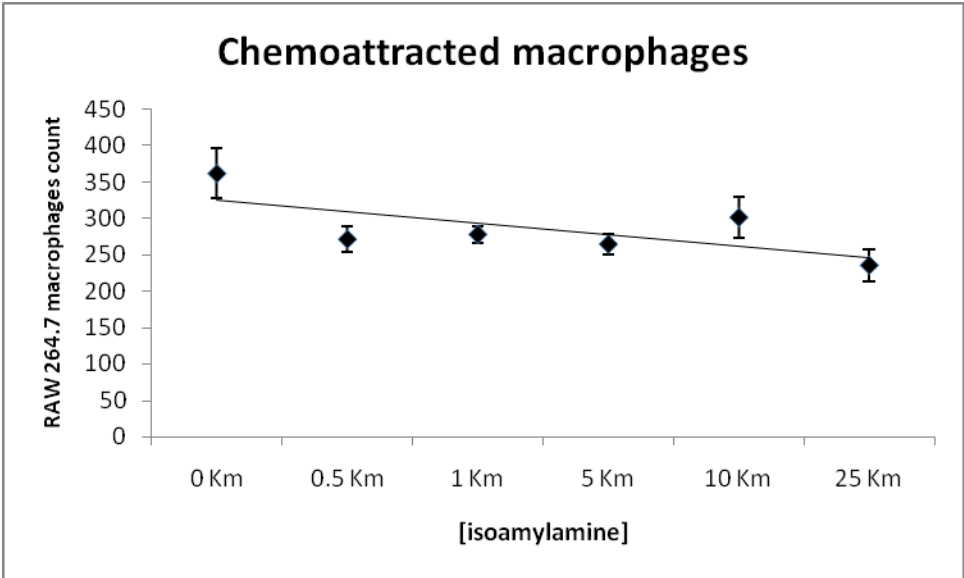
Figure 6.3- Dose response curve of RAW264.7 macrophages to media incubating 3T3-L1 adipocytes treated with 0 – 3.7 mM isoamylamine for 2 hours at 37°C and 5% CO_2. Chemotaxis was allowed to occur over 4 hours. (n = 2). R^2 = 0.473
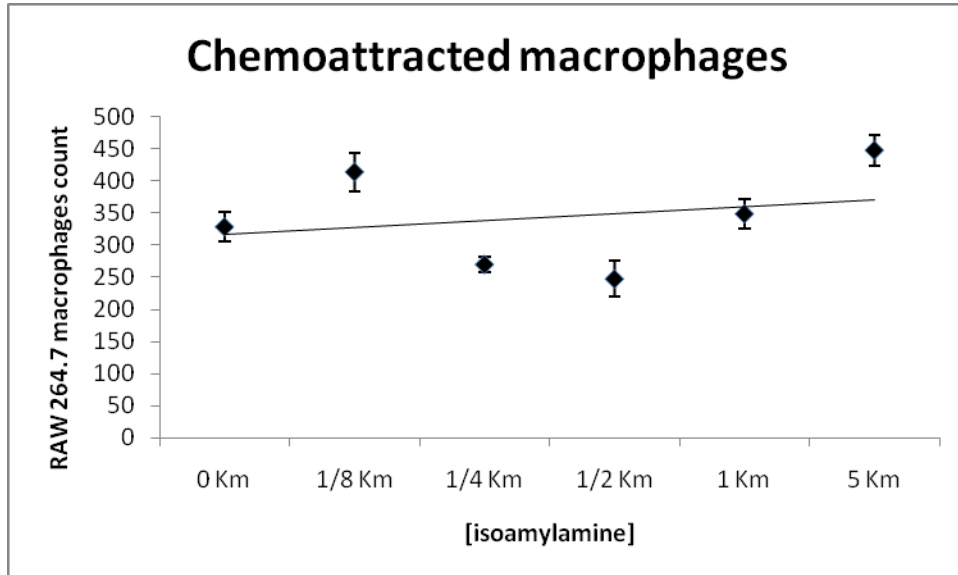
Figure 6.4- Dose response curve of RAW264.7 macrophages to supernatant derived from adipocytes incubated at lower levels of isoamylamine ranging from 0 – 740 uM for 2 hours at 37°C and 5% CO_2. Chemotaxis was allowed to occur over 4 hours. (n=2) R^2 = 0.066
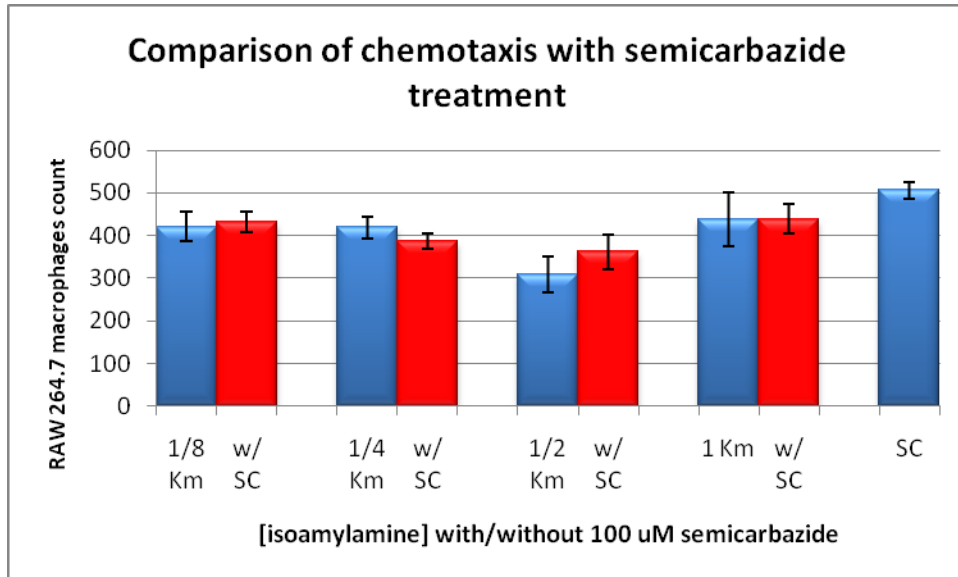
Figure 6.5- Comparison of chemotaxis by RAW 264.7 macrophages between adipocytes with or without 100 uM semicarbazide pretreatment.